

UNIVERSITY OF CALIFORNIA

Santa Barbara

Age, Provenance, and Facies Architecture of an arid-land fluvial system in equatorial  
Pangaea: The Cloud Chief Formation in western Oklahoma, U.S.A.

A Thesis submitted in partial satisfaction of the  
requirements for the degree Master of Science  
in Marine Science

by

Vanessa May De Belen Brillo

Committee in charge:

Professor Alexander R. Simms, Chair

Professor John M. Cottle

Professor Susannah M. Porter

December 2015

The thesis of Vanessa May De Belen Brillo is approved.

---

John M. Cottle

---

Susannah M. Porter

---

Alexander R. Simms, Committee Chair

December 2015

## ACKNOWLEDGEMENTS

I first would like to thank U. S. Geological Survey under Award #G14AC00277 for providing the funds that made this study possible. A heartfelt thank you to my research advisor, Dr. Alex Simms, for providing me with the opportunity to work with this exciting project and for all the patience and guidance throughout the process. I am a better field scientist because of him. A special thank you to my committee members, Dr. John Cottle and Dr. Susannah Porter, for constructive criticisms and help in editing my thesis. Thank you to Justin Steinmann for field assistance in collecting samples and measuring sections. I thank Dr. Gregg Hudson and Paul Clark from the United States Department of Agriculture Natural Resources Conservation Service for allowing me to obtain a core through the Cloud Chief Formation. Many thanks to Wagner Petrographic for help in making my thin sections. Thank you to Dr. Douglas Walker of the Isotope Geochemistry Laboratories in University of Kansas for conducting Strontium isotope analysis on my gypsum samples. I thank Dr. Andrew-Kylander Clark from the University of California Santa Barbara for running detrital zircon geochronology on my zircon samples. A special thanks to all the landowners in my study area, especially to Joni and Scott Sanderford, for giving me permission to gain access to their lands. Thank you to all my friends in UCSB, for all the moral support these past two years. To all the faculty at UCSB, thank you for providing me with a rich graduate school experience. I extend my deepest gratitude to my family, especially to mom, dad, Tito, Amy, and Ren, who stood by me through my ups and downs. Finally, a special thanks to my fiancé, James, for putting up with long hours of work. This thesis would not have been possible if not for the cumulative support that all of you provided me. My sincerest thanks.

## ABSTRACT

Age, Provenance, and Facies Architecture of an arid-land fluvial system in equatorial  
Pangaea: The Cloud Chief Formation in western Oklahoma, U.S.A.

by

Vanessa May De Belen Brillo

The Permian redbeds of the Midcontinent U.S.A. are thought to contain important clues to the climate history of western Pangaea. However, before these units can be used as paleoclimatic archives, better constraints are needed on their age, depositional environment, and provenance. In this study, 43 stratigraphic sections were measured within the Lopingian Cloud Chief Formation of western Oklahoma. The sections were complemented by strontium isotope analysis and detrital zircon geochronology. Nine facies were recognized within the measured sections. These facies include massive gypsum, gypsiferous sandstones, channelized very fine sandstones, thickly-bedded sandstones, siltstones, variegated mudstones, ripple cross-laminated very fine sandstones, interbedded sandstones and mudstones, and silty claystones. These facies are interpreted to represent subenvironments of widespread arid-land fluvial systems flowing into a sabkha. These interpretations fit well with other recent work calling for arid conditions within the midcontinent during the middle Permian. Detrital zircon geochronology points to a dominant sediment source to the east (Ouachita Mountains) with a subordinate source to the west (Ancestral Rocky Mountains in Colorado and New Mexico). Strontium isotope values of the massive gypsum facies provide

evidence for marine encroachment during periods of high relative sea level. These isotope values point to an age for the Cloud Chief of  $262 \pm 3$  Ma to  $255 \pm 3$  Ma, providing some of the first numerical ages from the redbeds of western Oklahoma.

## TABLE OF CONTENTS

I. Introduction .....	1
II. Background .....	2
A. Tectonic Setting .....	2
B. Climatic Setting.....	4
B. Age constraints on the Cloud Chief .....	5
III. Methods.....	6
IV. Results .....	8
A. Sedimentary Facies .....	8
B. Paleocurrent measurements.....	15
C. Detrital Zircon Geochronology .....	15
D. Sr Isotope Analysis .....	15
V. Discussion.....	16
A. Sedimentary Facies Interpretations.....	16
B. Paleogeography .....	20
C. Stratigraphic Architecture .....	22
D. Provenance.....	23
E. Age and Relationships to Global Sea Level .....	24
VI. Conclusion.....	25
VII. Figures .....	27
References.....	42
Appendix.....	47

## LIST OF TABLES

Table 1. Strontium isotope values.....	38
--	----

## LIST OF FIGURES

Figure 1. Study area .....	27
Figure 2. Evaporite and siliciclastic facies .....	29
Figure 3. Channel outcrop and associated structures.....	31
Figure 4. Petrographic thin sections .....	32
Figure 5. Variegated mudstone facies.....	33
Figure 6. Variegated mudstone outcrop.....	34
Figure 7. Sandstone and mudstone facies .....	35
Figure 8. Ternary diagram .....	36
Figure 9. Regional paleocurrent.....	37
Figure 10. Probability density plot.....	38
Figure 11. Paleogeographic map.....	39
Figure 12. Stratigraphic architecture.....	40
Figure 13. Water Table level curve.....	41



## I. Introduction

With the goal of understanding Permian global climate, recent studies have painted a new picture of the environmental conditions present within the Permian rocks of the US midcontinent. Originally thought to have been deposited as a fluvial-deltaic system, many of these rocks are now thought to represent non-marine deposition dominated by eolian and lacustrine processes (Foster et al., 2014; Poland and Simms, 2012; Sweet et al., 2013). The mere presence of evaporites and inferred coeval relationships with sandstones in southwestern Oklahoma were initially utilized to suggest a marine origin for these units while sedimentological studies and whole rock geochemistry on the abundant evaporites suggest that these systems came from nonmarine sources (Benison and Goldstein, 2001; Fay, 1964; Foster et al., 2014). In addition, new depositional models suggest that the relative influence of fluvial processes seems to have been minimal, which supports a nonmarine interpretation (Foster et al., 2014; Poland and Simms, 2012; Sweet et al., 2013).

Only one numerical age has been determined for the entire Permian section (600-2000 m thick) of western Oklahoma— a mid-Leonardian age for the Blaine Formation based on strontium isotope ratios of its gypsum beds (Denison et al., 1998). Although some biostratigraphic constraints are available (rare fossils and burrows), they assign only a broad age to each stratigraphic unit (Johnson et al., 1989; G. Soreghan et al., 2012). These unknowns leave uncertainty on updated paleoclimate models concerning global tropical climate patterns. The purpose of this paper is to provide new ages and insights on the depositional conditions of one of these Permian units within the midcontinent of the US, the Cloud Chief Formation, a unit that has thick gypsum beds ideal for dating. We provide the first detailed facies analysis of the Cloud Chief as well as additional numerical ages for the

Permian rebeds of western Oklahoma and compliment this data with detrital zircon geochronology to determine the sources of the thick clastic units. Our results support recent work on some of the older Permian rebeds within the midcontinent, calling upon the presence of salinas, marine-sourced evaporites, and a major sediment source from the east.

## **II. Background**

### ***A. Tectonic Setting***

The Cloud Chief Formation was deposited over an area of  $\sim 12,500$  km<sup>2</sup> in west-central Oklahoma within the Anadarko basin (Fig. 1). A second group of outcrops is exposed in the Oklahoma Panhandle, but better, more accessible exposures and more laterally extensive outcrops are found within the west-central part of the state. The thickness of the Cloud Chief is about 3-39 m (10—130 ft) in southwestern Oklahoma, about 38—46 m (124—150 ft) in northwestern Oklahoma, and about 53—63 m (175—190 ft) in west-central Oklahoma (Becker, 1930; Evans, 1931; Fay, 1978).

The Anadarko basin is a foreland basin formed during the late Mississippian to Pennsylvanian. Its formation represents the compressional stage following the building of the supercontinent Pangaea in the late Paleozoic (Perry, 1989; Scotese et al., 1979). Most of the basin fill is sedimentary, with Pennsylvanian rocks composing the thickest section of about 4600 m (15,000 feet) (Sweet et al., 2013). Permian strata regionally dip to the southwest at extremely low angles (Fay, 1964). Rarely was the basin a topographic depression because, in general subsidence rates did not outpace sedimentation rates (Perry, 1989; G. Soreghan et al., 2012).

The basin is bounded to the south by the Wichita Mountains, formed from the same compressional forces during the Late Paleozoic. The Wichita Mountains are composed of Precambrian to Upper Ordovician rocks (Dott, 1952; Johnson et al., 1989). Presently, the uplift strikes approximately N60°W and has a maximum width of ~100 km (~60 mi) (Becker, 1930). The area first developed as an aulacogen filled with volcanic rocks during Precambrian rifting (Johnson et al., 1989). From the Cambrian to early Mississippian, the thermally-buoyant rift zone subsided, and a passive margin developed throughout the trough (Perry, 1989).

Sedimentary rocks, such as the Upper Cambrian Timbered Hills Group, Lower Ordovician Arbuckle Group, and Upper Devonian to Lower Mississippian Woodford Shale, unconformably overlie the Precambrian rift volcanic rocks (Dott, 1941; Johnson et al., 1989; Perry, 1989). The formation of the supercontinent Pangaea, with Laurentia (North America) colliding with Gondwana (South America/Africa continent), disrupted this tectonic setting through reverse reactivation of the Precambrian normal faults, creating thrust faults and consequently the Wichita and Arbuckle Mountains to the east. The Anadarko basin is separated from the Wichita Mountains by the Frontal thrust zone with about 12 km of buried relief (G. Soreghan et al., 2012; Ye et al., 1996).

Correlation of Permian units throughout the Midcontinent presents one of the biggest challenges in studying its regional history. The absence of definitive fossils, limited lateral extent of most marker beds, a highly weathered nature, and disagreements on formation boundaries are some of the largest barriers preventing robust unit correlations (Gould, 1926; Johnson et al., 1989). Two such correlations by Dott (1941) and Fay (1978) summarize multiple studies across the Permian of North Texas, Oklahoma, Kansas, and Nebraska. Based on their classifications, the Cloud Chief Formation in western Oklahoma is correlative

with the Whitehorse Group of North Texas, Seven Rivers Formation of New Mexico, and the Day Creek dolomite in Kansas. It is not exposed in Nebraska.

The Cloud Chief Formation is mostly composed of gypsum, fine-grained sandstones, and siltstones. The gypsum is most voluminous and thickest at the base, and gypsum volume and thickness decrease up section. Previous workers considered it to be Guadalupian (271-260 Ma) in age (Dott, 1941; Fay, 1978; Foster et al., 2014). Originally, Gould (1924) defined the Cloud Chief Formation to include the basal gypsum beds above the Weatherford Bed as well as the overlying sandstones and siltstones. The formation's lower and upper boundaries have been revised on multiple occasions, at one point demoted from a formation and termed 'Cloud Chief gypsum'. The rest of the sandstones and siltstones were grouped into the Quartermaster Formation along with the overlying resistant, reddish-brown Doxey Formation (Evans, 1931). Fay (1978) redefined the upper part of the Cloud Chief to include the sandstones and siltstones above the massive gypsum beds. This upper boundary is delineated by a thin layer of greenish-gray claystone that separates the lighter colored Cloud Chief from the darker colored Doxey Formation. The lower boundary of the Cloud Chief has also been a source of disagreement (Dott, 1941; Evans, 1931; Fay, 1964; Gould, 1924). For the purposes of this paper, we follow Green (1936), who defined the Cloud Chief Formation as the rocks stratigraphically above the Weatherford Bed of the Rush Springs Formation and below the reddish-brown Doxey Formation.

### ***B. Climatic Setting***

The late Paleozoic, in particular the Permo-Carboniferous witnessed extensive polar ice caps and records the greatest glaciation of the Phanerozoic (Crowell, 1983; Fielding et al., 2008; M. Soreghan et al., 2008). As Pangaea was gradually assembled, climate within the

interior of the continent (western North America) was increasingly arid and warm. This brought about the widespread development of eolian dunes (Poland and Simms, 2012). Rearranging of the continental crust due to the formation of Pangaea greatly influenced global atmospheric wind patterns, possibly impacting the source of some of the fine-grained Permian units in western Oklahoma (Foster et al., 2014; M. Soreghan et al., 2008). Strong evidence exists for a change in paleowind direction, from eastern (zonal) to a more northwestern (monsoonal) circulation (Foster et al., 2014; Heavens et al., 2015; Poland and Simms, 2012; M. Soreghan et al., 2002; M. Soreghan et al., 2008; Tabor and Montanez, 2002). Shifting of the Intertropical Convergence Zone (ITCZ) is called upon as a likely cause of the onset of the northwestern winds along tropical Pangaea. The change in atmospheric circulation was well-established by the earliest Permian (M. Soreghan et al., 2002; Tabor and Montanez, 2002).

By the end of the Lopingian (late Permian), Gondwanan ice sheets had completely melted, signaling a global change to a greenhouse (Montanez et al., 2007). The cause for the end of the glaciation is not well understood, although one hypothesis calls upon high atmospheric carbon dioxide values as an effective agent for glacial termination (Barron and Moore, 1994; Montanez et al., 2007). The transition from Paleozoic (Permian) to Mesozoic (Triassic) shows abundant evidence for an arid climate within the supercontinent interior (Barron and Moore, 1994).

### *C. Age Constraints on the Cloud Chief*

Spatial and temporal correlation among Permian units in the midcontinent of North America has historically been considered a significant problem for those studying these rocks, so much so that early workers referred to it as "The Permian problem" (Dott, 1941;

Evans, 1931; Fay, 1978; Gould, 1926). Because of mostly discontinuous marker beds, very few fossils, and similar lithologies, constant revision of these units' boundaries and ages were a common topic of debate among those who study them.

Many attempts were made to establish a robust stratigraphic column for these redbeds. Clifton (1930) suggested using trace malachite concentrations to correlate one of the gypsum beds in the Cloud Chief with those to the southwest. However, this method was not reliable because other gypsum and dolomite beds stratigraphically below and above also have copper compound traces (Clifton, 1930). Areal mapping of these units, such as that mentioned by Dott (1941), is not a reliable method as well due to their very similar lithologies. In addition, burial by the Tertiary Ogallala Formation prevents tracing the Cloud Chief to west Texas (Fay, 1978). More recently, Foster et al. (2014) used magnetostratigraphy to estimate an age for the Cloud Chief and other Permian units. Their results place the Cloud Chief as early Capitanian (~265 Ma) in age. Their results differ from those of Johnson et al. (1989) and Norton (1939), who placed the Cloud Chief at ~260 Ma and ~270 Ma, respectively. After more than 80 years of study, the Cloud Chief Formation's absolute age remains to be determined. In this study, we resolve this issue by providing the first numerical ages for the massive basal gypsum of the Cloud Chief Formation in western Oklahoma from Sr isotope ratios of the Weatherford Bed and the basal gypsum beds of the Cloud Chief.

### **III. Methods**

Thin section analysis, detrital zircon geochronology, and Sr isotope analysis were conducted on hand samples collected in the field and an 18 m (56 ft) long core taken from the Barnitz Creek dam near Putnam, OK (Fig. 1). The Cheyenne NW quadrangle within

Roger Mills County was mapped at the 1:24000 scale. Extensive Cloud Chief Formation outcrops occur within this band.

Thin sections were used to characterize the degree of maturity, grain composition, and other textural characteristics of six siliciclastic samples. Sr isotopes were measured to identify the depositional environment of the evaporite (gypsum) facies and their ages. Paleocurrent measurements were summarized using Stereonet 9 (Allmendinger et al., 2012; Cardozo and Allmendinger, 2013). To determine the provenance of the Cloud Chief Formation, detrital zircon ages from one of the siliciclastic subfacies, the white very fine sandstones, were measured. Other units were attempted but contained too few ( $n = <10$ ) zircons for a robust analysis.

Detrital zircons were separated from the channelized very fine sandstone facies using standard crushing, heavy liquid, and magnetic separation techniques. The resulting zircon grains were randomly selected, mounted on epoxy resin disks, and polished for U-Pb analysis using laser ablation multi collector inductively coupled plasma mass spectrometry (LA-MC-ICP-MS) at the University of California, Santa Barbara. The laboratory contains a Nu Plasma MC-ICP-MS, coupled with a Photon Machines Excite ArF Excimer laser ablation system. Each analysis lasted for 20 seconds, with a repetition rate of 4 Hz and laser fluency of  $\sim 1 \text{ J/cm}^2$ . The 91500 zircon (Wiedenbeck, 1995) was used as the primary reference material, while GJ1 (Jackson et al., 2004) and Plesovice (Slama et al., 2008) were used for quality control. Weighted mean ages were within 1% of their reported values, with  $2\sigma$  uncertainties in the unknown ages. A U-Pb Concordia diagram was created to check for discordance and a probability density graph was plotted to determine zircon age groupings. The density graph utilized the  $^{207}\text{Pb}/^{206}\text{Pb}$  ratio for ages  $>1200 \text{ Ma}$  and the  $^{207}\text{Pb}$ -corrected  $^{206}\text{Pb}/^{238}\text{U}$  ratio for ages  $<1200 \text{ Ma}$ .

The  $^{87}\text{Sr}/^{86}\text{Sr}$  analyses were conducted on six samples, producing 7 to 16 mg of powdered gypsum each, using a Sector-54 Thermal Ionization Mass Spectrometer (TIMS) at the University of Kansas Isotope Geochemistry Laboratories. Samples were dissolved in 3.5 N  $\text{HNO}_3$  and enriched with a pure  $^{84}\text{Sr}$  tracer. Strontium-spec resin within ion-exchange columns was used to isolate strontium from other cations. The measured isotope ratios were fractionation corrected to  $^{86}\text{Sr}/^{88}\text{Sr} = 0.1194$  and were reported with respect to a value of 0.710250 for NBS987. The NBS987 was repeatedly determined to calculate and maintain the precision of each  $^{87}\text{Sr}/^{86}\text{Sr}$  measurement ( $\pm 0.000015$ ).

## **IV. Results**

### ***A. Sedimentary Facies***

Nine sedimentary facies were identified within the Cloud Chief Formation. Most of the unit is composed of very fine-grained sandstones and siltstones, with gypsum and dolomite as the major evaporite and carbonate facies, respectively. In Beckham County (Fig. 1), only the silty claystone and the topmost part of the channelized very fine sandstone facies are exposed. On the other hand, only the basal Cloud Chief is exposed in southeastern Washita County (Fig. 1).

Thin sections were taken from six samples, the channelized very fine sandstones, thickly-bedded sandstones, laminated sandstones, siltstones, silty claystones, and gypsiferous sandstones. In general, they exhibit well-rounded, well-sorted grains. Iron oxide and clay cements ranged from extremely well-covered to absent. The Cloud Chief Formation is composed of 72-88% rounded to well-rounded quartz grains, the most abundant and ubiquitous constituents.



## 1. Gypsum and dolomite

Massive thick-bedded gypsum occurs as beds typically 1-2 m in thickness but as great as 4 m within the basal part of the Cloud Chief. Massive gypsum beds are thickest, most abundant, and most laterally extensive along the southern portion of the study area, and occur less commonly and are less extensive within the northernmost areas. Most of the gypsum within the formation pinches out north of Camargo (Fig. 1; [Evans, 1931](#)). The gypsum beds are mostly white to pinkish-white (Fig. 2a). Alabaster is the most common texture, with some samples displaying a selenite (glassy) texture. Recrystallization zones, most commonly consisting of celestite crystals, are present in some of the gypsum outcrops. Only rarely is chickenwire texture with shales found. Throughout the study area, an interbedded sandstone-siltstone layer with varying thickness (~3m to 15 m) separates the Weatherford Bed from the lowest massive gypsum bed of the Cloud Chief. To the north, the massive gypsum beds grade laterally into sandstones, siltstones, and shales.

Thin (10-20 cm thick), resistant ledges of dolomite occur locally, usually in close association with gypsum but in isolation as well. Dolomite beds are normally silty to sandy, contain burrows, and occasionally oolitic (Fig. 2b, c). Unlike the thick, massive gypsum, dolomite beds are normally only a few centimeters thick and are most common within the lower middle part of the Cloud Chief. Basinward, dolomite beds laterally grade into gypsum ([Clifton, 1930](#)).

## 2. Gypsiferous sandstone

Between beds of massive gypsum but below the fluvial channels is a facies that displays a mixed evaporite/clastic system. This resistant facies is found only in the basal Cloud Chief.

It typically exhibits gypsum crystal growth within a massive sandstone matrix but sometimes occurs as small-scale channel-like features within parallel laminated sandstones (Fig. 2f-g).

Aside from the massive gypsum facies, the gypsiferous fine sandstones have the highest gypsum content of all the facies in the Cloud Chief. Alabaster gypsum is the most common texture observed and the most abundant cement. Feldspar grains are mostly tabular prismatic and sometimes show albite twinning. Quartz grains are subrounded to rounded and have normal extinction (Fig. 4a). The approximate percentages of the framework grains are as follows: 76% quartz, 9% feldspars, 9% muscovite, and 2% biotite and 4% opaques (Fig. 8).

### 3. Channelized very fine sandstone

This facies includes two subfacies: brown fine sandstone and very fine white sandstone. Their distinctive characteristic is their channel geometry. These sandstones usually directly overlie the massive basal gypsum. Brown fine sandstones are resistant, ledge-forming, well-sorted, and display convoluted bedding (Fig. 3). They are relatively thick beds, about a meter thick on average, and sometimes exhibit climbing ripples, trough-cross bedding, scour-and-fill, and rip-up clasts (Fig. 3; Fig. 7b; Fig. 7f). Beds of this facies are commonly overprinted by satin-spar gypsum veins within both bedding planes and fractures within these sandstones. These gypsum fracture fills are more abundant along the northern part of the study area.

The other subfacies, very fine white sandstones, are commonly structureless, well-sorted, poorly consolidated, and their beds have wavy lower and upper boundaries (Fig. 2e). This facies is locally gypsiferous and usually interbedded with the brown fine sandstone mentioned above. This subfacies also exhibits channelized geometry that is more subtle than that of the other subfacies.

Grains of both subfacies are generally well-sorted and rounded, with occasional subangular grains, and have a clay mineral matrix. Quartz grains are mostly subangular to rounded. Feldspar grains, most commonly orthoclase, are tabular prismatic with rare tartan plaid twinning. Cements are mainly composed of iron oxides and calcite. A few small, euhedral, tabular prismatic, highly birefringent muscovite grains are also present. Opaques and isotropic minerals are less common. Laminae within this facies vary in cement and matrix content. Some laminae are clay-rich, displaying a grey cloudy appearance, while some are thickly covered with iron oxides making the grains indistinguishable. Coarser-grained sandstones typically have less porosity and cement cover is not as extensive as the finer-grained sandstones (Fig. 4b). The rocks contain approximately 88% quartz, 5% orthoclase and microcline, 2% muscovite, 3% opaques (zircons and hematite), and 2% plagioclase (Fig. 8).

#### 4. Siltstone

Siltstone beds are usually interbedded with the channelized units. These very fine siltstones are brown or white in color and usually massive, but can display planar laminations (Fig. 2d). This facies sometimes exhibits ripple cross laminations and sparsely climbing ripples. This facies is geographically extensive and stratigraphically common. Near the top of the Cloud Chief, satin-spar gypsum fills fractures within this facies.

Quartz intergrowths are commonly found on the coarser grains. Much like the other facies, the coarser, more rounded grains have less iron oxide cement coatings than the finer grains (Fig. 4c). Finer quartz grains tend to be more euhedral than their coarser counterparts. Similar to the channelized very fine sandstone facies, orthoclase is the most common feldspar. A few prismatic biotite grains were observed, though in lesser abundance than

within the thickly-bedded sandstone facies. Of the framework grains, the rock contains approximately 75% quartz, 13% orthoclase, 6% muscovite, 4% opaques, and 2% plagioclase (Fig. 8).

#### 5. Variegated mudstone

Along the northern portion of the study area, the presence of multi-colored mudstones point to an environment not indicated in the previous facies. One particular feature this facies exhibits is the presence of vertical color gradients in outcrops, beginning with reddish-white, to brown, to white (Fig. 5a). Structures within this facies include thin (<5 cm) calcite beds, diagenetic halos, granular texture, and slickenlines (Fig. 5b-e). Immediately above most variegated mudstone layers are relatively thick (0.5-1.5 m) beds of thickly-bedded sandstones, a facies discussed below (Fig. 6).

#### 6. Thickly-bedded sandstone

These well-sorted, very fine sandstones occur as resistant, thick beds about a meter thick. Many of these sandstones contain diagenetic halos and gypsum. The structureless subfacies is typically found in the basal to middle Cloud Chief and tends to exhibit little variation in bed thickness throughout an outcrop (Fig. 7a). In addition, these sandstones are found directly overlying variegated mudstones, exhibiting a sharp lower boundary (Fig. 6).

The thickly-bedded sandstone facies contains abundant quartz and muscovite. Quartz grains are subrounded to well-rounded while muscovite and biotite grains are prismatic and aligned with the laminae length. Calcite cement is present in some areas, although non-cemented grains are also observed. Iron oxide cement and a clay matrix sometimes completely coat the quartz grains. No feldspar was observed, although it is possible that they

were replaced by clay minerals. This facies contains approximately 86% quartz, 7% muscovite, and 7% opaques (Fig. 8).

In one outcrop, this facies exhibited fine lamination. When viewed under the microscope, the color difference was found to reflect the grain size and degree of iron oxide cementing. White laminae are composed of larger grains with little to no iron oxide cement, while the opposite is true for the red laminae (Fig. 4d). In addition to iron oxides, calcite cement is also ubiquitous. However, cementation by calcite does not vary as a function of grain size; both types are affected equally. Coarser and finer laminae commonly pinch-out. Quartz grains are angular to rounded. Similar to within the thickly-bedded sandstone facies, biotites are aligned with the length of the laminae. No feldspars were observed. Based on the relative mineral assemblages and proportions, this rock is part of the thickly-bedded sandstone facies. It contains approximately 86% quartz, 7% opaques, 6% muscovite, and 1% biotite and is a product of a recycled orogen environment (Fig. 8).

#### 7. Ripple-cross laminated very fine sandstone

These well-sorted sandstones are most common in the northern half of the study area (Fig. 7c). The highest concentration of this facies are found near the stratigraphic top of the Cloud Chief Formation, although they are also found interbedded with the channelized sandstone facies. Climbing ripples are also present and the beds that contain them are sometimes channelized. Most paleocurrent measurements were taken from this facies.

#### 8. Interbedded sandstone and mudstone

Stratigraphically above the ripple-cross laminated sandstones are tabular, fining-upward, decimeter-thick interbedded sandstones and mudstones (Fig. 7d). The sandstone beds are generally thicker (tens of cm) than the mudstone beds (<10 cm on average). One instance of

a Bouma-like sequence was observed and oscillation ripples are locally present within the sandstone beds. Occasionally, a hummocky sequence is seen within this facies (Fig. 7e). Much like the ripple-cross laminated sandstones, this facies is found most commonly along the northern portions of the study area and near the stratigraphic top of the Cloud Chief.

#### 9. Silty claystone

This facies underlies the contact between the Cloud Chief and the overlying Doxey Formation. These silty claystones generally lack gypsum, except for rare diagenetic satin-spar gypsum-filled fractures north and west of the study area. They are usually structureless, dark brown in color and widespread throughout the study area. A thin band of greenish claystone a few centimeters thick is present within beds of this facies typically 20 cm below the contact with the Doxey Formation (Fig. 2h).

This facies has a very fine, clayey matrix and abundant floating muscovite, quartz, feldspars and less commonly biotite grains. Most of the coarse quartz grains are well-sorted, subangular to rounded. Floating feldspar grains are mostly angular, tabular prismatic, and rarely exhibit Carlsbad twinning. Most feldspars have high first-order level birefringence, displaying dark pink to orange colors. Zircon and hematite grains are the most common well-rounded opaque minerals. Iron oxide and gray clay minerals are the most common cements within this facies, affecting both individual grains and rock fragments. Some of these clay minerals are surrounded by a thick layer of iron oxide cement. Less porous areas with coarser grains typically have less cement around them. Of the grains larger than 100  $\mu\text{m}$ , this facies contains approximately 72% quartz, 13% feldspars, 5% muscovite, 4% opaques, 4% biotite, and 2% rock fragments larger than 150  $\mu\text{m}$  (Fig. 8).

### ***B. Paleocurrent measurements***

Sixty-one paleocurrent measurements were taken from ripple-cross laminations and less frequently trough cross bedding. Limited exposures and their highly weathered nature restricted the number of sedimentary structures to take measurements from within the Cloud Chief. The mean of the paleocurrent measurements is  $8.3^{\circ}$  (Fig. 9). A radial pattern with a general northward trend is observed within the overall distribution.

### ***C. Detrital Zircon Geochronology***

Detrital zircons were isolated from the very fine white sandstone subfacies of the channelized very fine sandstone facies. Too few ( $n = <10$ ) zircon grains for a robust analysis were found in the other facies. All resultant ages fall within error of or on the Concordia curve (see Appendix). Three major groupings are found within the probability density graph (Fig. 10). These ages are 920-1360 Ma (51%), 1520-2080 Ma (25%), and 2640-2800 Ma (24%). No zircons with ages of ~500-600 Ma were found.

### ***D. Sr Isotope Analysis***

Sr isotope ratios were measured from the massive gypsum of the basal to lower middle Cloud Chief. Gypsum is essentially an impermeable rock and considered to be a good seal for trapping fluids (Denison et al., 1998). As such, it tends to resist isotope exchanges with pore waters, and thus retains its original strontium isotope ratios. In particular, the Permian redbeds of the midcontinent were subject to minimal burial (<1 km) (Carter et al., 1998; Foster et al., 2014; Giles et al., 2013; Hemmerich and Kelley, 2000); thus, not subject to intense pressure and cementation or flushing with deep basinal brines. Hydration of anhydrite back to gypsum is also unlikely to alter the original ratios (Denison et al., 1998). A mole of anhydrite usually contains 13 000 to 15 000 micrograms of strontium, compared to

two moles of rainwater, which contain 0.1 to 0.5 micrograms (Denison et al., 1998). In this case, the system itself acts as a buffer to changes in strontium ratios from foreign waters.

Strontium isotope ratios from the Weatherford Gypsum Bed and five gypsum beds from the Cloud Chief all suggest a marine source based on the strontium ratio of the late Permian seawater and thus provide only the second set of numerical ages for the Permian redbeds of western Oklahoma (Table 1). According to the Sr isotope timescale of Denison et al. (1994), our new ages range from  $262 \pm 3$  Ma to  $255 \pm 3$  Ma. These ages fall within the Lopingian Age based on the 2012 timescale of the Geological Society of America (GSA), the Leonardian Age based on the timescale of Denison et al. (1994), and the Kungurian-Roadian Age based on the timescale of Korte et al. (2006). For consistency, we use GSA's 2012 timescale throughout this paper. The oldest age of  $\sim 262$  Ma, as expected, was taken from the Weatherford Gypsum Bed (Table 1). Our results are similar to those found by Foster et al. (2014). They used magnetostratigraphy to analyze multiple Permian redbeds in western Oklahoma and assigned an age of younger than  $\sim 266$  Ma for the equivalent of the Cloud Chief in south Central Kansas, the Whitehorse and Big Basin formations.

## **V. Discussion**

### ***A. Sedimentary Facies Interpretations***

#### **1. Sabkha assemblage**

Based on the marine strontium isotope values, the extensive, thick, massive basal gypsum facies of the Cloud Chief is interpreted to represent a marine sabkha (Fig. 11). Chickenwire textures, though rare, also support a sabkha interpretation (Giles et al., 2013). The lateral extent of the basal gypsum constrains the minimum area of the ancient sabkha



that formed adjacent to the near-buried Wichita-Amarillo Mountains immediately to the south (Fig. 1).

The dolomite beds are also interpreted to have been deposited within a sabkha. Ooids and burrows within these dolomitic siltstones provide additional support for a sabkha interpretation. The presence of siliciclastic rocks interbedded with these rare, thin dolomite beds suggests that sediment flux continued even during periods when the sabkha was flooded by marine waters (Foster et al., 2014). The gypsiferous sandstones between the massive gypsum beds and the other siliciclastic facies assemblage are interpreted to be relatively protected, intertidal sandflat deposits based on gypsum grain growth within the siliciclastics (Fig. 2f), their fine-grained nature, and channel-like structures within laminated sandstones (Fig. 2g).

## 2. Fluvial assemblage

The widespread channelized very fine sandstones are interpreted as fluvial deposits. This interpretation is based on their channelized nature, current ripples, and absence of marine indicators. Evidence of climbing ripples suggests areas of locally high sediment supply. In addition, the absence of abundant trough cross-bedding, fining upwards sequences, and lateral accretion structures suggest deposition within an anastomosing river system rather than a meandering fluvial system. Modern anastomosing river systems are characterized by high mud proportions, low stream power and gradient profiles, features that fit the environments proposed for the western tropical Pangaea during the Lopingian (Foster et al., 2014; Nanson and Croke, 1992).

The close association between the channelized very fine sandstones and the siltstone facies suggest they formed under similar depositional conditions. The structureless siltstone

subfacies indicates suspension load deposition, likely within the floodplains of the anastomosing fluvial systems characterized by the channelized very fine sandstones (Fig. 11). Occasionally, this facies exhibit small, bumpy, popcorn-like structures, a texture also seen in the siltstone facies of the Wellington Formation (Giles et al., 2013). Due to close morphological similarity, we interpret these features to be from the precipitation of salt crusts in the highly permeable siltstones. These structures most likely formed from evaporation of groundwater brought to the surface via capillary action as a result of aridity.

The floodplain deposits were overprinted by pedogenesis, represented by the variegated mudstones facies. Evidence for paleosols within the variegated mudstones include granular texture, slickenlines, diagenetic halos, and calcitic beds (Fig. 5b-e). The noneffervescent white color at the topmost portion of these mudstones suggests abundance of gypsum (Fig. 5a). Granular texture is considered to be synonymous with hackly texture and, in conjunction with slickenlines, indicate the presence of swelling clays within these mudstones (Retallack, 1988). The presence of organic matter is indicated by widespread diagenetic halos of locally reducing conditions. The thin calcitic beds are interpreted to be B<sub>k</sub> horizons, which result from accumulation of calcite within the B horizon (Retallack, 1988). Based on Retallack's classification, we interpret these paleosols to be vertisols and aridisols. Based on a pedogenetic overprint, this facies is cited as strong evidence that the deposits in the later stages of the Cloud Chief Formation experienced periods of desiccation.

The well-sorted nature of the massive sandstone subfacies within the thickly-bedded sandstone facies and their placement immediately above variegated mudstones suggest burial rapid enough to preserve the pedogenic structures within the mudstones. As such, this subfacies within the thickly-bedded sandstone facies is interpreted to be crevasse splay deposits (Fig. 11). Sudden deposition of fine-grained sediments from a levee breach could

easily bury terrestrial soils developed within the adjacent floodplains of a river. Rapid deposition of these sandstones is also supported by the general absence of sedimentary structure within this subfacies.

### 3. Terminal splay assemblage

The ripple-cross laminated sandstone facies is interpreted as proximal terminal splay deposits. Increased abundance of ripple-cross laminations, but more importantly climbing ripples, support rapid deposition of this facies. Proximal terminal splay deposits are generally marked by relatively thick beds (>10 cm) of abundant ripple-cross laminations (Fisher et al., 2008). This interpretation fits its stratigraphic position within the Cloud Chief system and its association with the interbedded sandstone and mudstone facies. The absence of deltaic characteristics (e.g. coarsening upward sequence, prodelta deposits) argues against a mouthbar interpretation. We suggest that the ancient fluvial systems feed terminal splays and deposited fine-grained sediments across a subaerial to mudflat/shallow lake/marine sabkha environment, whose representative facies (silty claystone) is discussed below (Fig. 11). For simplicity, we will use the term ‘mudflat’ to denote the latter assemblage.

The proximity of the interbedded sandstones and mudstones facies to the ripple-cross laminated facies both laterally and vertically suggests that the former has a similar, if not closely associated, depositional setting. The absence of current ripples and cross-bedding provide evidence that this facies is dominated by suspension processes, while the presence of oscillation ripples suggests areas of wave action. Hummocky sequences found within this facies are interpreted to be tempestites deposited during storm events (Fig. 13; Snedden et al., 1988). Based on the relatively thin and massive nature of the beds (10-60 cm), the interbedding of sandstones and mudstones, presence of storm deposit sequences and

oscillation ripples, and the absence of current ripples, this facies is interpreted to represent distal terminal splay deposits interbedded with a mudflat assemblage. The presence of mudstones represents waning flow as waters move farther away from the main channels and flow transitions into an unconfined flow regime (Fig. 11; Fisher et al., 2008; Treece, 2007). As fluvial channels emptied into a low-lying basin to the north, the area was marked by either distal splay lobes when dry or shallow water mudflats when wet. During prolonged wet periods, storms and standing bodies of water allowed tempestites and oscillation ripples to form.

#### 4. Mudflat assemblage

The absence of defining structures and the fine-grained nature of the silty claystone facies suggest deposition in a relatively quiet and stable setting. In addition, the presence of thin (~20 cm) greenish beds along its topmost portion points to a reducing environment. Based on these characteristics, the silty claystone facies is interpreted as mudflat deposits indicating a rise in local base levels during the end of Cloud Chief times and the beginning of Doxey Formation deposition. These silty claystones, including the basal Doxey Formation, were found to be radioactive and contain uranium (Al-Shaieb et al., 1977; Fay, 1964; Finch, 1967). The presence of uranium within these silty claystones, the greenish-gray siltstone beds and sharp bases within this facies also suggest a mudflat depositional environment.

#### ***B. Paleogeography***

A paleogeographic and depositional model for western Oklahoma during the deposition of the Cloud Chief Formation is shown in Figure 11. The massive gypsum beds are concentrated in the south and become thinner to the north. We interpret this as the outline of

maximum accommodation within the Anadarko basin allowing thick evaporites to precipitate during the initial stages of Cloud Chief deposition. As the accommodation within the Anadarko basin decreased, western Oklahoma was dominated by fluvial systems flowing from the south and becoming less confined to the north (Fig. 11). Similar to the massive gypsum, the river channels generally become thinner to the north in proportion to their distance from the Wichita uplift (Fig. 1; Fig. 11). On average, channel thicknesses range from 20-30 cm in Sayre and Weatherford, thicken to 70-90 cm in Cheyenne and near Foss Lake, and thin to 15-25 cm in northern Roger Mills and Dewey Counties (Fig. 1). Their floodplains dominantly fall into Class C2b of Nanson and Croke (1992), which are low-gradient, low-energy floodplains, characterized by anastomosing rivers. Class C2b systems are also characterized by sparse vegetation and the presence of vertisols, features that fit the Cloud Chief.

Nichols and Fisher (2007) introduced a term for a fluvial system that has a distal zone that varies depending on the regional climate. A 'fluvial distributary system' is characterized by a decrease in flow discharge from proximal to distal regions and could terminate at a dry alluvial plain, terminal splays, or a lake delta. Here, we argue that the Cloud Chief fluvial system falls into this category. Notable characteristics of a fluvial distributary system such as thin, horizontally stratified sand sheets in the distal zone (interbedded sandstone and siltstone facies in this study), absence of incised channel fill, and a radial paleocurrent pattern are all observed within the deposits of the Cloud Chief Formation. We argue that the Cloud Chief is a fluvial distributary system with terminal splays in its distal zone except for times when the sabkha is flooded by marine waters.

### *C. Stratigraphic Architecture*

The measured cross-sections and observed locations were compiled to create a stratigraphic model for the Cloud Chief. The surface section line runs from the SE (Washita County) to the NW (Roger Mills County) (Fig. 1). Within the study area, the Cloud Chief is thickest (~60 m) around the town of Cheyenne and thinnest (< 20-30 m) around the town of Sayre and northern Roger Mills County (Fig. 1).

The Weatherford Bed and the massive basal gypsum beds of the Cloud Chief, are thickest to the south and pinch out to the north, where they grade into the channelized very fine sandstones or thickly-bedded sandstones (Fig. 12). The latter two facies compose the thickest portion of the Cloud Chief and the most common facies occurring in outcrops. The channelized very fine sandstones laterally grade into ripple-cross laminated sandstones, which grade into interbedded sandstones and mudstones basinward (Fig. 12). Overlying these facies is the sheet-like silty claystone facies, the stratigraphic top of the Cloud Chief (Fig. 12).

The succession of facies within the Cloud Chief reflects the evolution of the Anadarko basin. As compressional forces caused by the formation of Pangaea relaxed during the mid to late Permian, subsidence of the Anadarko basin slowed (G. Soreghan et al., 2012). Accommodation within the basin during the early to middle Permian allowed marine waters to accumulate and precipitate thick beds of evaporites. Nonetheless, the replacement of evaporites by conformable channel fills higher within the Cloud Chief is evidence that accommodation within the Anadarko basin was filled by late Cloud Chief times. As such, fluvial systems from the south dominated the landscape as the basin transitioned from an underfilled to an overfilled basin (Carroll and Bohacs, 1999). The presence of large unconformities above the Cloud Chief, such as those between it and the Cretaceous Kiowa

Formation or the Tertiary Ogallala Formation, also suggest that accommodation within the Anadarko basin was filled and hence subsidence had ceased (Johnson et al., 1989). We propose that the Cloud Chief Formation marks the last of the Anadarko basin fill as a consequence of the cessation of basinal compression.

#### *D. Provenance*

A high-density crustal mafic load underneath the Wichita Mountains is thought to have been emplaced during the time when the Anadarko basin was part of an aulacogen during the early Paleozoic, ultimately causing load-induced subsidence and burial of the uplift by Pennsylvanian and Permian sedimentary strata (G. Soreghan et al., 2008; G. Soreghan et al., 2012; Soreghan and Soreghan, 2013). As a consequence of subsidence, the Wichita uplift was not a major source of sediments for the Permian redbeds in Oklahoma. Our paleocurrent measurements do point to a source south of the study area, but they provide local flow directions, not the provenance. The absence of zircons with ages of Wichita Mountains basement (~535 Ma) reinforce the idea of burial of the Wichitas (Fig. 10).

In addition, our results support earlier work conducted on the Permian Dog Creek Formation and the Permian Wellington Formation within western Oklahoma (Foster et al., 2014; Giles et al., 2013). Their results yielded two major age groups that correspond to known ages of the Grenville basement and early Paleozoic terranes. The three major age groupings of the zircons within the Cloud Chief are similar to those found for other Permian units in Oklahoma. According to M. Soreghan et al. (2008), our age groupings correspond to the Grenville basement, the Yavapai-Mazatzal basement, and cratonic Laurentia (Fig. 10). Much of Laurentia was covered with sediments during the late Paleozoic, therefore this age grouping most likely represents reworked zircons (M.Soreghan et al., 2008). Based on this,

two major sources are identified for the deposits of the Cloud Chief Formation, the Ouachita Mountains (Grenville age) and the western Ancestral Rockies (Yavapai-Mazatzal age).

Based on our detrital zircon results, most of Cloud Chief is composed of sediments from the Ouachitas with minor contributions from the western Ancestral Rockies. These uplifts are to the southeast and west of the Anadarko basin, respectively.

Two sources for the Cloud Chief may reflect shifting in the ITCZ allowing monsoonal circulation to contribute to sediment flux to the Anadarko basin from both the east and the west (M. Soreghan et al., 2002; Tabor and Montanez, 2002). During the Permian, large Oklahoma streams originated from the southeast and flowed northwest (Fay, 1964). Fluvial systems from the Ouachitas and the western Ancestral Rockies reached the southern Anadarko basin, which served as a sink for the sediments reworked to become Cloud Chief deposits (Soreghan and Soreghan, 2013). Fluvial systems originating from the south adjacent to the buried Wichita Mountains then transported these sediments north to their present location.

#### *E. Age and Relationships to Global Sea Level*

All strontium isotope ratios point to a dominantly marine origin imprint, putting the Cloud Chief within the Lopingian Epoch of the Late Permian based on the 2012 Geological Society of America (GSA) Geologic Time Scale (Table 1; Fig. 13). The data suggest the presence of a low-lying sabkha adjacent to the open ocean, episodically flooded by marine waters (Fig. 11). This conclusion is similar to interpretations of gypsum beds within the older Blaine Formation of western Oklahoma (Denison et al., 1998). The Blaine Formation's gypsum beds were deposited within a salina with dominantly marine imprint for the lower gypsum beds and increasingly continental source signal for the upper gypsum (Denison et



al., 1998). Other strontium isotope measurements from the San Andres Formation in the Texas panhandle (El Reno Group correlative) also suggest marine-sourced waters (Foster et al., 2014; Hovorka et al., 1993). Our findings support a marine-influenced sabkha, providing an improved understanding of the Permian evaporites of the midcontinent.

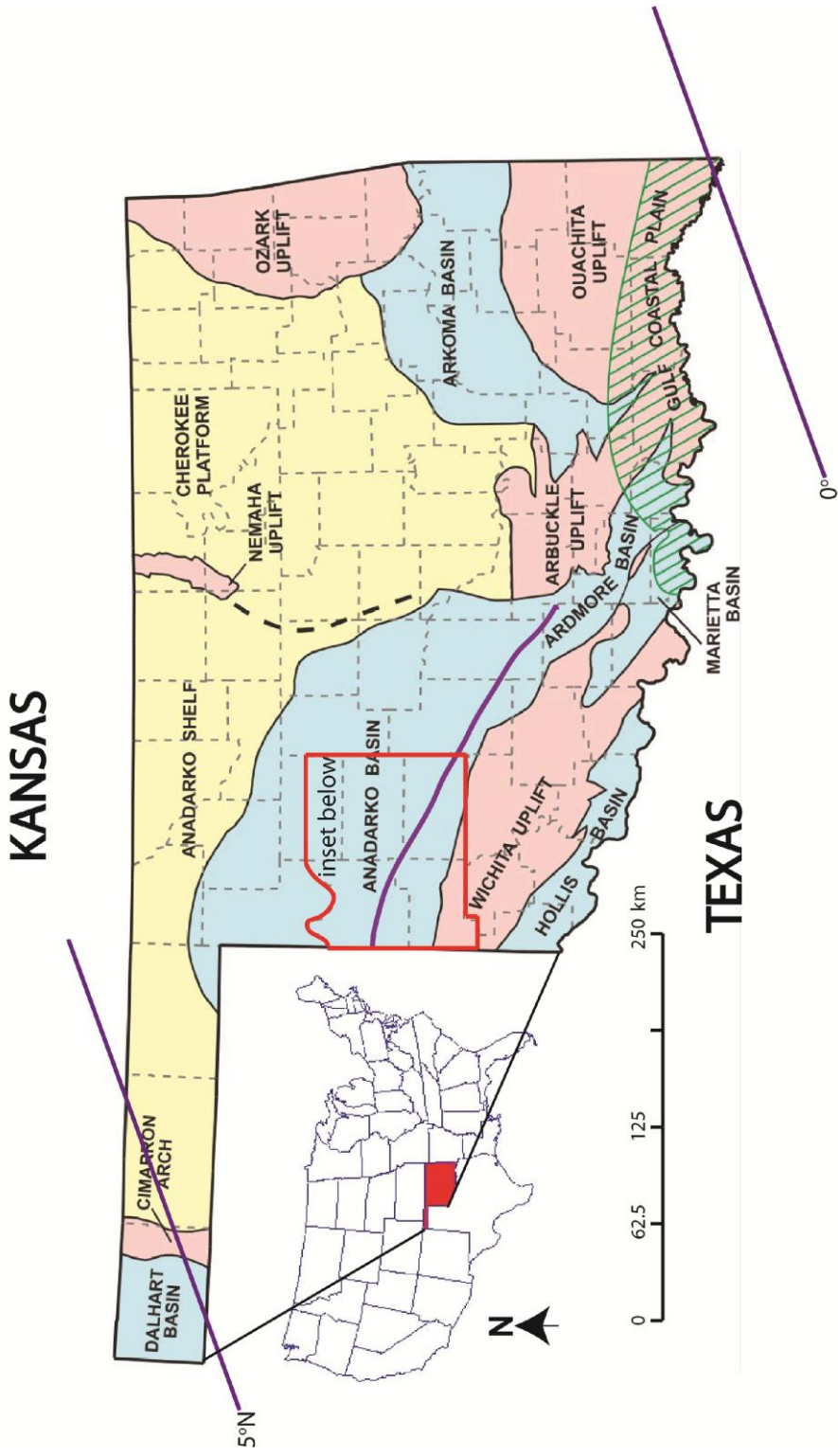
A marine encroachment over the eolian erg of the Rush Springs Formation is attributed to the rise in sea levels as a consequence of the Gondwanan deglaciation during the late Permian to early Triassic (Fig. 13; Crowell, 1978; Fielding et al., 2008; Montanez et al., 2007; Poland and Simms, 2012; Poulsen et al., 2007; Ross and Ross, 1988; Ruban, 2015; Veevers and Powell, 1987). As creation of accommodation within the Anadarko basin stopped and the basin became overfilled, fluvial channels, terminal splays, and paleosols filled the basin, but episodic marine encroachment continued as eustatic sea levels continued to rise (Fig. 11; Fig. 13). Unlike the older marine waters that precipitated the massive gypsum beds, waters from these encroachments were relatively ephemeral and thus precipitated much thinner and lenticular gypsum (Fig. 11). The overlying Doxey Formation is composed of shales with prevalent oscillation ripples most likely deposited in a subaqueous environment when either sea level was high enough to flood the overfilled Anadarko basin or a large lake formed (Fig. 13).

## **VI. Conclusion**

The Cloud Chief Formation of western Oklahoma was deposited as a marginal-marine sabkha system. The lower gypsum beds within the Cloud Chief were marine in origin and yield ages that range from  $262 \pm 3$  Ma to  $255 \pm 3$  Ma. These ages are only the second set of numerical ages for the Permian rocks of western Oklahoma. The upper Cloud Chief marks the progradation of a series of arid-land anastomosing rivers onto mudflats forming terminal

splays to the north. The rivers flowed from the south into the Anadarko basin but the detrital zircons suggest the ultimate source of that sediment was from the Ouachitas of southeastern Oklahoma with a minor contribution from the western Ancestral Rockies. These river deposits mark the last deposition within the Anadarko basin as all accommodation was filled after subsidence ended.

VII. Figures



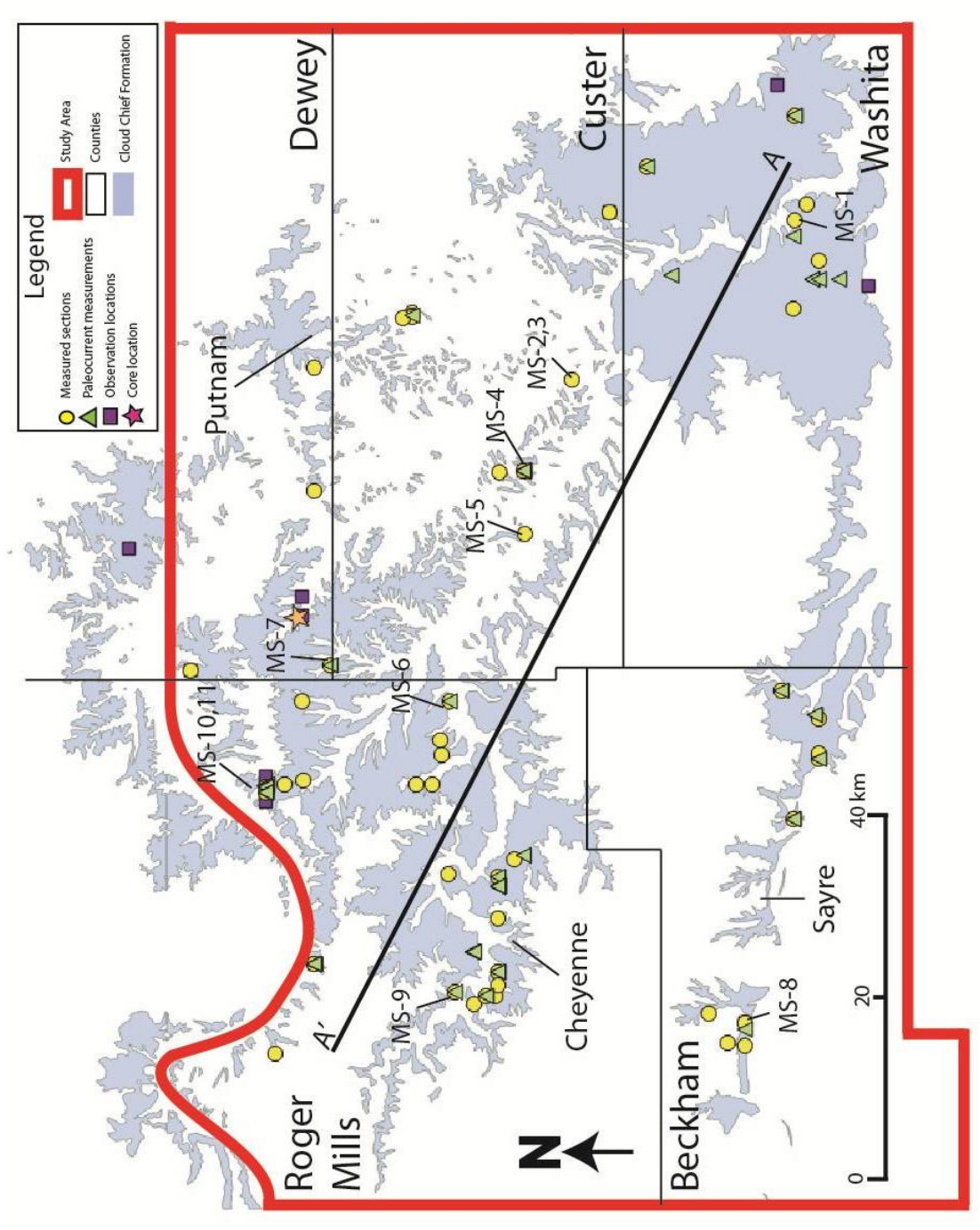
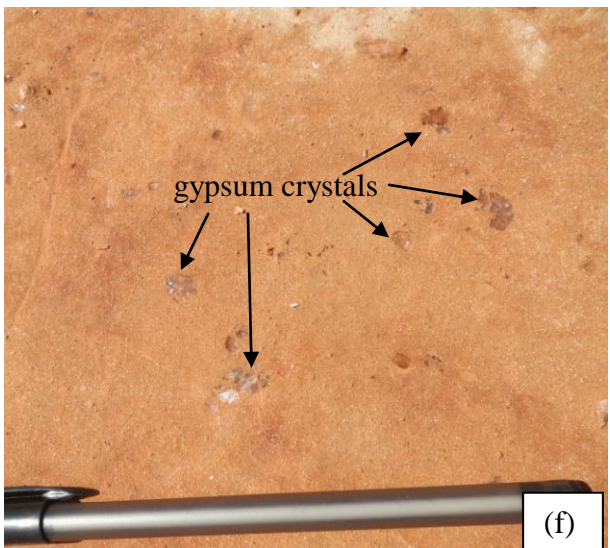
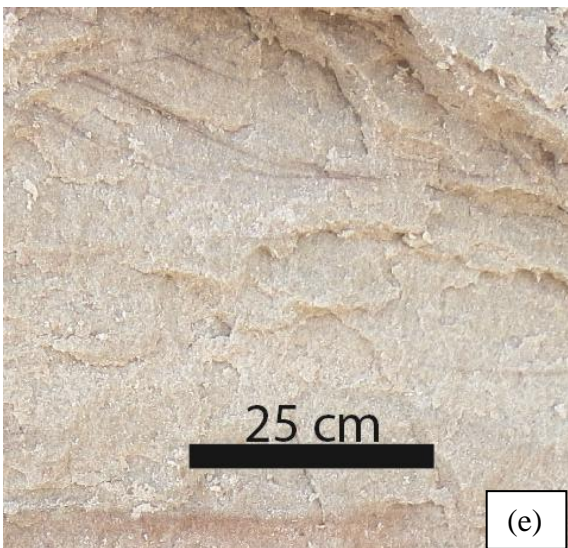
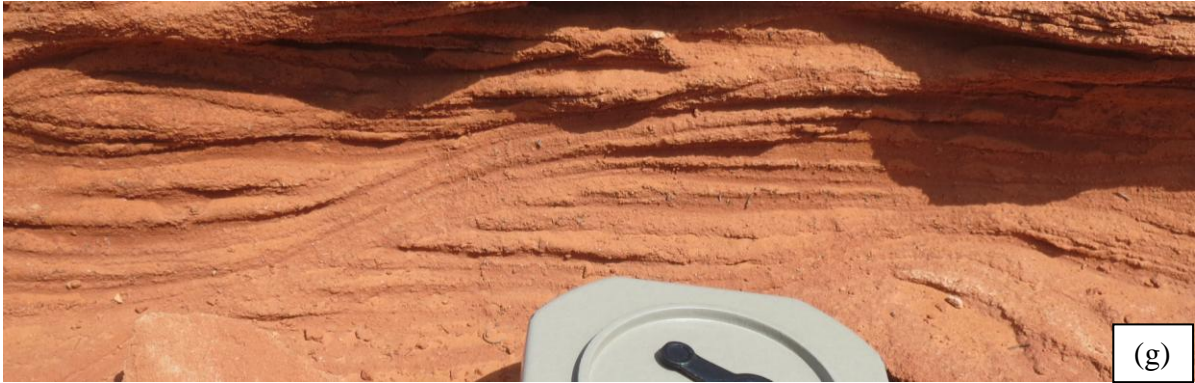
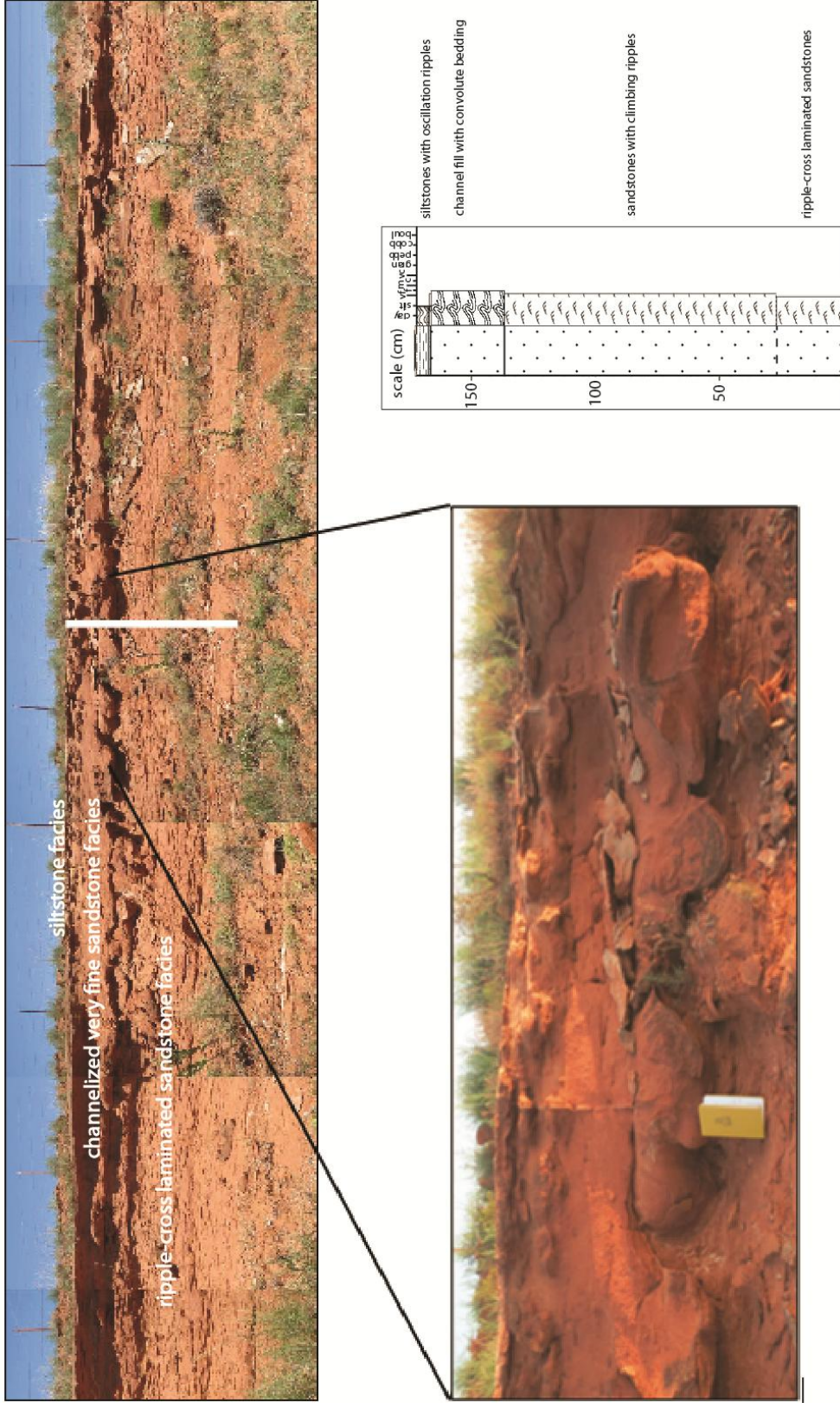


Figure 1. Study area – Geologic map showing the Cloud Chief Formation outcrop belt and the approximate location of the study area (red border) within Oklahoma and the U.S. The purple line in the state map is the approximate axis of the Anadarko basin. Approximate paleolatitude lines are from Kocurek and Kirkland (1998). The numbers, letters, and Line AA' are explained in Figure 12. MS = select measured sections. The geologic provinces map and the outcrop belt shapefiles are courtesy of the Oklahoma Geological Society.





**Figure 2. Evaporite and siliciclastic facies - (a) massive basal gypsum facies (b) Sandy dolomite with burrows; (c) Oolitic dolomite; (d) siltstone facies; (e) very fine sandstone subfacies; (f) gypsiferous sandstone type 1 (gypsum crystal growth within massive sandstones); (g) gypsiferous sandstone type 2 (channel-like features within laminated sandstones); (h) silty claystone facies, inferred contact with the overlying Doxey Formation is denoted by the dashed blue line. Arrow points to the light greenish claystone beds ~20 cm below the actual contact.**



**Figure 3. Channel outcrop and associated structures - an along strike section showing convoluted beds near the base. The measured stratigraphic column corresponds to the white vertical line on the outcrop image.**

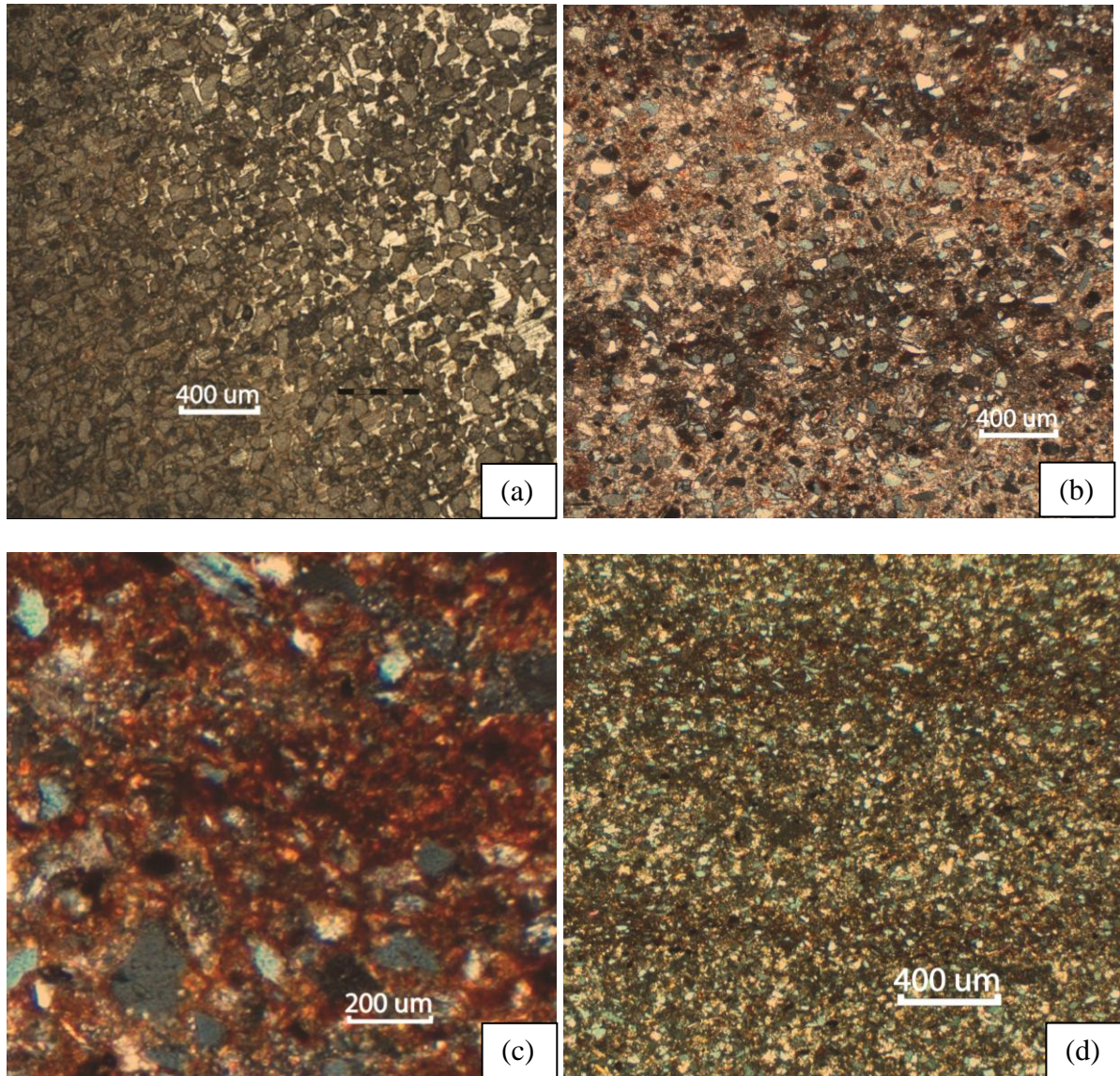


**Figure 4. Petrographic thin sections - (a) gypsiferous sandstone, cross-polars; (b) channelized very fine sandstone, laminae indicated by varying clay and hematite cement concentrations (cement-rich laminae = darker colored, and vice versa), cross-polars; (c) siltstone facies, with thick cement cover around quartz grains, cross-polars; (d) laminated sandstone subfacies, showing varying degrees of hematite cement (high = dark bands, and vice versa), cross polars**



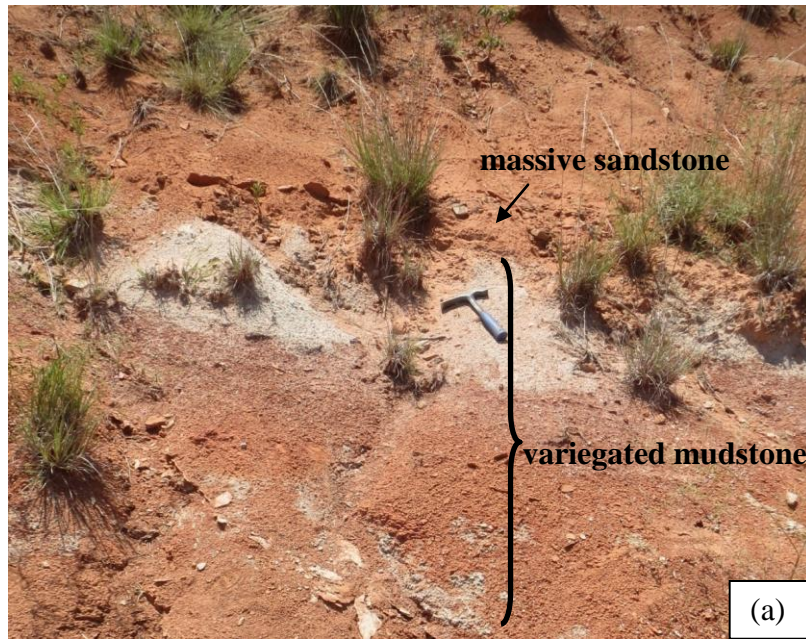


**Figure 5. Variegated mudstone facies - (a) one typical section, showing color gradation from reddish-white (bottommost portion), to brown, to dark brown, to whitish-red, to white (topmost portion). Stratigraphically above most of these facies is a light brown thickly-bedded sandstone layer; (b) slickenlines; (c) granular texture; (d) diagenetic halos; (e) calcitic layer**



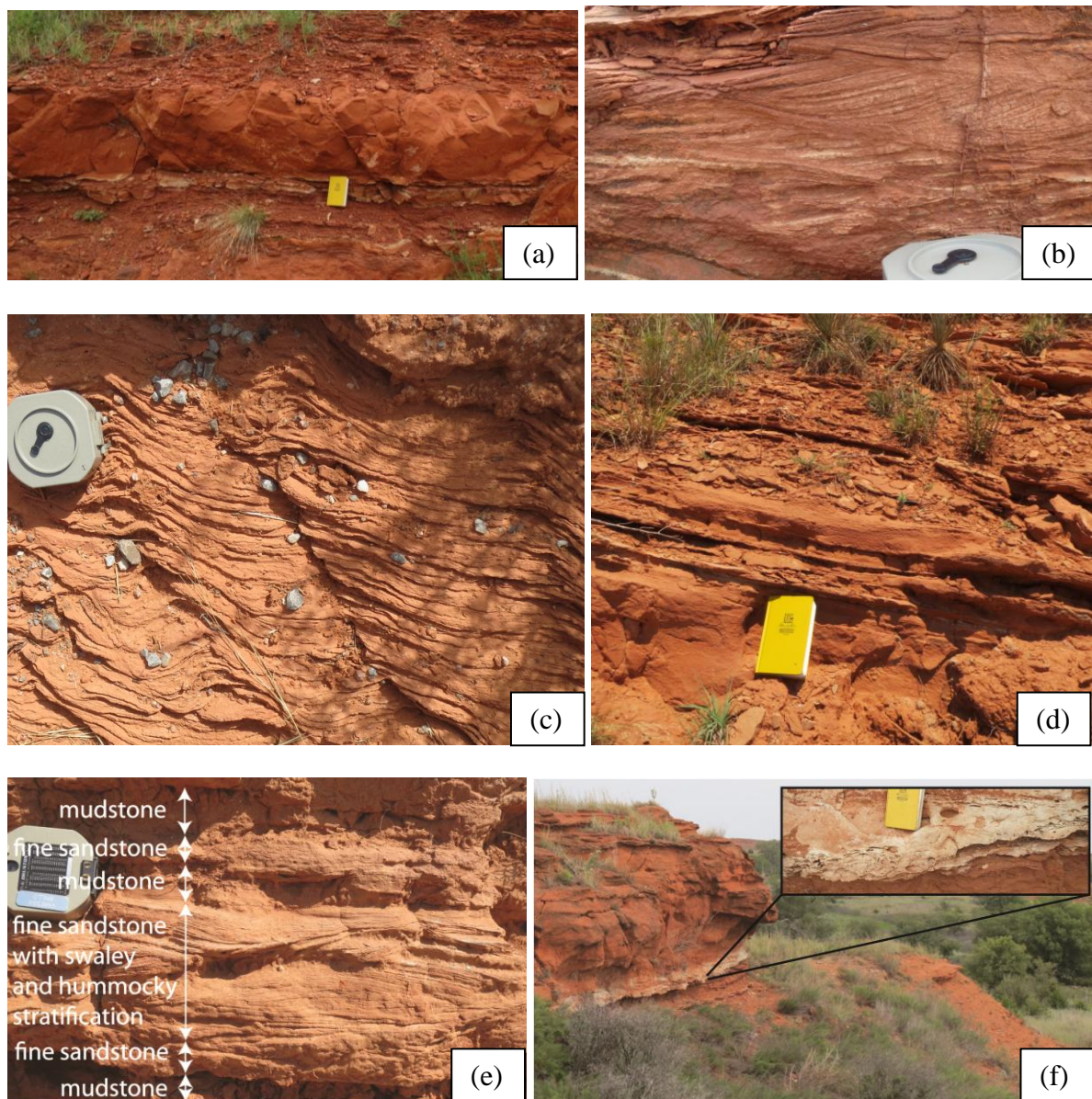


**Figure 7. Sandstone and mudstone facies - (a) massive sandstone; (b) trough-cross bedded sandstone; (c) ripple-cross laminated sandstone; (d) interbedded sandstone and mudstone, talus cover near the top of the section; (e) tempestite sequence within the interbedded sandstone and mudstone facies (interpreted as distal splays); (f) rip-up clasts at the base of an unusually thick (4.33 m) channel fill**

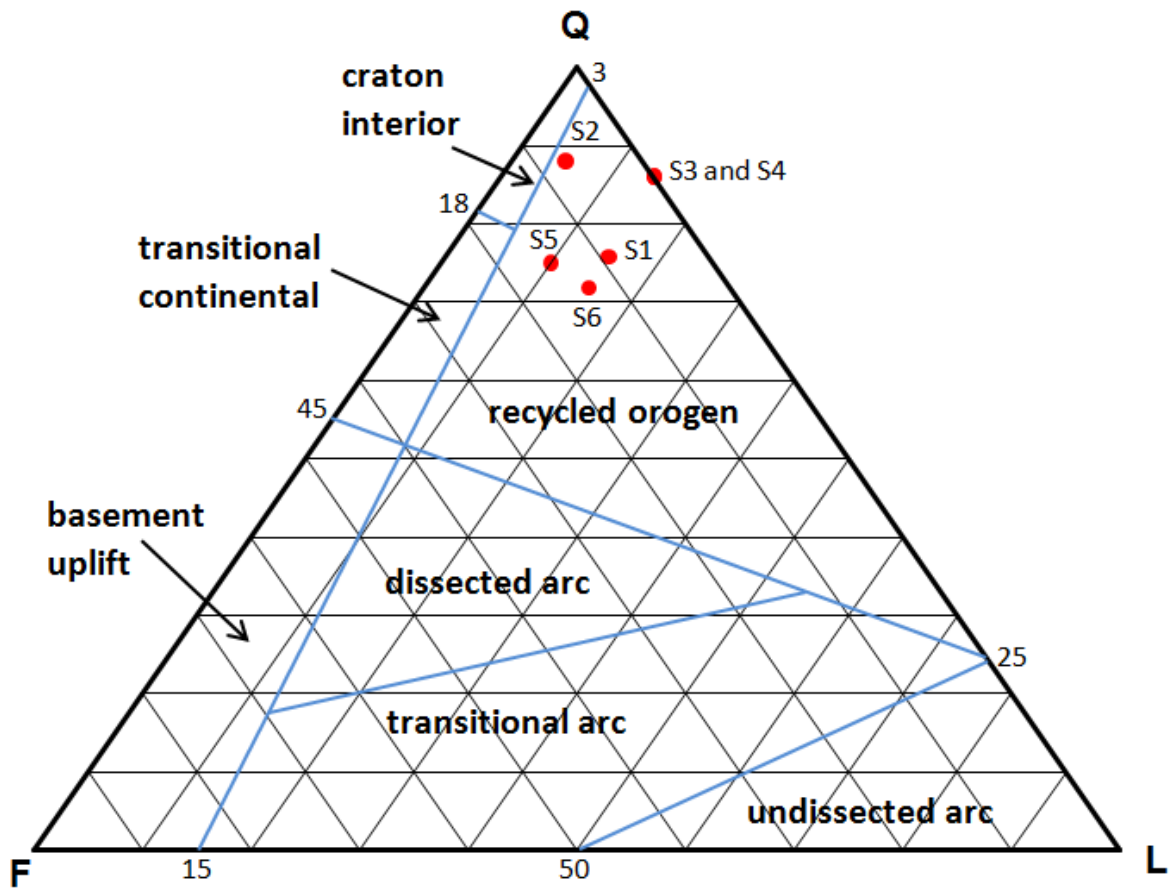
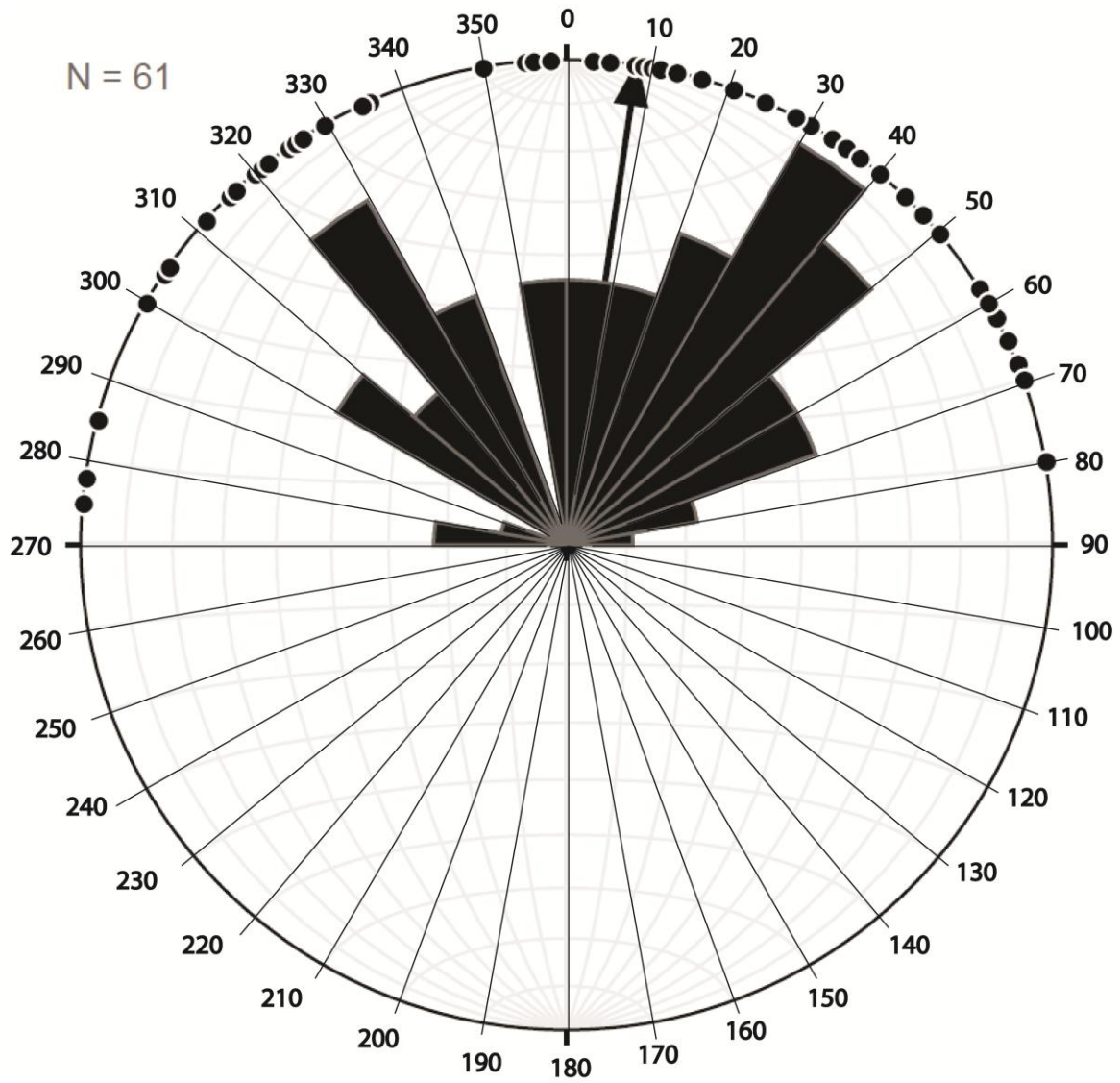
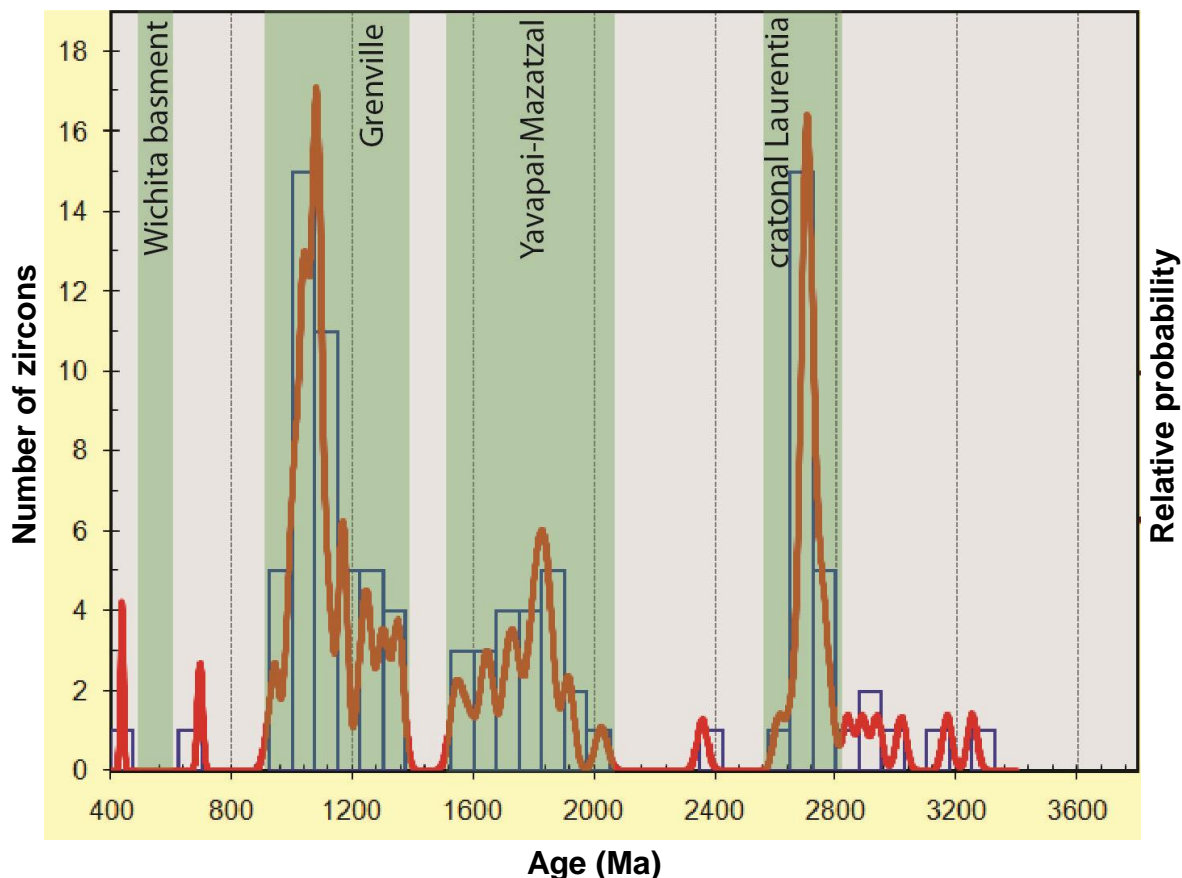


Figure 8 - Ternary diagram - QFL diagram after Dickinson et al. (1983) showing the parent rock type of each the six samples taken for thin-section analysis. S1 = gypsiferous sandstone subfacies, S2 = channelized very fine sandstone facies, S3 = thickly-bedded sandstone facies, S4 = laminated sandstone subfacies, S5 = siltstone facies, S6 = silty claystone facies.



**Figure 9. Regional Paleocurrent – Distribution of 61 paleocurrent measurements from the study area. See Fig. 1 for locations from which these were taken. Note the unimodal, radial flow originating from present-day south. The mean vector ( $8.3^\circ$ ) is denoted by the black arrow. The program ‘Stereonet 9’ by Dr. Richard Allmendinger from Cornell University was used to create this paleocurrent figure.**



**Figure 10. Probability density plot** – The histogram is created from the 'best age' column of detrital zircon ages ( $^{207}\text{Pb}/^{206}\text{Pb}$  for ages 1200 Ma or older and the  $^{207}\text{Pb}$ -corrected  $^{206}\text{Pb}/^{238}\text{U}$  for anything younger than 1200 Ma). Blue bars show the number of zircons within each age interval. Each bin is 80 Ma. The red line indicates the cumulative probability distribution of the data. Green bars correspond to the three major age groupings. Note the lack of zircons aged ~500-600 Ma.

Sample Number	Sample weight (mg)	Sr ppm	Total Sr (mg)	$^{87}\text{Sr}/^{86}\text{Sr}$ exp corrected ( $\pm 0.000015$ )	delta SW
8-12-w	13.70	1179.39	16.16	0.707547	-162.61
9-18-440	10.10	430.59	4.35	0.707436	-173.67
8-17-SC	12.80	4342.34	55.58	0.707421	-175.18
9-18-480	16.20	462.83	7.50	0.707350	-182.30
BC-55	7.30	1320.30	9.64	0.707311	-186.19
9-16-H34	8.10	875.45	7.09	0.707261	-191.16

**Table 1. Strontium isotope values** - Each gypsum sample is ordered from oldest (top) to youngest (bottom). A modern seawater value of 0.709173 was used to normalize each corrected isotope ratio into delta SW (seawater). See Figure 13 for locations from which these samples were taken.

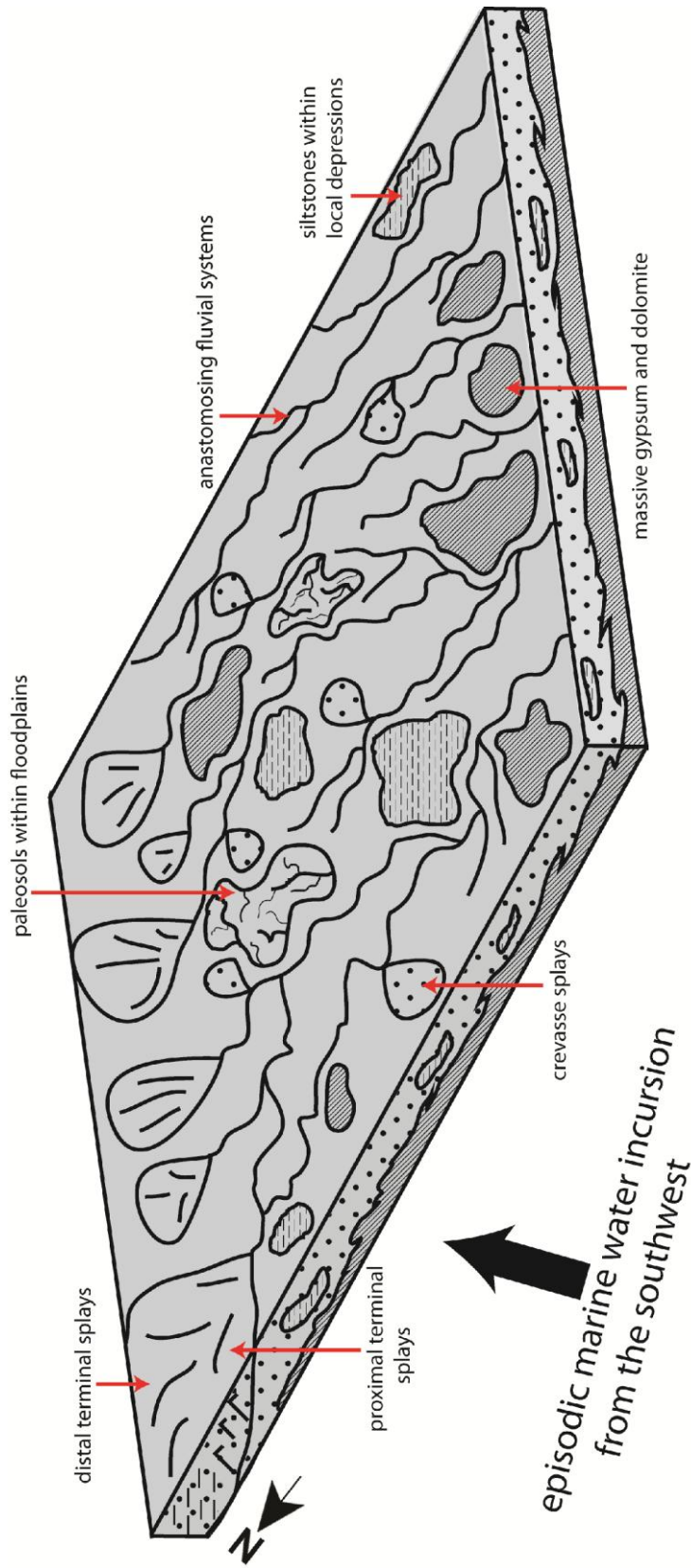


**Figure 11. Facies model – Idealized facies model for the paleoenvironment of western Oklahoma during the deposition of the Cloud Chief Formation. See text for facies interpretations. The silty claystone is not shown as it is interpreted to be a floodsheet deposit that covers the rest of the facies. Marine waters episodically flooded this sabkha from the present-day southwest.**

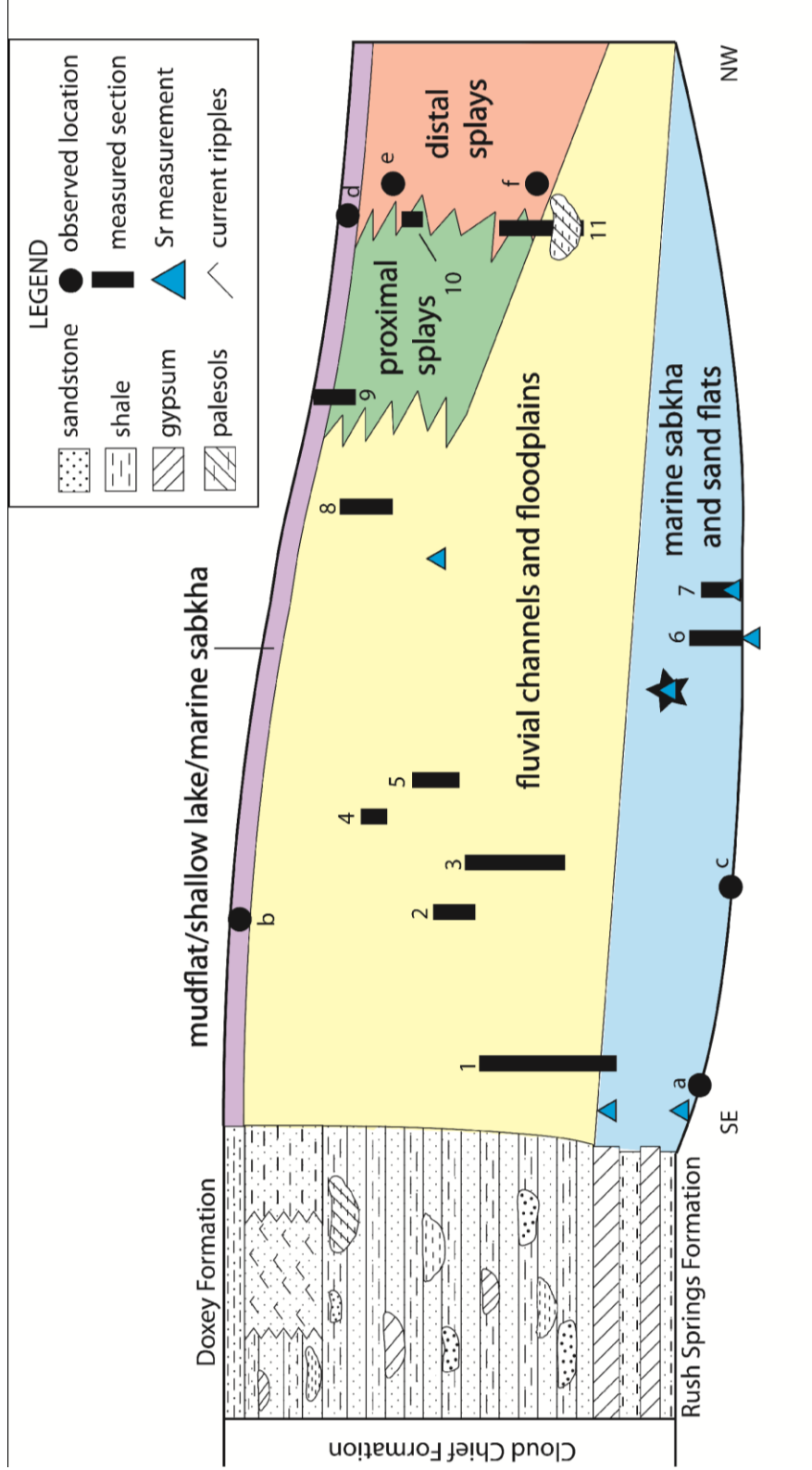


Figure 12. Stratigraphic architecture - Idealized cross section through the Cloud Chief from SE to NW. Numbers correspond to select measured sections, while letters correspond to select observation locations (See Figure 1). Line AA' in Figure 1 traces the approximate surface line of the cross-section.



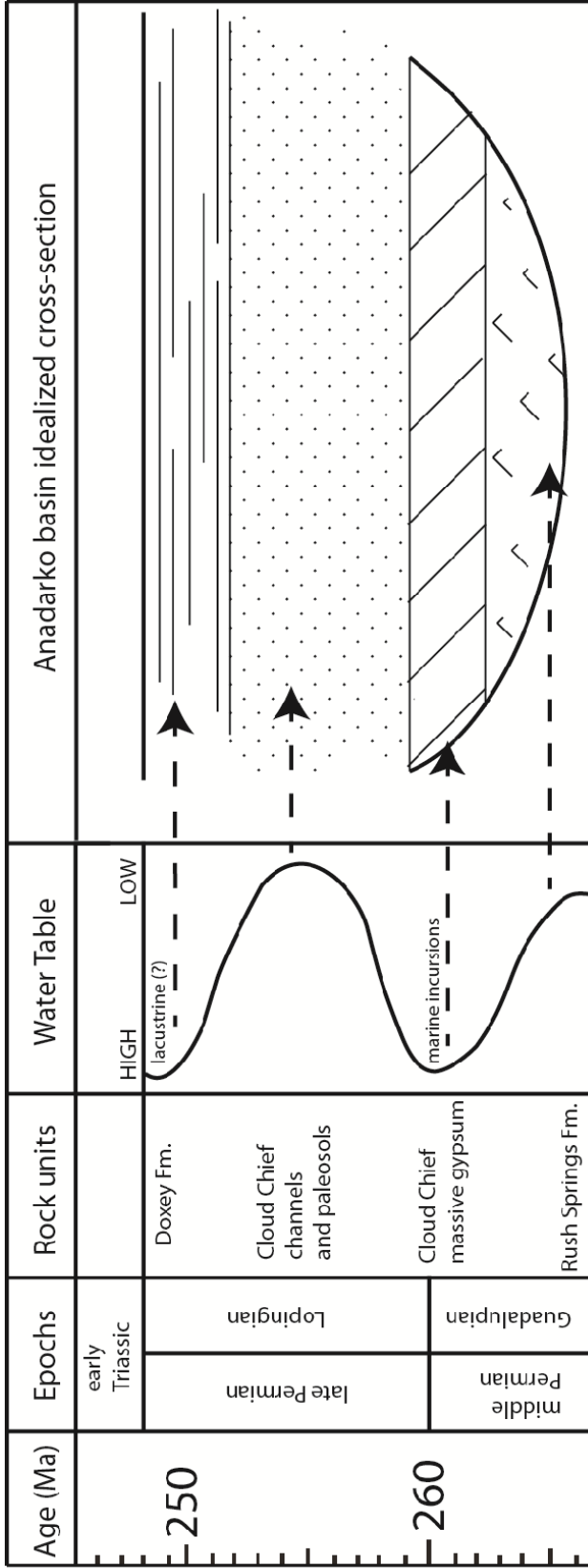


Figure 13. Water table level curve - A summary of the general trend of water table levels during the mid to late Permian. The idealized cross-section is vertically exaggerated to match the timescale. Note the abundance of sandstones and siltstones during periods of low water table and of evaporites and shales during high levels.

## References

1. R. W. Allmendinger, N. Cardozo, and D. Fisher, "Structural Geology Algorithms: Vectors & Tensors," Cambridge, England, Cambridge University Press 289 p. (2012).
2. Z. Al-Shaieb, R. W. Olmsted, J. W. Shelton, R. T. May, R. T. Owens, and R. E. Hanson, "Uranium Potential of Permian and Pennsylvanian Sandstones," *Amer. Assoc. Petroleum Geologists Bulletin*, Vol. 61, Iss. 3, pp. 360-375 (1977).
3. E. J. Barron and G. T. Moore, "Climate model application in paleoenvironmental analysis," *Soc. for Sed. Geol., Nature*, 339 p. (1994).
4. C. M. Becker, "Structure and Stratigraphy of Southwestern Oklahoma," *Amer. Assoc. of Petroleum Geologist Bulletin*, Vol. 14, pp.37-56 (1930).
5. K. C. Benison and R. H. Goldstein, "Evaporites and siliciclastics of the Permian Nippewalla Group of Kansas, USA: a case for non-marine deposition in saline lakes and saline pans," *Sedimentology*, Vol. 48, No. 1, pp. 165-188 (2001).
6. N. Cardozo and R. W. Allmendinger, "Spherical projections with OSXStereonet," *Computers & Geosciences*, Vol. 51, pp. 193-205 (2013).
7. A. R. Carroll and K. M. Bohacs, "Stratigraphic classification of ancient lakes: balancing tectonic and climatic controls," *Geology*, Vol. 27, pp. 99-102 (1999).
8. L. S. Carter, S. A. Kelley, D. D. Blackwell, and N. D. Naeser, "Heat flow and thermal history of the Anadarko Basin, Oklahoma," *Amer. Assoc. Petroleum Geologists Bulletin*, Vol. 82, pp. 291-316 (1998).
9. R. L. Clifton, "Permian structure and stratigraphy of north-western Oklahoma and adjacent areas," *Amer. Assoc. Petroleum Geologists Bulletin*, Vol. 14, No. 2, pp. 161-173 (1930).
10. J. C. Crowell, "Gondwanan Glaciation, Cyclothems, Continental Positioning, and Climate Change," *Amer. Jour. of Sci.*, Vol. 278, pp. 1345-1372 (1978).
11. J. C. Crowell, "Ice Ages recorded on Gondwanan continents," *Geol. Soc. S. Afr. Vol.* 86, pp. 238-262 (1983).
12. R. E. Denison, R. B. Koepnick, W. H. Burke, E. A. Hetherington, and A. Fletcher, "Construction of the Mississippian, Pennsylvanian and Permian seawater  $^{87}\text{Sr}/^{86}\text{Sr}$  curve," *Chemical Geology*, Vol. 112, pp. 145-167 (1994).
13. R. E. Denison, D. W. Kirkland, and R. Evans, "Using Strontium Isotopes to Determine the Age and Origin of Gypsum and Anhydrite Beds," *The Journal of Geology*, Vol. 106, No. 1, pp. 1-18 (1998).

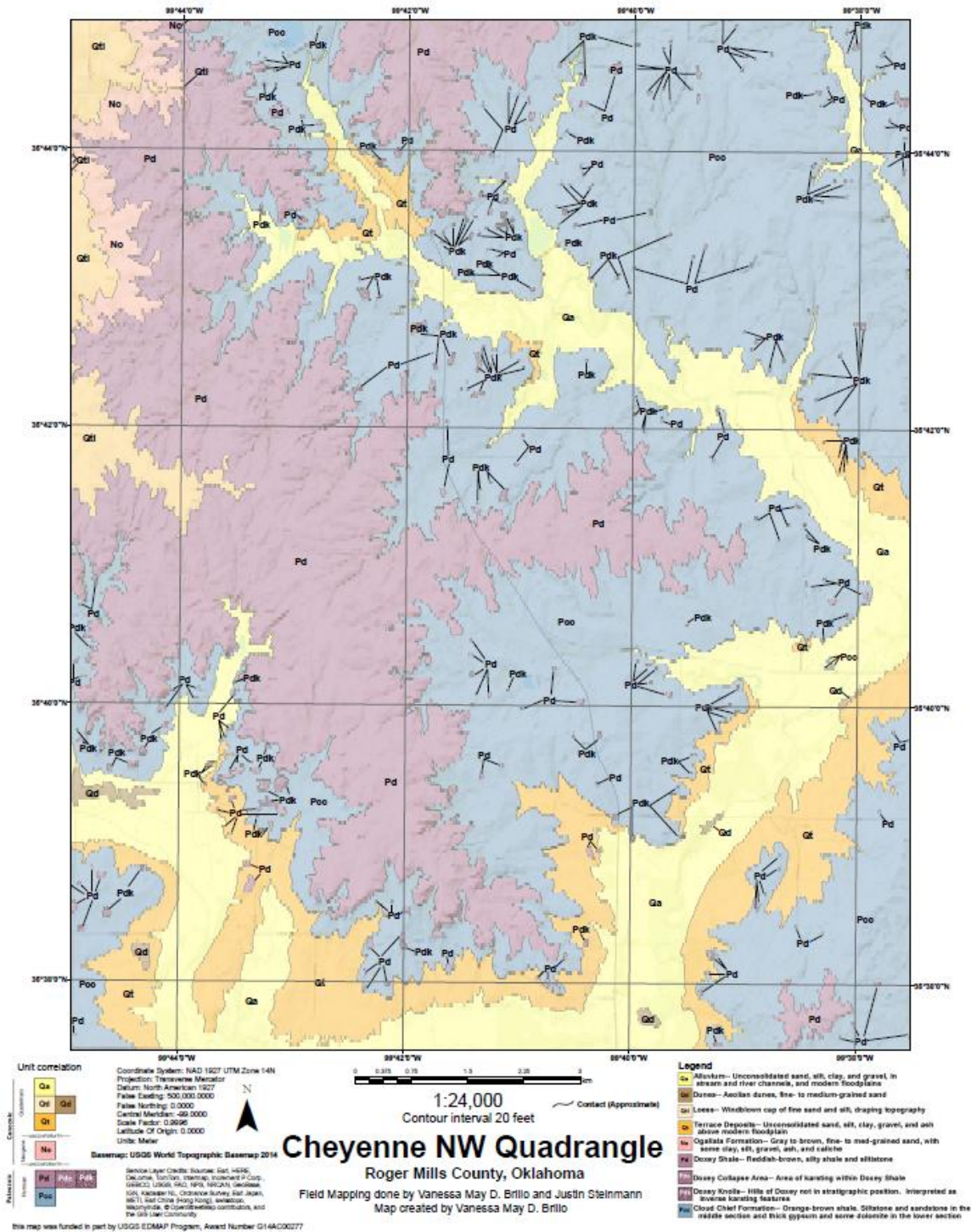
14. R. H. Dott, "Regional Stratigraphy of the Mid-continent," *Amer. Assoc. Petroleum Geologists Bulletin*, Vol. 25, No. 9, pp. 1619-1705 (1941).
15. R. H. Dott, "Stratigraphy of Oklahoma," *Tulsa Geological Society Digest*, Vol. 20, pp. 30-37 (1952).
16. N. Evans, "Stratigraphy of Permian beds of northwestern Oklahoma," *Amer. Assoc. of Petroleum Geologist*, Vol. 15, pp.405-439 (1931).
17. R. O. Fay, "The Blaine and Related Formations of Northwestern Oklahoma and Southern Kansas," *Oklahoma Geological Survey, Bulletin 98* (1964).
18. R. O. Fay, "Geology and Mineral Resources (Exclusive of Petroleum) of Custer County, Oklahoma," *Oklahoma Geological Survey, Bulletin 114* (1978).
19. C. R. Fielding, T. D. Frank, L. P. Birgenheier, M. C. Rygel, and A. T. Jones, "Stratigraphic imprint of the Late Paleozoic Ice Age in eastern Australia: A record of alternating glacial and nonglacial climate regime," *J. of the Geol. Soc.*, Vol 165, No. 1, pp. 129-140 (2008).
20. J. A. Fisher, C. B. E. Krapf, S. C. Lang, G. J. Nichols, and T. H. D. Payenberg, "Sedimentology and architecture of the Douglas Creek terminal splay, Lake Eyre, central Australia," *Sedimentology*, Vol. 55, pp. 1915-1930 (2008).
21. T. M. Foster, G. S. Soreghan, M. J. Soreghan, K. C. Benison, and R. D. Elmore, "Climatic and paleogeographic significance of eolian sediment in the Middle Permian Dog Creek Shale (Midcontinent U.S.)," *Paleogeography, Paleoclimatology, Paleoecology*, Vol. 40, pp. 12-29 (2014).
22. J. M. Giles, M. J. Soreghan, K. C. Benison, G. S. Soreghan, S. T. Hasiotis, "Lakes, loess, and paleosols in the Permian Wellington Formation of Oklahoma, U.S.A.: Implications for paleoclimate and paleogeography of the Midcontinent," *J. of Sed. Res.*, Vol. 83, pp. 825-846, (2013).
23. C. N. Gould, "A new classification of the Permian redbeds of southwestern Oklahoma," *Amer. Assoc. Petroleum Geologists Bulletin*, Vol. 8, pp. 322-341 (1924).
24. C. N. Gould, "The Correlation of the Permian of Kansas, Oklahoma, and northern Texas," *Amer. Assoc. Petroleum Geologists Bulletin*, Vol. 10, pp. 144-153 (1926).
25. N. G. Heavens, N. M. Mahowald, G. S. Soreghan, M. J. Soreghan, C. A. Shields, "A model-based evaluation of tropical climate in Pangaea during the late Paleozoic icehouse," *Paleogeography, Paleoclimatology, Paleoecology*, Vol. 425, pp. 109-127 (2015).
26. M. J. Hemmerich and S. A. Kelley, "Patterns of Cenozoic denudation on the southern high plains," *Amer. Assoc. Petroleum Geologists Bulletin*, Vol. 84, 1239 p. (2000).

27. S. Hovorka, L. P. Knauth, R. S. Fisher, and G. Gao, "Marine to nonmarine facies transition in Permian evaporites of the Palo Duro Basin, Texas: Geochemical response," *Geol. Soc. Amer. Bulletin*, Vol. 105, No. 8, pp. 1119-1134 (1993).
28. S. E. Jackson, N. J. Pearson, W. L. Griffin, and E. A. Belousova, "The application of laser ablation inductively coupled plasma mass spectrometry to *in situ* U-Pb zircon geochronology," *Chemical Geology*, Vol. 211, pp. 47-69 (2004).
29. K. S. Johnson, T. W. Amsden, R. E. Denison, S. P. Dutton, A. G. Goldstein, B. Rascoe Jr., P. K. Sutherland, D. M. Thompson, "Geology of the Southern Midcontinent," Oklahoma Geol. Surv. Spec. Pub. 89-2, 53 p. (1989).
30. C. Korte, T. Jasper, H. W. Kozur, and J. Veizer, "<sup>87</sup>Sr/<sup>86</sup>Sr record of Permian seawater," *Paleogeography, Paleoclimatology, Paleoecology*, Vol. 240, pp. 89-107 (2006).
31. I. P. Montanez, N. J. Tabor, D. Niemeier, W. A. DiMichele, T. D. Frank, C. R. Fielding, J. L. Isbell, L. P. Birgenheier, and M. C. Rygel, "CO<sub>2</sub>-Forced Climate and Vegetation Instability During Late Paleozoic Deglaciation," *Science*, Vol. 315, No. 5808, pp. 87-91 (2007).
32. G. C. Nanson and J. C. Croke, "A genetic classification of floodplains," *Geomorphology*, Vol. 4, Iss. 6, pp. 367-490 (1992).
33. G. J. Nichols and J. A. Fisher, "Processes, facies and architecture of fluvial distributary system deposits," *Sedimentary Geology*, Vol. 195, pp. 75-90 (2007).
34. G. H. Norton, "Permian Redbeds of Kansas," *Amer. Assoc. Petroleum Geologists Bulletin*, Vol. 23, No. 12, pp. 1751-1819 (1939).
35. W. J. Perry, Jr., "Tectonic Evolution of the Anadarko Basin region, Oklahoma," *U.S. Geological Survey, Bulletin, Report No. B 1866-A*, pp. 1-19 (1989).
36. Z. A. Poland and A. R. Simms, "Sedimentology of an Erg To An Erg-Margin Depositional System, the Rush Springs Sandstone of Western Oklahoma, U.S.A.: Implications For Paleowinds Across Northwestern Pangaea during the Lopingian (Middle Permian)," *Journal of Sedimentary Research*, Vol. 82, pp. 345-363 (2012).
37. C. J. Poulsen, D. Pollard, I. P. Montanez, and D. Rowley, "Late Paleozoic tropical climate response to Gondwanan deglaciation," *Geology*, Vol. 35, No. 9, pp. 771-774 (2007).
38. G. Retallack, "Field recognition of paleosols," *Geol. Soc. Am. Spec. Paper 216*, pp. 1-20 (1988).
39. C. A. Ross and J. R. P. Ross, "Late Paleozoic Transgressive-Regressive Deposition," *SEPM Special Publication No. 42*, pp. 227-247 (1988).

40. D. A. Ruban, "Mesozoic long-term eustatic cycles and their uncertain hierarchy," *Geoscience Frontiers*, Vol. 6, pp. 503-511 (2015).
41. C. R. Scotese, R. K. Bambach, C. Barton, R. Van de Voo, and A. M. Ziegler, "Paleozoic base maps," *Journal of Geology*, Vol. 87, pp. 217-277 (1979).
42. J. Slama, J. Kosler, D. J. Condon, J. L. Crowley, A. Gerdes, J. M. Hanchar, M. S. A. Horstwood, G. A. Morris, L. Nasdala, N. Norberg, U. Schaltegger, B. Schoene, M. N. Tubrett, M. J. Whitehouse, "Plesovice zircon -- A new natural reference material for U-Pb and Hf isotopic microanalysis," *Chemical Geology*, Vol. 249, pp. 1-35 (2008).
43. J. W. Snedden, D. Nummedal, and A. F. Amos, "Storm- and fair-weather combined flow on the central Texas continental shelf," *Journal for Sed. Pet.*, Vol. 58, No. 4, pp. 580-595 (1988).
44. G. S. Soreghan, M. J. Soreghan, and M. A. Hamilton, "Origin and significance of loess in late Paleozoic western Pangaea: A record of tropical cold?," *Paleogeography, Paleoclimatology, Paleoecology*, Vol. 268, pp. 234-259 (2008).
45. G. S. Soreghan, G. R. Keller, M. C. Gilbert, C. G. Chase, D. E. Sweet, "Load-induced subsidence of the Ancestral Rocky Mountains recorded by preservation of Permian landscapes," *Geosphere*, Vol. 8, No. 3, pp. 654-668 (2012).
46. G. S. Soreghan and M. J. Soreghan, "Tracing Clastic Delivery to the Permian Delaware Basin, U.S.A.: Implications for Paleogeography and Circulation in Westernmost Equatorial Pangaea," *J. of Sed. Res.*, Vol. 83, pp. 786-802 (2013).
47. M. J. Soreghan, G. S. Soreghan, and M. A. Hamilton, "Paleowinds inferred from detrital-zircon geochronology of upper Paleozoic loessite, western equatorial Pangaea," *Geology*, Vol. 30, No. 8, pp. 695-698 (2002).
48. M. J. Soreghan, G. S. Soreghan, and M. A. Hamilton, "Glacial-interglacial shifts in atmospheric circulation of western tropical Pangaea," *Paleogeography, Paleoclimatology, Paleoecology*, Vol. 268, pp. 260-272 (2008).
49. A. C. Sweet, G. S. Soreghan, D. E. Sweet, M. J. Soreghan, and A. S. Madden, "Permian dust in Oklahoma: Source and origin for Middle Permian (Flowerpot-Blaine) redbeds in Western Tropical Pangaea," *Sedimentary Geology*, Vol. 284-285, pp. 181-196 (2013).
50. N. J. Tabor and I. P. Montanez, "Shifts in late Paleozoic atmospheric circulation over western equatorial Pangaea: Insights from pedogenic mineral  $\delta^{18}\text{O}$  compositions," *Geology*, Vol. 30, No. 12, pp. 1127-1130 (2002).

51. T. Treece, "Depositional Environments of a North American Mid-continent Red Bed: The El Reno Group of Central Oklahoma, USA," Thesis submitted to Oklahoma State University, Stillwater, Oklahoma, 63 pp. (2007).
52. J. J. Veevers and C. McA. Powell, "Late Paleozoic glacial episodes in Gondwanaland reflected in transgressive-regressive depositional sequences in Euramerica," *Geol. Soc. Amer. Bulletin*, Vol. 98, pp. 475-487 (1987).
53. M. Wiedenbeck, "An example of reverse discordance during ion microprobe zircon dating: an artifact of enhanced ion yields from radiogenic labile Pb," *Chemical Geology*, Vol. 125, No. 3, pp. 197-218 (1995).
54. H. Ye, L. Royden, C. Burchfiel, and M. Schuepbach, "Late Paleozoic Deformation of Interior North America: The Greater Ancestral Rocky Mountains," *Amer. Assoc. Petroleum Geologists Bulletin*, Vol. 80, No. 9, pp. 1397-1432 (1996).

# Appendix



**Cheyenne NW Quadrangle - Geologic map created for the Cheyenne NW Quadrangle in Roger Mills County.**

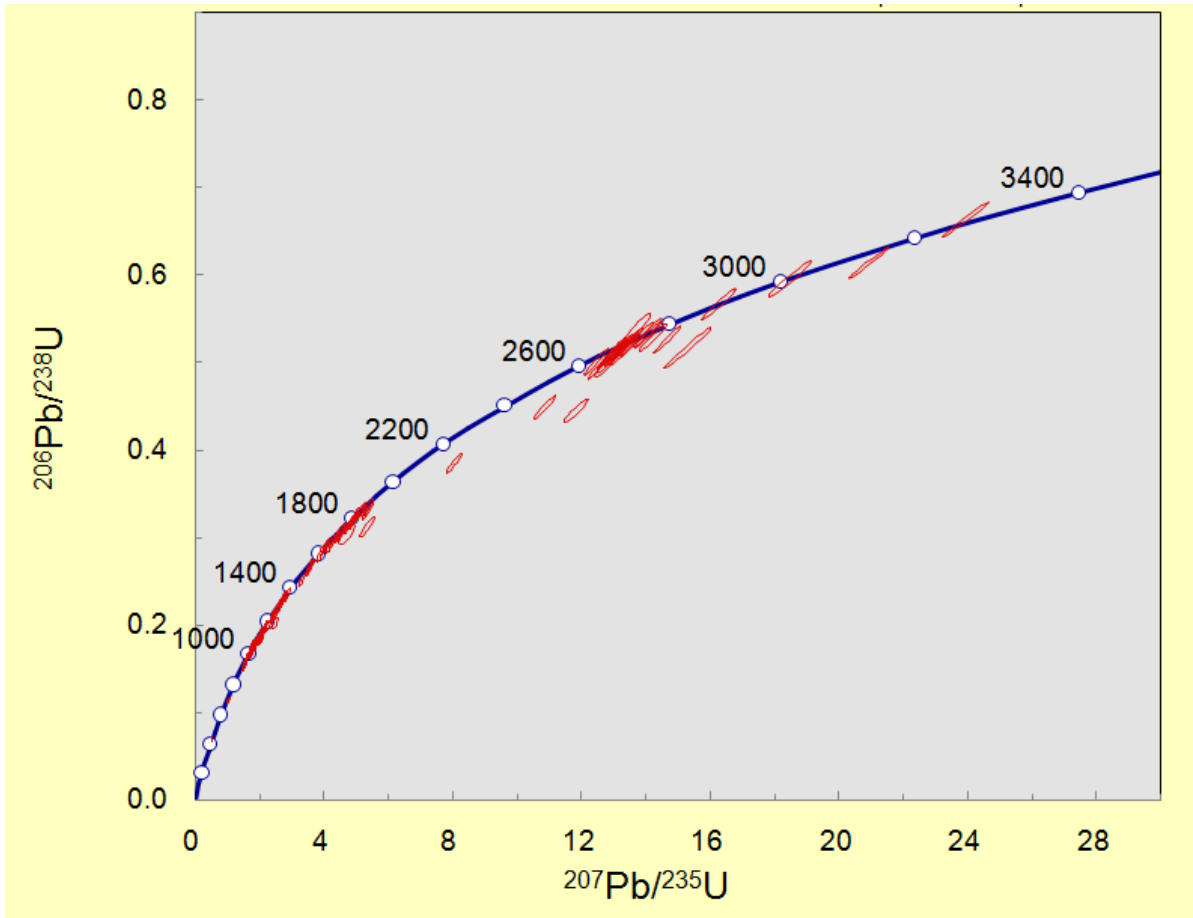
Sample	U (ppm)	Th (ppm)	206Pb/ 204Pb	207Pb /235U	$\pm 2\sigma$	206Pb /238U	$\pm 2\sigma$	rho	207Pb/ 206Pb	$\pm 2\sigma$	Apparent Age (Ma)
9-3-ws-s1-99	650	195	11724	11.84	0.304	0.4456	0.011	0.930	0.1919	0.004	2758
9-3-ws-s1-42	18	11	1747	5.36	0.193	0.3123	0.009	0.924	0.1246	0.003	2022
9-3-ws-s1-48	20	9	-992	2.481	0.083	0.2024	0.005	0.741	0.0887	0.003	1396
9-3-ws-s1-70	165	52	-12660	8.05	0.195	0.3851	0.009	0.955	0.1510	0.003	2358
9-3-ws-s1-23	561	225	24371	15.31	0.595	0.517	0.019	0.988	0.2140	0.004	2936
9-3-ws-s1-79	205	56	12681	10.87	0.270	0.4494	0.011	0.967	0.1754	0.004	2610
9-3-ws-s1-80	221	106	8463	1.044	0.026	0.1143	0.003	0.927	0.0662	0.001	698
9-3-ws-s1-37	99	62	1536	2.019	0.060	0.1821	0.004	0.794	0.0800	0.002	1078
9-3-ws-s1-13	29	14	978	4.72	0.194	0.304	0.009	0.779	0.1124	0.003	1837
9-3-ws-s1-72	139	56	-8873	1.759	0.045	0.1672	0.004	0.911	0.0760	0.002	996
9-3-ws-s1-76	21	7	-567	2.06	0.063	0.1861	0.006	0.643	0.0788	0.002	1100
9-3-ws-s1-30	47	23	1386	1.822	0.057	0.1718	0.005	0.873	0.0762	0.002	1022
9-3-ws-s1-4	70	21	3656	2.269	0.073	0.1993	0.005	0.840	0.0823	0.002	1252
9-3-ws-s1-46	92	90	3818	3.33	0.079	0.2525	0.006	0.927	0.0954	0.002	1535
9-3-ws-s1-41	12	6	513	1.553	0.064	0.1549	0.006	0.885	0.0724	0.002	928
9-3-ws-s1-88	352	100	44333	14.68	0.344	0.5267	0.012	0.979	0.2015	0.004	2839
9-3-ws-s1-68	130	91	-8303	12.79	0.292	0.4979	0.011	0.922	0.1857	0.004	2704
9-3-ws-s1-1	75	38	3198	1.964	0.057	0.1823	0.005	0.894	0.0782	0.002	1079
9-3-ws-s1-18	352	46	17968	5.377	0.142	0.3307	0.009	0.973	0.1175	0.002	1919
9-3-ws-s1-96	133	44	2990	2.541	0.082	0.2154	0.005	0.891	0.0855	0.002	1325
9-3-ws-s1-22	150	124	1824	2.014	0.055	0.1857	0.004	0.842	0.0785	0.002	1098
9-3-ws-s1-5	195	90	45700	12.6	0.322	0.4967	0.013	0.985	0.1851	0.004	2699
9-3-ws-s1-20	60	95	1413	1.824	0.049	0.174	0.004	0.866	0.0759	0.002	1034
9-3-ws-s1-10	134	86	-20176	3.595	0.089	0.2658	0.007	0.953	0.0978	0.002	1583
9-3-ws-s1-69	27	30	-1017	1.826	0.051	0.1742	0.004	0.747	0.0748	0.002	1035
9-3-ws-s1-38	68	34	1043	2.042	0.061	0.1879	0.005	0.718	0.0792	0.002	1110
9-3-ws-s1-26	130	72	4643	2.416	0.063	0.2095	0.005	0.944	0.0834	0.002	1277
9-3-ws-s1-50	23	8	-1073	2.476	0.073	0.2128	0.006	0.647	0.0836	0.002	1281
9-3-ws-s1-71	56	41	-1325	1.721	0.043	0.1677	0.004	0.826	0.0738	0.002	999
9-3-ws-s1-63	551	239	-24559	4.572	0.111	0.3051	0.007	0.989	0.1087	0.002	1777
9-3-ws-s1-66	117	60	-9730	20.94	0.504	0.6145	0.014	0.992	0.2475	0.005	3169
9-3-ws-s1-100	169	227	9133	4.964	0.134	0.3193	0.008	0.986	0.1121	0.002	1834
9-3-ws-s1-98	99	136	6404	12.88	0.303	0.5041	0.012	0.940	0.1857	0.004	2704
9-3-ws-s1-77	284	92	-19507	2.197	0.054	0.1979	0.005	0.955	0.0792	0.002	1164
9-3-ws-	250	114	5979	1.919	0.055	0.1811	0.005	0.953	0.0767	0.002	1073



s1-15												
9-3-ws-s1-86	103	44	8311	2.717	0.063	0.2263	0.005	0.878	0.0869	0.002	1358	
9-3-ws-s1-33	47	16	1402	4.22	0.119	0.2928	0.008	0.885	0.1046	0.002	1707	
9-3-ws-s1-81	141	43	9311	1.969	0.044	0.1843	0.004	0.845	0.0771	0.002	1090	
9-3-ws-s1-95	25	15	2385	2.097	0.064	0.1922	0.005	0.669	0.0789	0.002	1133	
9-3-ws-s1-94	206	107	24269	4.478	0.104	0.3028	0.007	0.955	0.1064	0.002	1738	
9-3-ws-s1-85	203	83	6327	1.743	0.045	0.1701	0.004	0.903	0.0743	0.002	1013	
9-3-ws-s1-27	102	59	3161	5.396	0.135	0.335	0.008	0.945	0.1168	0.002	1907	
9-3-ws-s1-83	269	136	137100	13.16	0.337	0.5109	0.012	0.994	0.1868	0.004	2714	
9-3-ws-s1-19	94	113	3190	4.773	0.121	0.3139	0.008	0.946	0.1099	0.002	1798	
9-3-ws-s1-55	34	23	-1419	2.609	0.064	0.2213	0.006	0.765	0.0847	0.002	1318	
9-3-ws-s1-89	48	1	2921	1.835	0.043	0.1763	0.004	0.642	0.0749	0.002	1047	
9-3-ws-s1-44	137	33	5481	2.871	0.080	0.2348	0.006	0.902	0.0877	0.002	1375	
9-3-ws-s1-28	104	79	2463	4.315	0.117	0.2974	0.008	0.961	0.1049	0.002	1712	
9-3-ws-s1-59	74	89	-7094	14.23	0.348	0.5289	0.013	0.972	0.1947	0.004	2782	
9-3-ws-s1-92	56	157	5796	13.35	0.366	0.515	0.014	0.979	0.1865	0.004	2712	
9-3-ws-s1-17	206	130	-36560	1.921	0.047	0.1821	0.004	0.937	0.0759	0.002	1079	
9-3-ws-s1-43	68	45	1997	1.803	0.049	0.1746	0.004	0.897	0.0747	0.002	1037	
9-3-ws-s1-78	41	16	-3962	3.901	0.094	0.2817	0.007	0.879	0.1001	0.002	1626	
9-3-ws-s1-90	139	168	6419	1.728	0.044	0.1697	0.004	0.946	0.0740	0.002	1010	
9-3-ws-s1-74	108	48	-3863	2.79	0.070	0.2315	0.006	0.956	0.0872	0.002	1364	
9-3-ws-s1-6	87	40	-4713	1.932	0.050	0.1831	0.004	0.799	0.0759	0.002	1087	
9-3-ws-s1-53	43	18	-983	2.044	0.050	0.1901	0.004	0.800	0.0778	0.002	1122	
9-3-ws-s1-82	92	44	5799	12.47	0.302	0.5017	0.012	0.982	0.1798	0.004	2651	
9-3-ws-s1-73	70	41	-1484	1.904	0.050	0.1815	0.005	0.899	0.0760	0.002	1075	
9-3-ws-s1-75	204	102	-12706	4.846	0.113	0.3182	0.007	0.980	0.1102	0.002	1803	
9-3-ws-s1-54	76	148	-7816	13.05	0.306	0.5121	0.012	0.958	0.1854	0.004	2702	
9-3-ws-s1-57	115	102	-10891	12.92	0.321	0.51	0.013	0.986	0.1835	0.004	2685	
9-3-ws-s1-58	93	90	-2740	2.185	0.052	0.1988	0.005	0.851	0.0801	0.002	1169	
9-3-ws-s1-84	159	88	4257	3.568	0.081	0.2685	0.006	0.917	0.0962	0.002	1551	
9-3-ws-s1-60	42	31	-3379	13.05	0.335	0.5126	0.012	0.967	0.1848	0.004	2696	
9-3-ws-s1-67	86	122	-3404	4.912	0.125	0.3209	0.008	0.930	0.1117	0.002	1827	
9-3-ws-s1-31	130	84	9161	13.36	0.317	0.518	0.012	0.977	0.1875	0.004	2720	
9-3-ws-s1-64	338	130	-21886	4.036	0.101	0.2884	0.007	0.979	0.1016	0.002	1654	
9-3-ws-s1-93	133	66	26088	5.171	0.118	0.3302	0.007	0.958	0.1137	0.002	1859	
9-3-ws-s1-9	44	32	-5011	2.439	0.072	0.2137	0.006	0.880	0.0828	0.002	1268	


9-3-ws-s1-65	251	162	-5953	1.823	0.046	0.1768	0.004	0.954	0.0747	0.002	1049
9-3-ws-s1-87	82	109	12845	13.35	0.340	0.5189	0.013	0.976	0.1862	0.004	2709
9-3-ws-s1-61	75	64	-5562	13	0.341	0.5133	0.013	0.979	0.1835	0.004	2684
9-3-ws-s1-32	84	132	8079	13.23	0.326	0.5173	0.013	0.971	0.1855	0.004	2703
9-3-ws-s1-62	118	76	-2337	1.623	0.040	0.1635	0.004	0.888	0.0719	0.002	976
9-3-ws-s1-91	351	202	58636	1.906	0.047	0.1824	0.004	0.938	0.0757	0.002	1080
9-3-ws-s1-51	67	29	-2746	4.538	0.117	0.3085	0.007	0.902	0.1065	0.002	1740
9-3-ws-s1-34	121	42	6421	1.926	0.050	0.1838	0.005	0.948	0.0759	0.002	1087
9-3-ws-s1-25	55	21	1606	5.1	0.173	0.3288	0.009	0.938	0.1128	0.002	1845
9-3-ws-s1-49	42	32	-1389	1.844	0.054	0.1787	0.005	0.846	0.0743	0.002	1060
9-3-ws-s1-56	130	162	68480	14.07	0.329	0.5323	0.012	0.977	0.1915	0.004	2755
9-3-ws-s1-45	133	100	14708	4.058	0.100	0.2906	0.007	0.962	0.1012	0.002	1646
9-3-ws-s1-2	140	67	-8425	4.935	0.138	0.3235	0.009	0.972	0.1109	0.002	1815
9-3-ws-s1-3	48	32	-9408	13.72	0.407	0.527	0.015	0.977	0.1885	0.004	2729
9-3-ws-s1-14	401	184	30365	1.538	0.040	0.1579	0.004	0.917	0.0703	0.001	945
9-3-ws-s1-8	38	18	-10845	18.48	0.537	0.596	0.017	0.974	0.2250	0.005	3017
9-3-ws-s1-21	82	93	3568	13.48	0.368	0.5238	0.014	0.962	0.1863	0.004	2710
9-3-ws-s1-12	42	36	-12644	16.28	0.429	0.5671	0.014	0.976	0.2075	0.004	2886
9-3-ws-s1-39	146	124	3469	0.535	0.015	0.0699	0.002	0.902	0.0557	0.001	435
9-3-ws-s1-47	153	85	-6425	2.58	0.068	0.2229	0.006	0.959	0.0838	0.002	1287
9-3-ws-s1-97	52	52	9634	14.06	0.363	0.5342	0.013	0.971	0.1903	0.004	2745
9-3-ws-s1-35	153	168	7239	1.745	0.045	0.173	0.004	0.907	0.0735	0.002	1029
9-3-ws-s1-11	117	51	-6505	2.759	0.071	0.2332	0.006	0.913	0.0857	0.002	1332
9-3-ws-s1-16	123	132	12871	23.96	0.588	0.6647	0.016	0.993	0.2608	0.005	3252
9-3-ws-s1-29	71	59	-2933	1.787	0.049	0.1777	0.005	0.870	0.0729	0.002	1054
9-3-ws-s1-36	182	13	5923	1.754	0.044	0.1756	0.004	0.907	0.0724	0.002	1043
9-3-ws-s1-40	18	14	4581	13.72	0.358	0.539	0.015	0.938	0.1847	0.004	2695

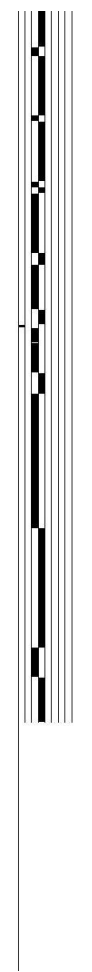
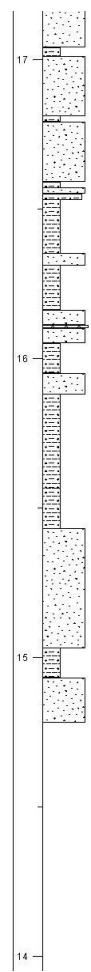
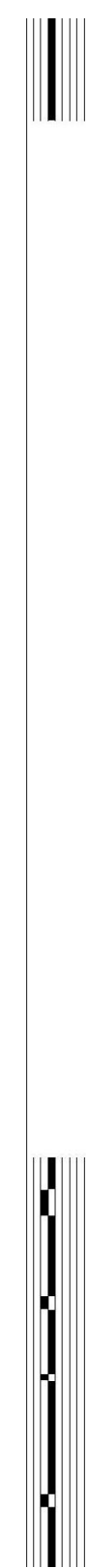
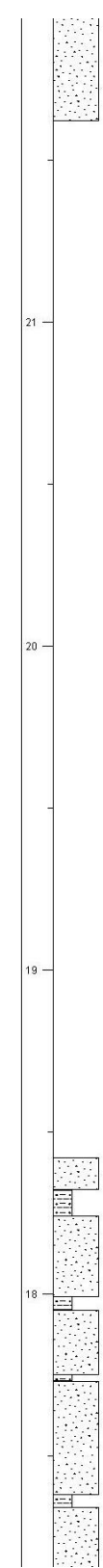
**U-Pb detrital zircon table – Data from the channelized very fine sandstone facies. Analyses were conducted using a laser ablation multi collector inductively coupled plasma mass spectrometer (LA-MC-ICP-MS) at University of California Santa Barbara. See text for further explanations.**

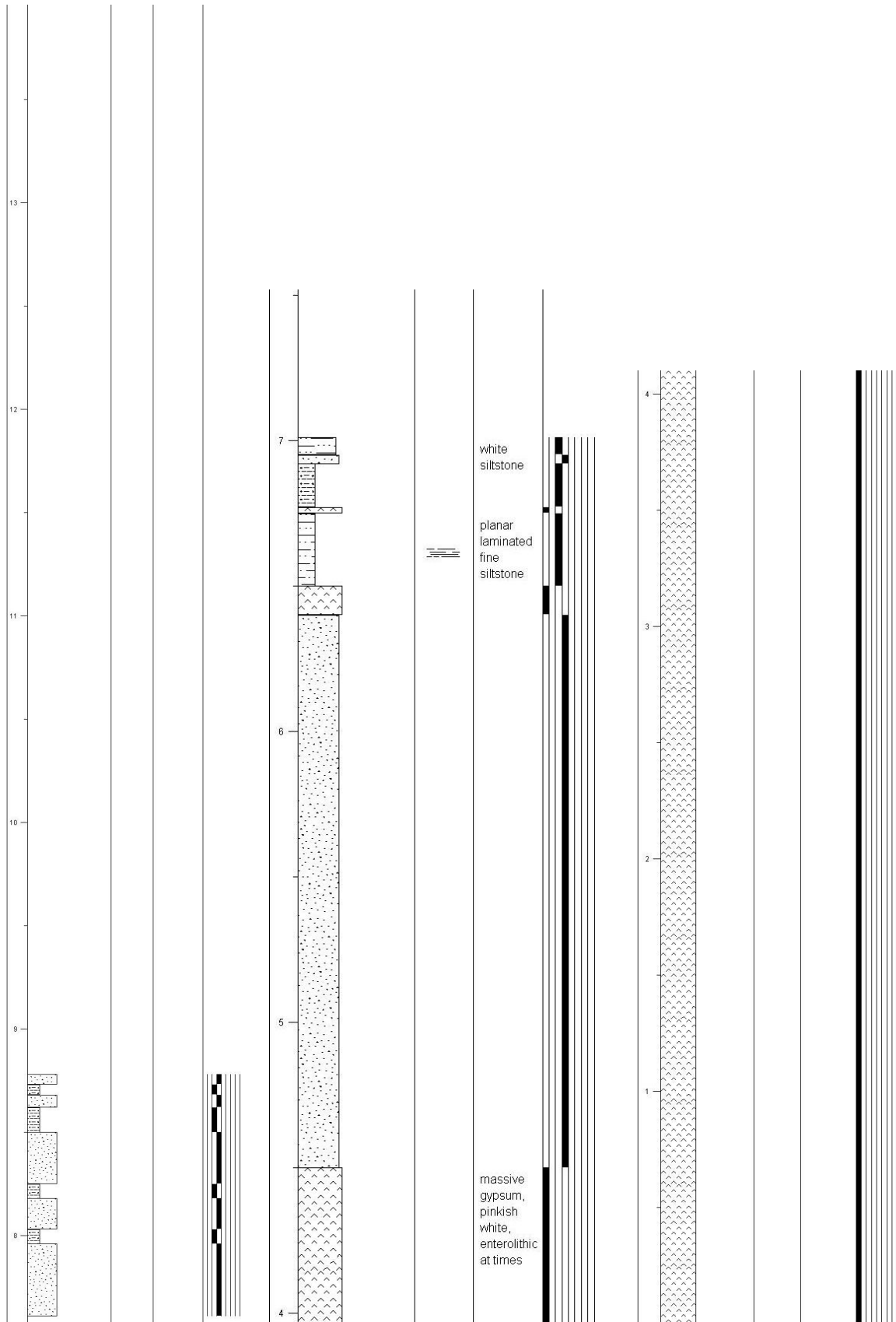


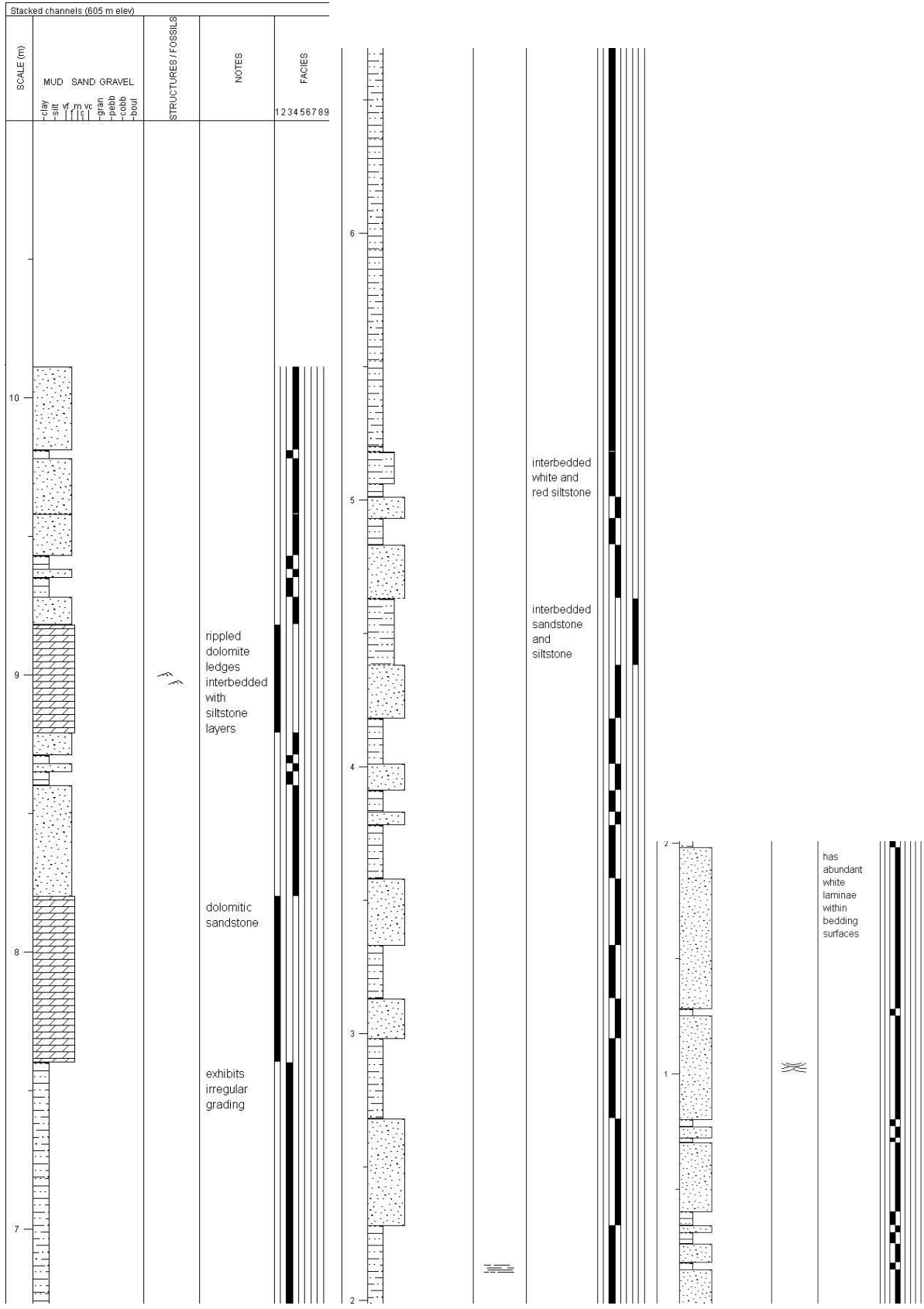
**Concordia plot – U-Pb Concordia Plot of detrital zircons. No discordant ages were found. Data-point error ellipses are  $2\sigma$  (95% confidence).**

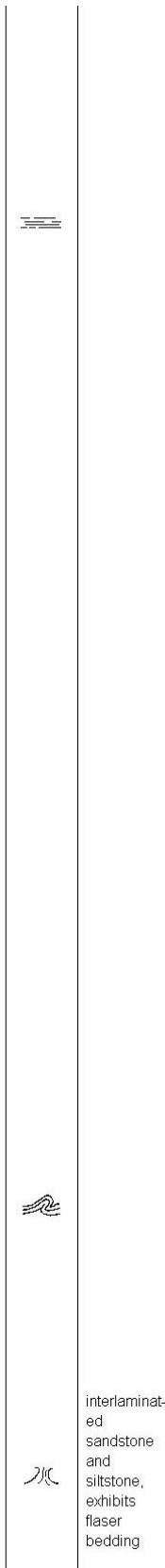
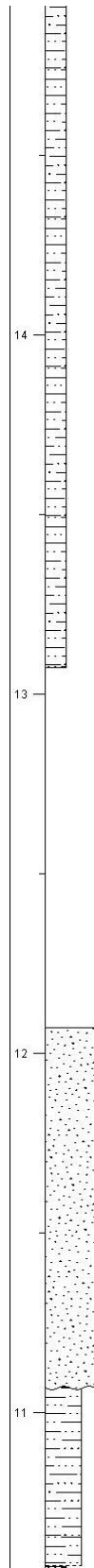
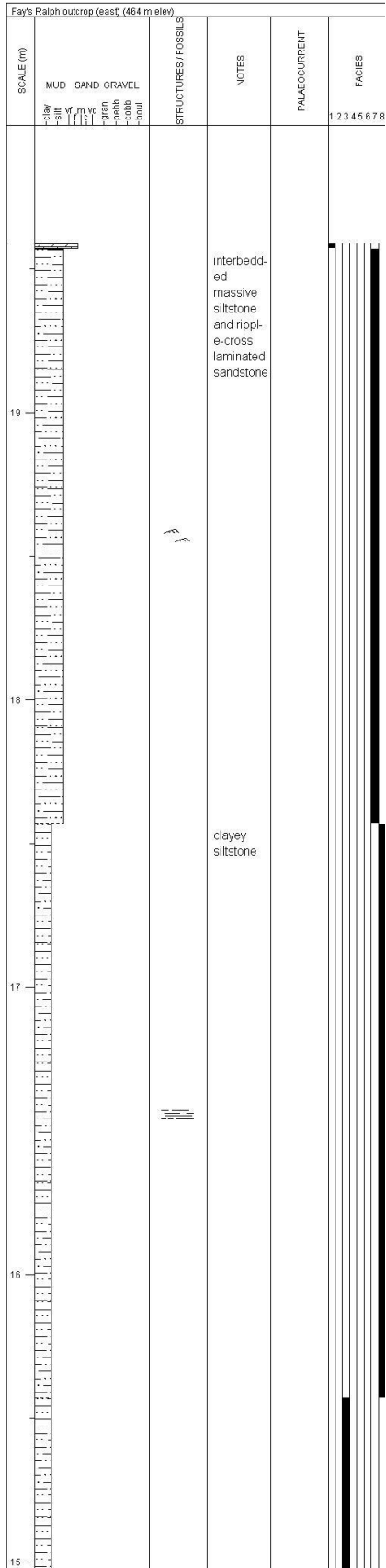
Extended CC outcrop (429 m - 493 m elev)

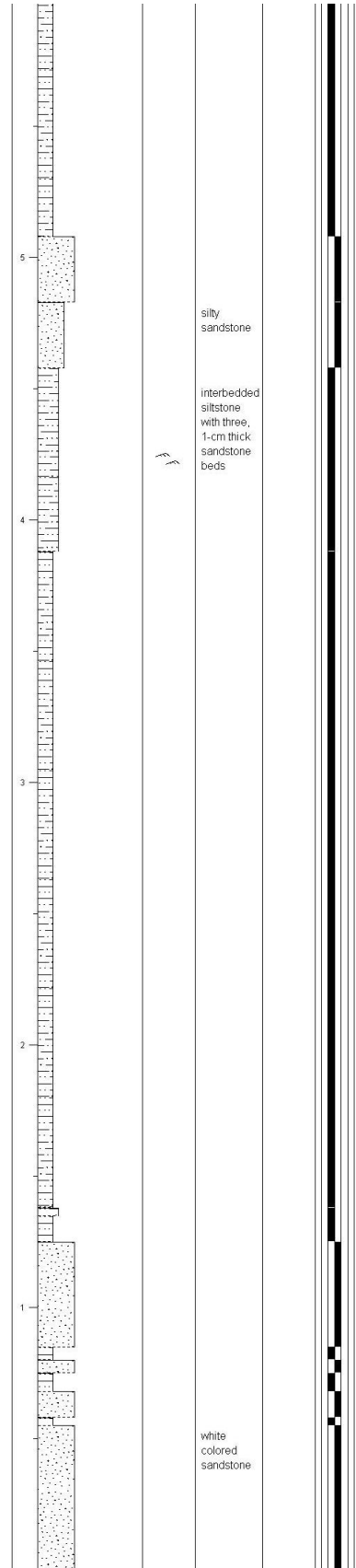
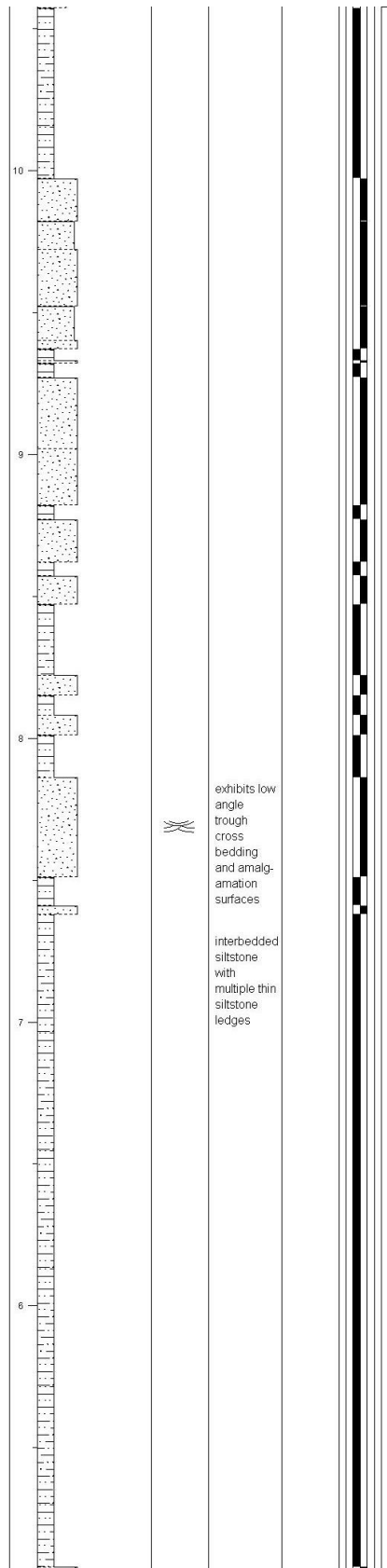
SCALE (m)	MUD SAND GRAVEL	STRUCTURES / FOSSILS	NOTES	FACIES
22	- clay - silty - m. vc - grain - fine - med - float			123456789
23				
24				
25			<p>                      sandstone with amalgamation (current) surface in the top 15 cm                 </p>	
26				



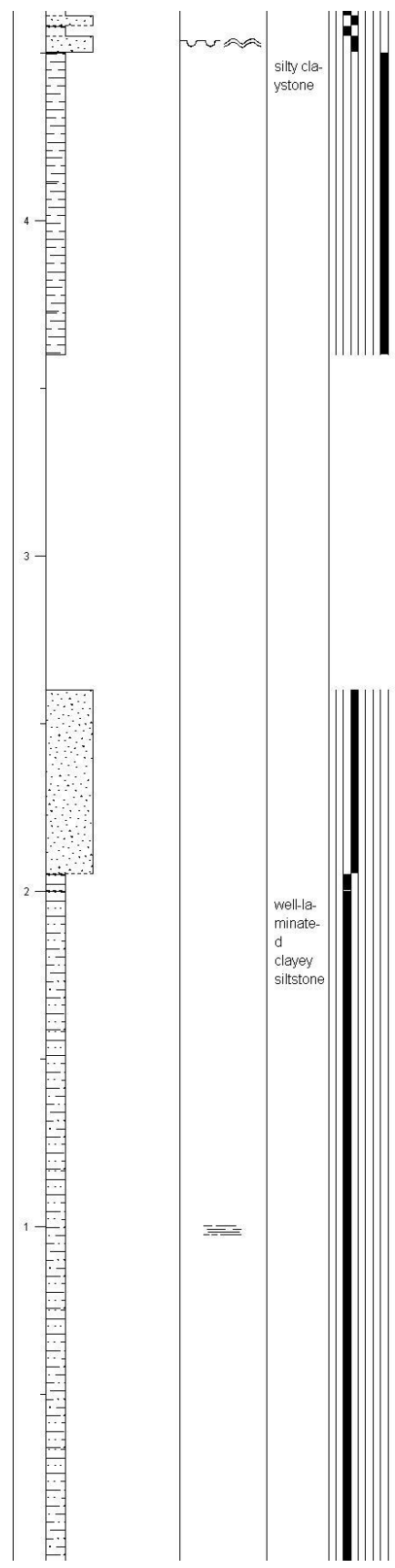
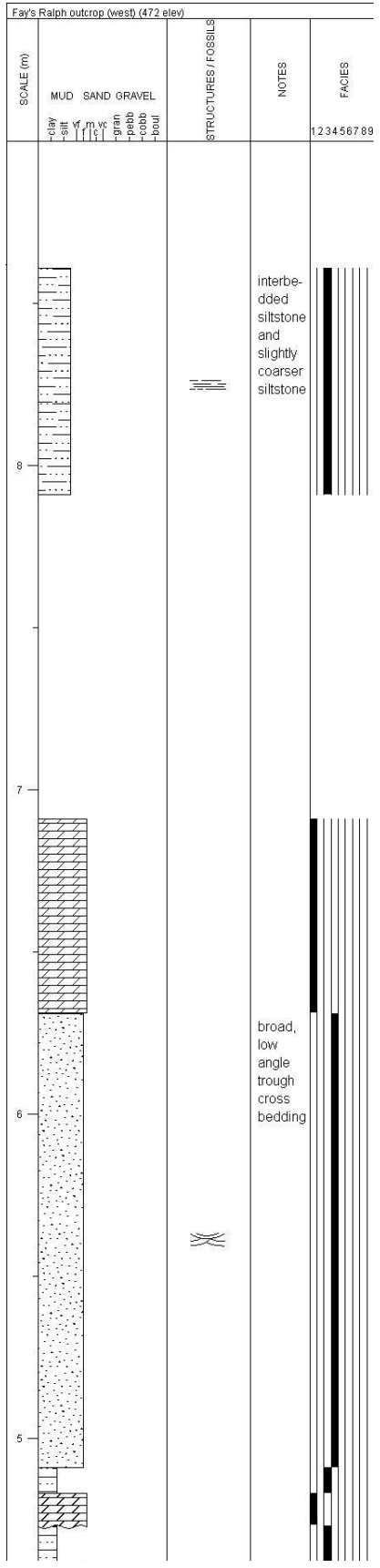




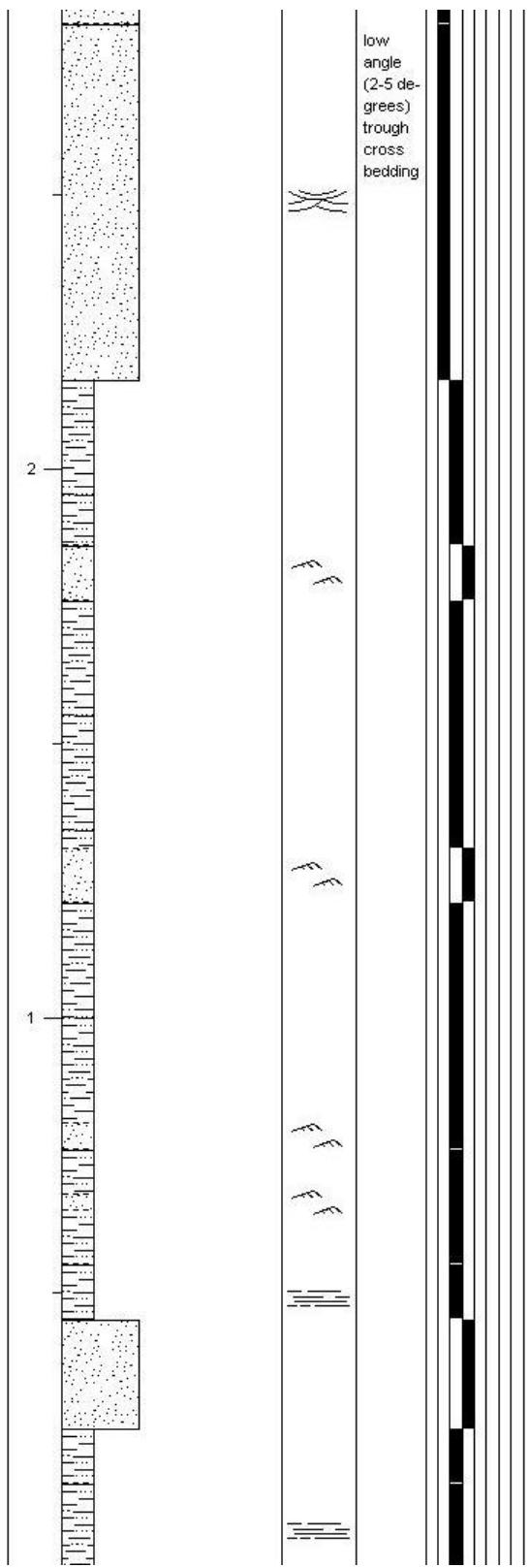
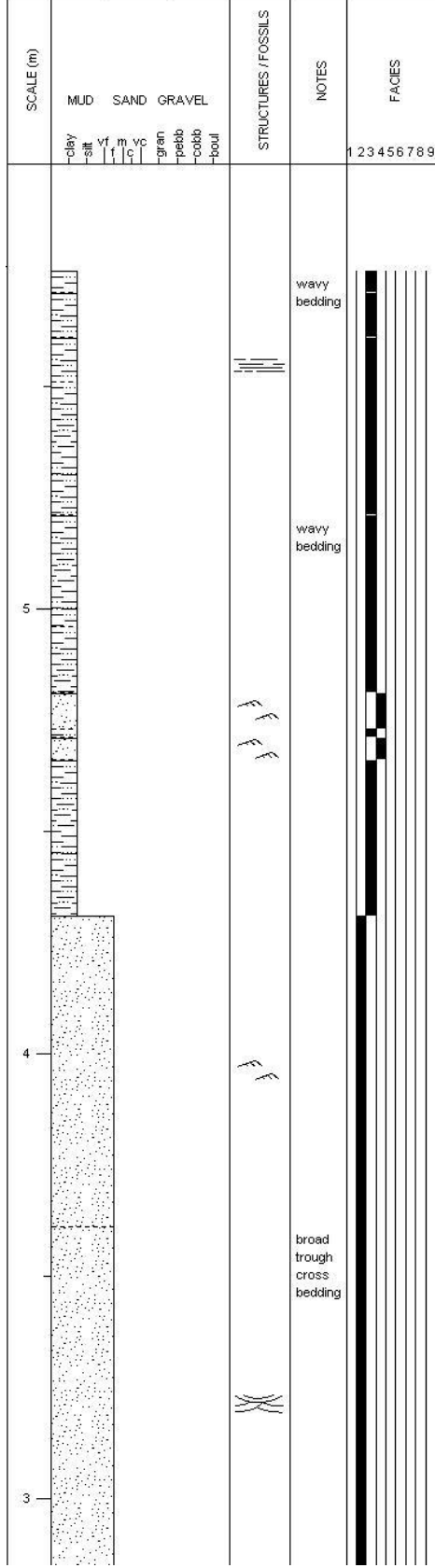


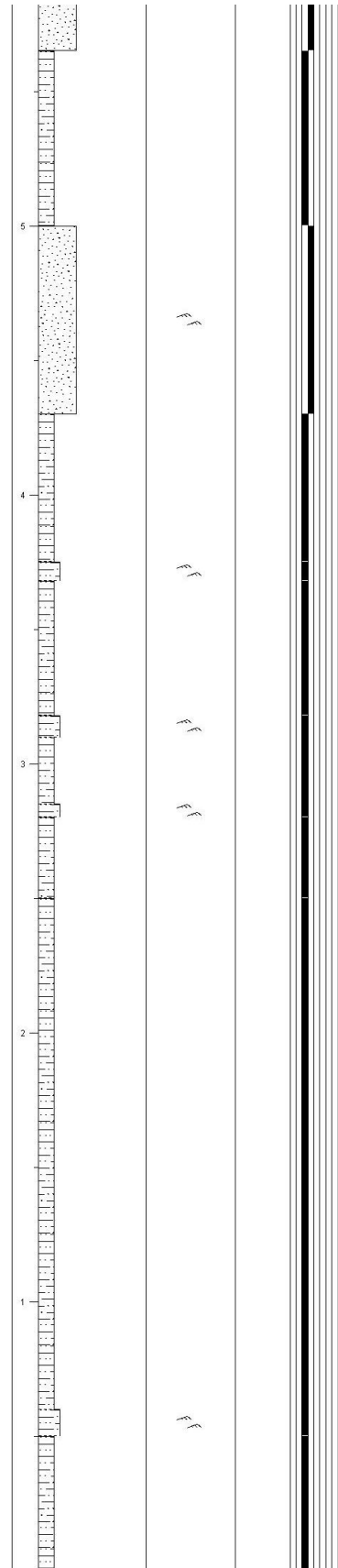
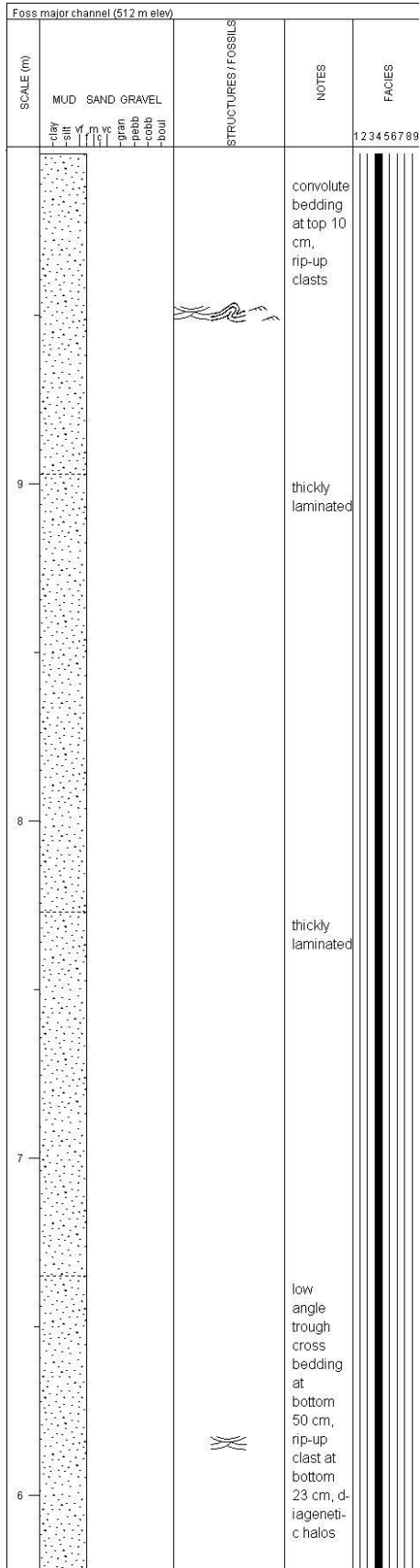


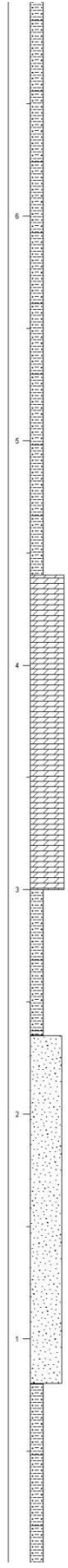
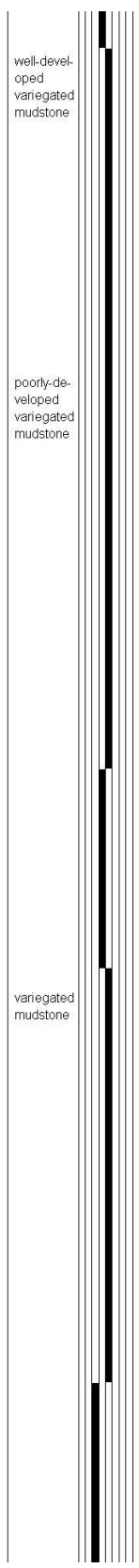
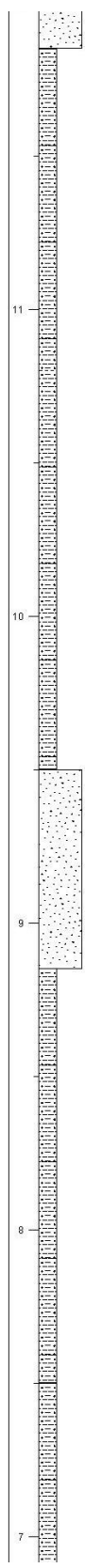
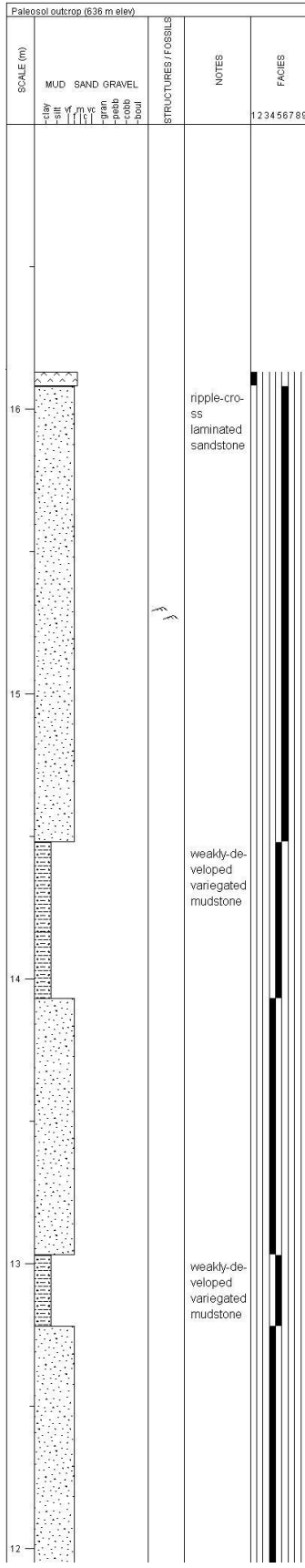


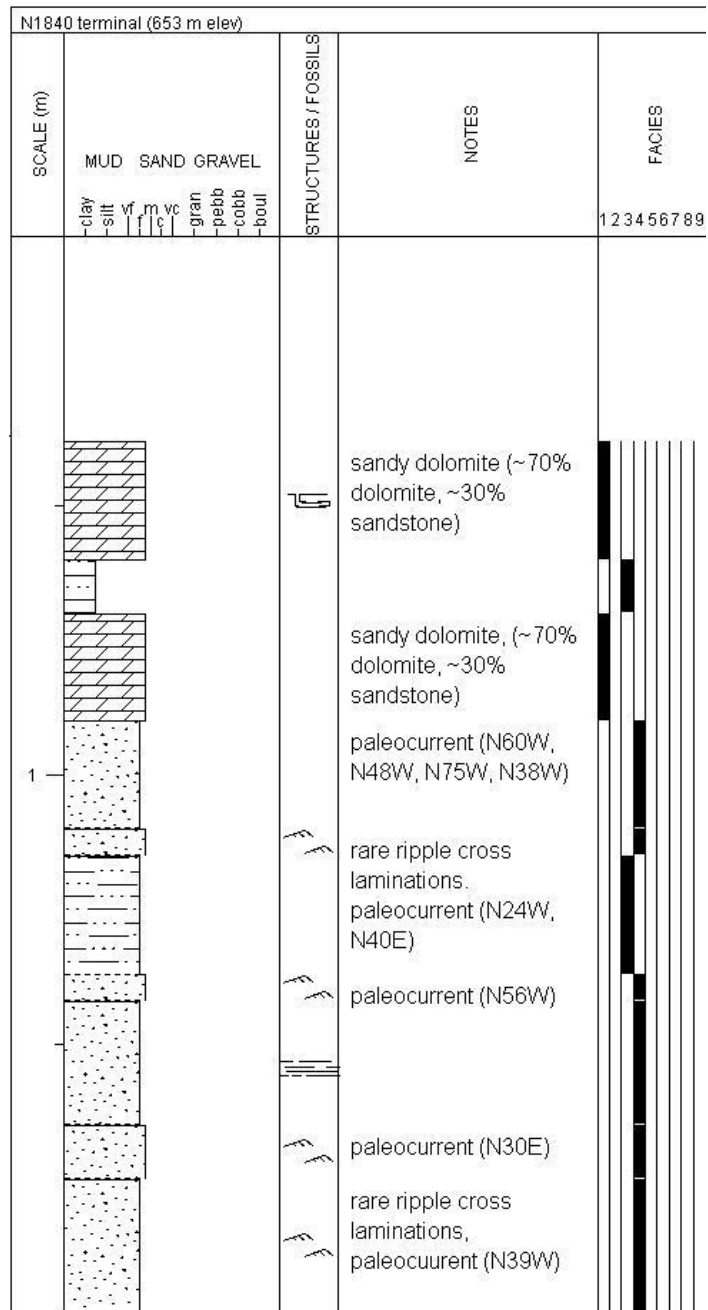
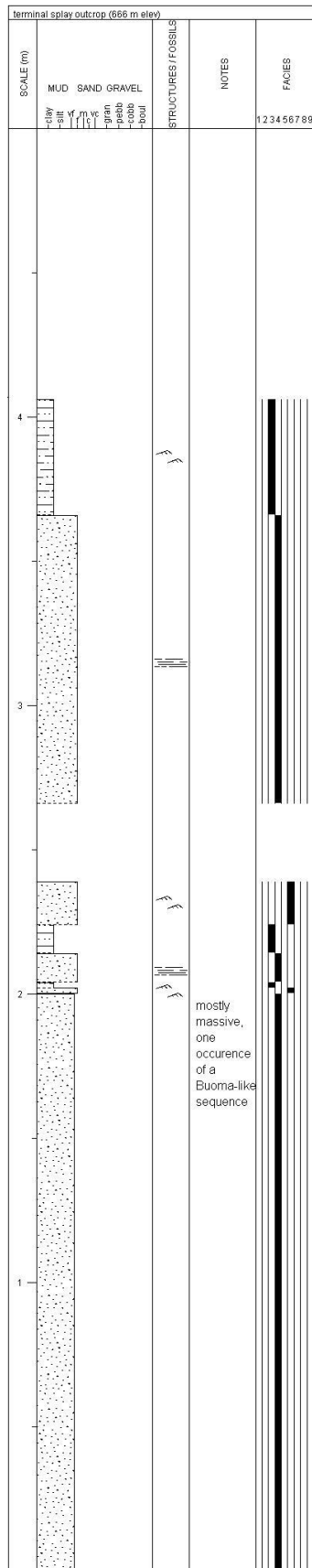


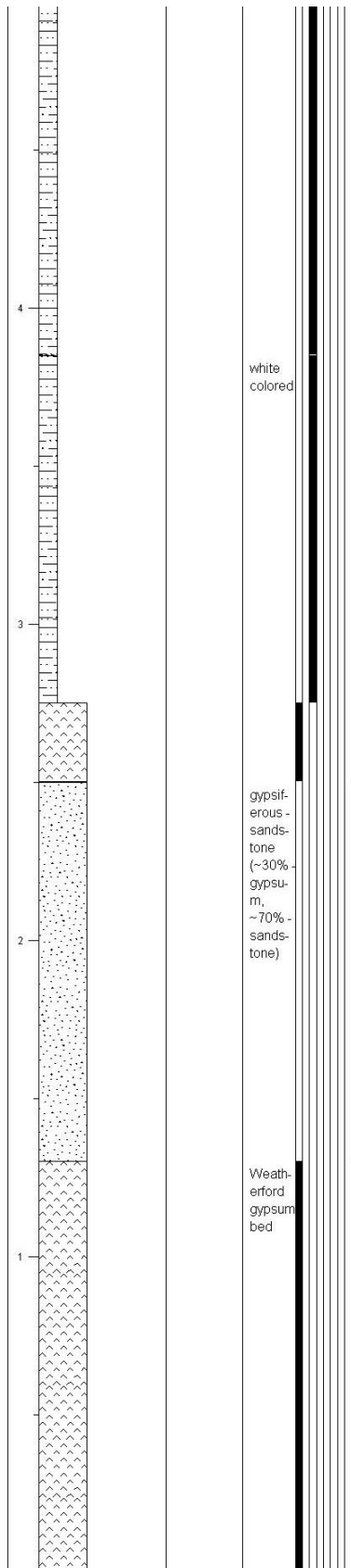
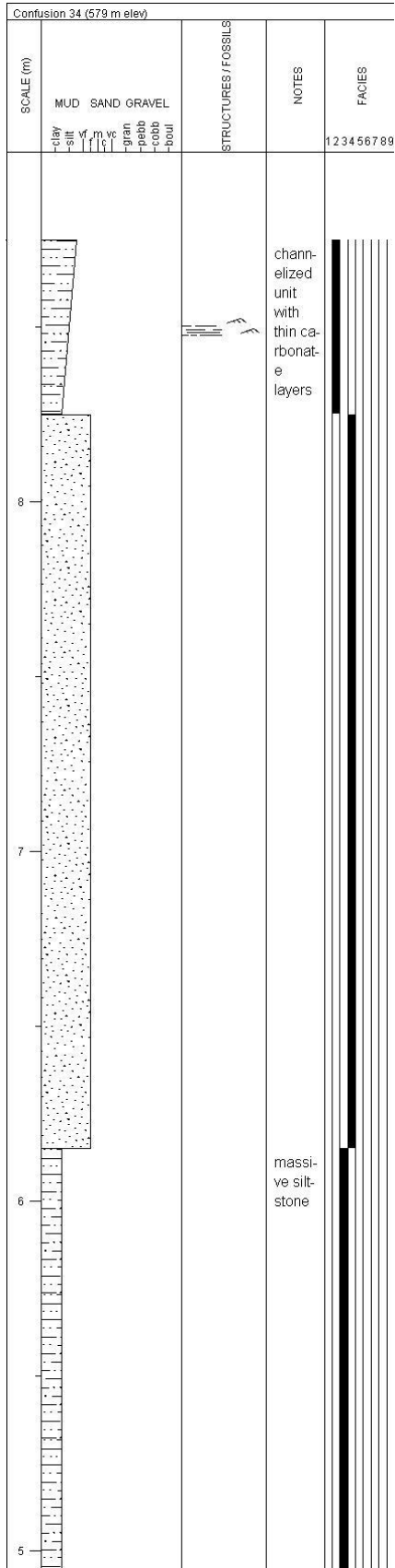
Foss Reservoir (525 m elev)





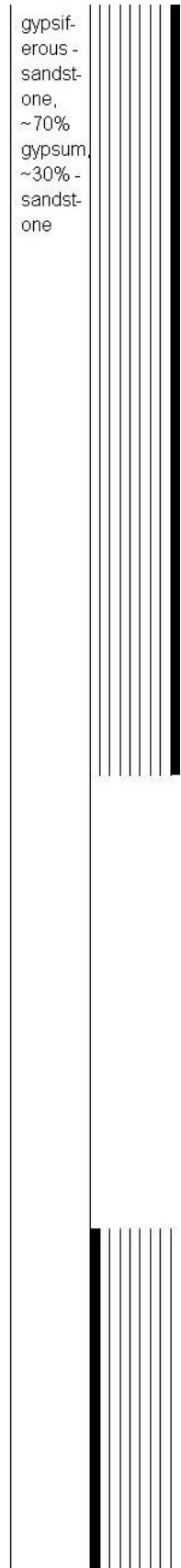
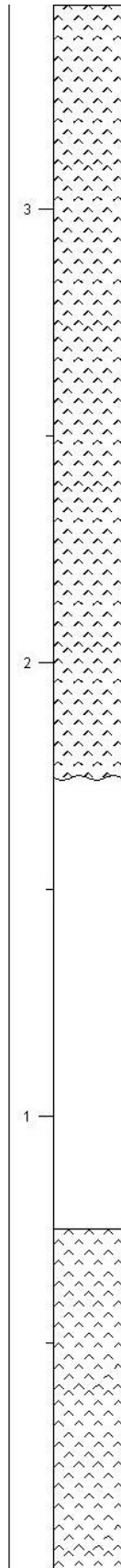
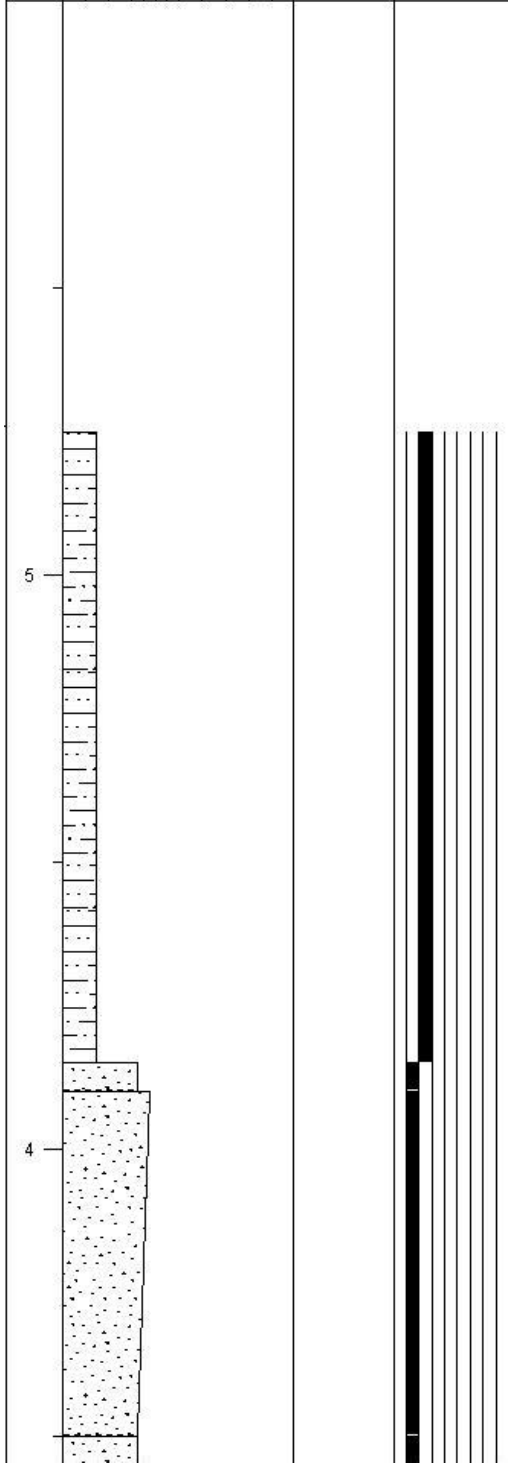




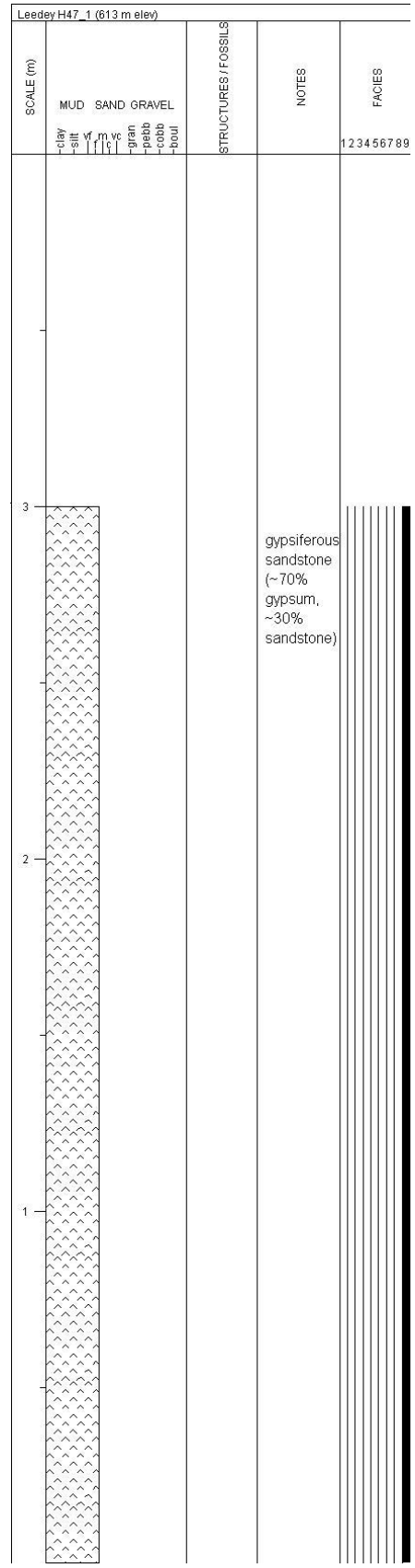
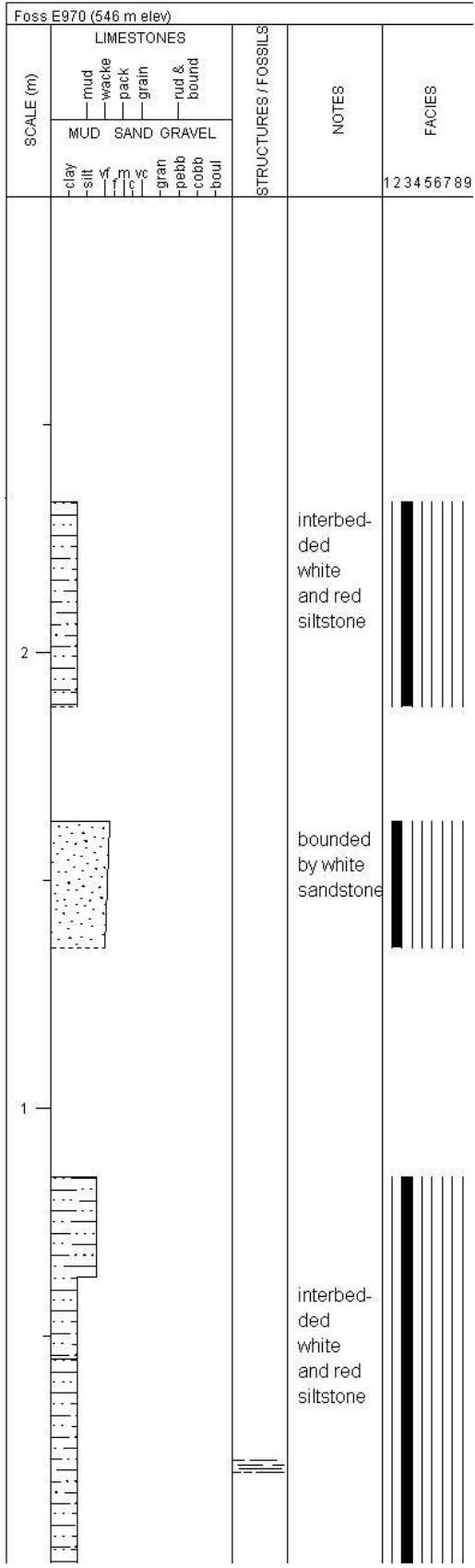


Strong City N1960\_1 (584 m elev)

SCALE (m)	MUD SAND GRAVEL			NOTES	FACIES
	clay silt vf m vc c	gran pebb cobb boul			

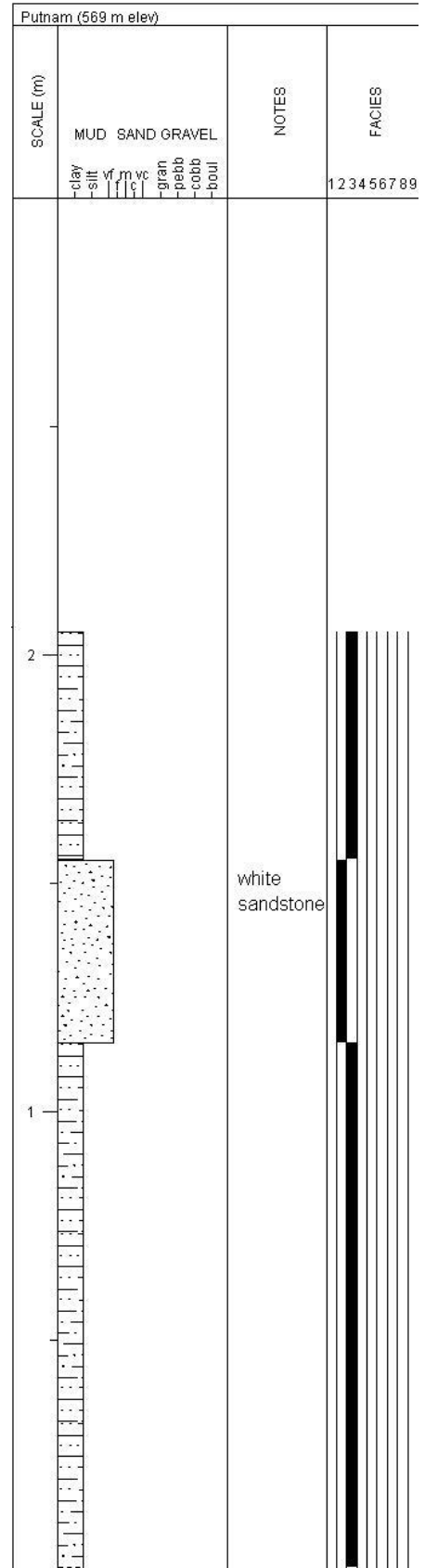
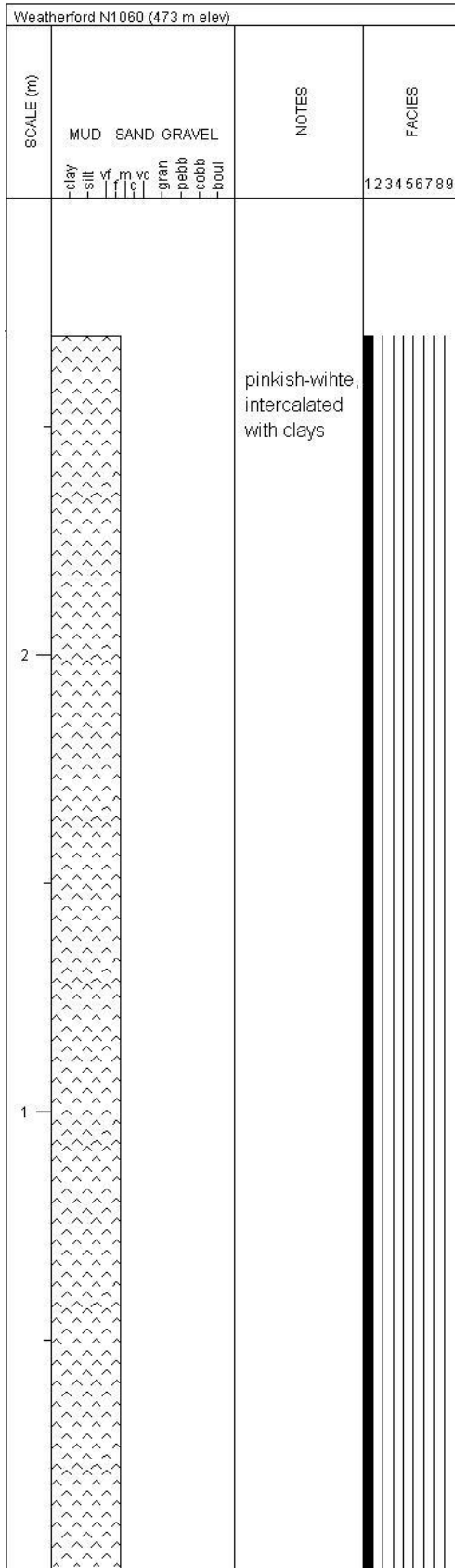


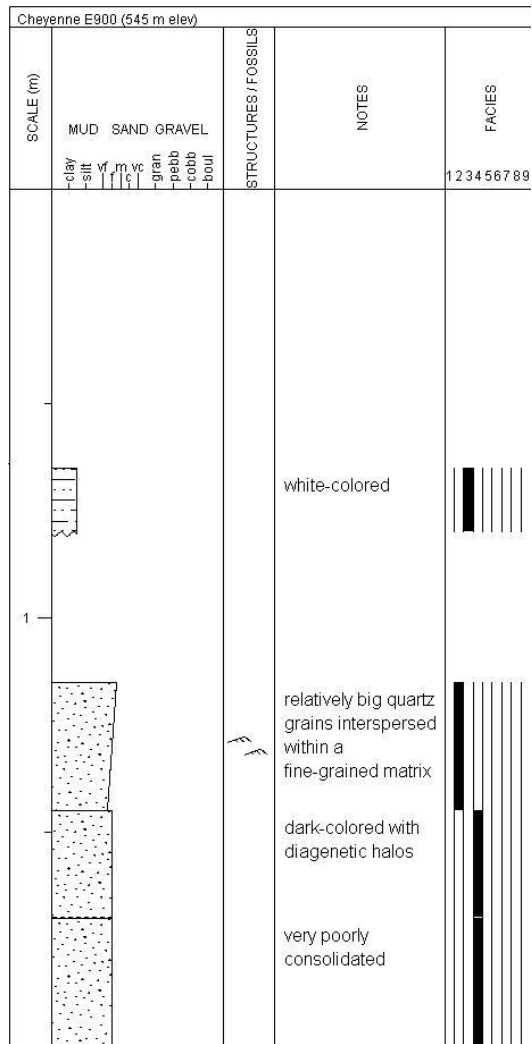
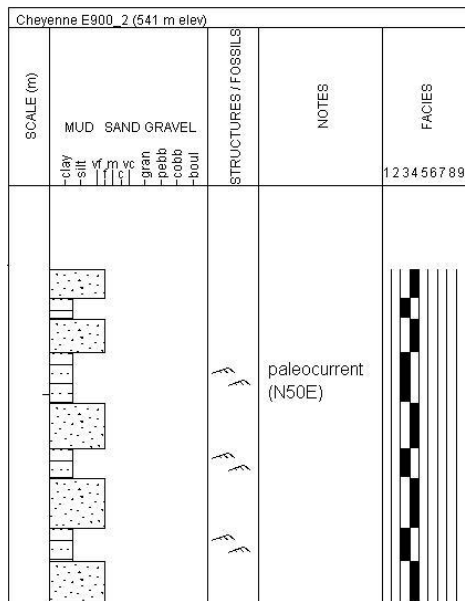
gypsiferous - sandstone, ~70% gypsum, ~30% - sandstone

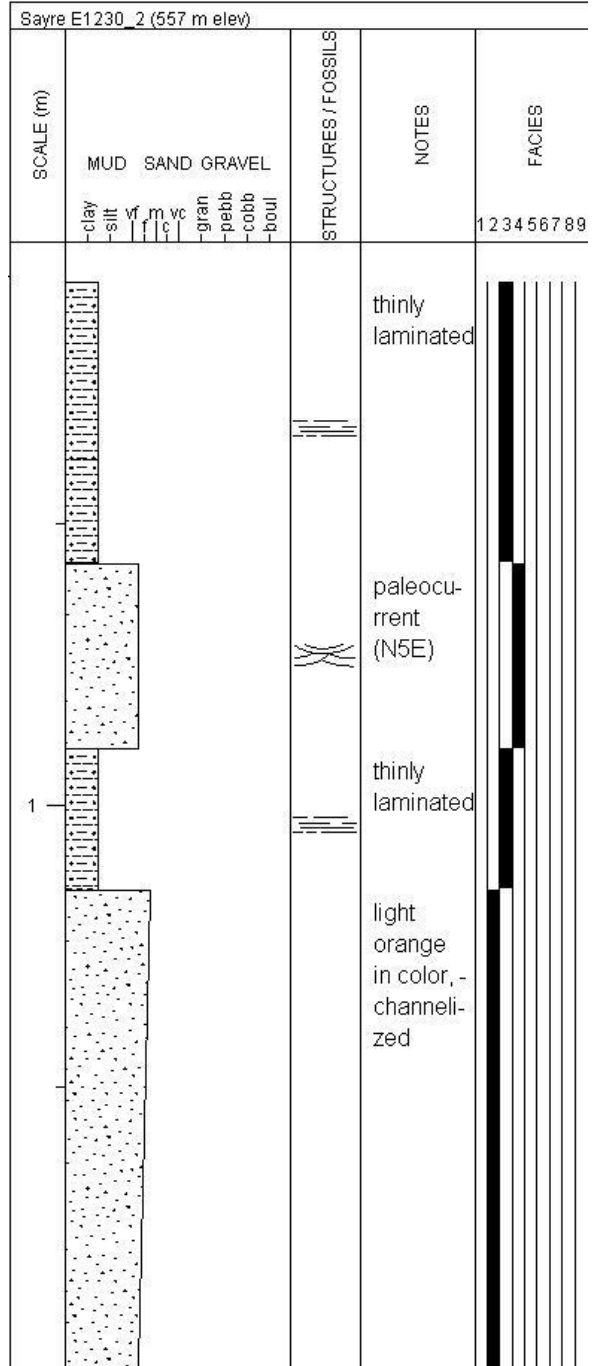
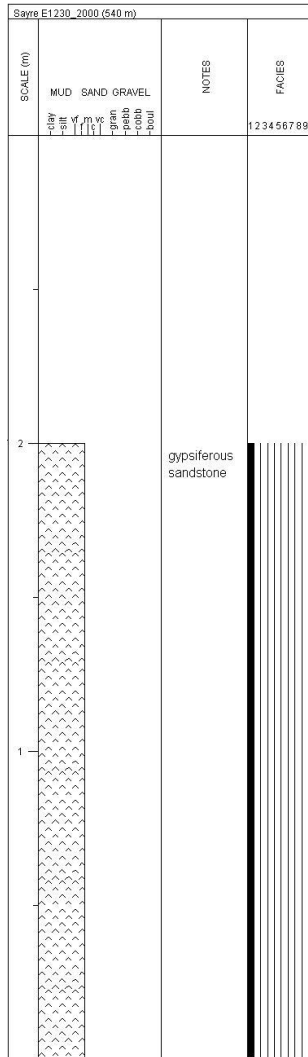


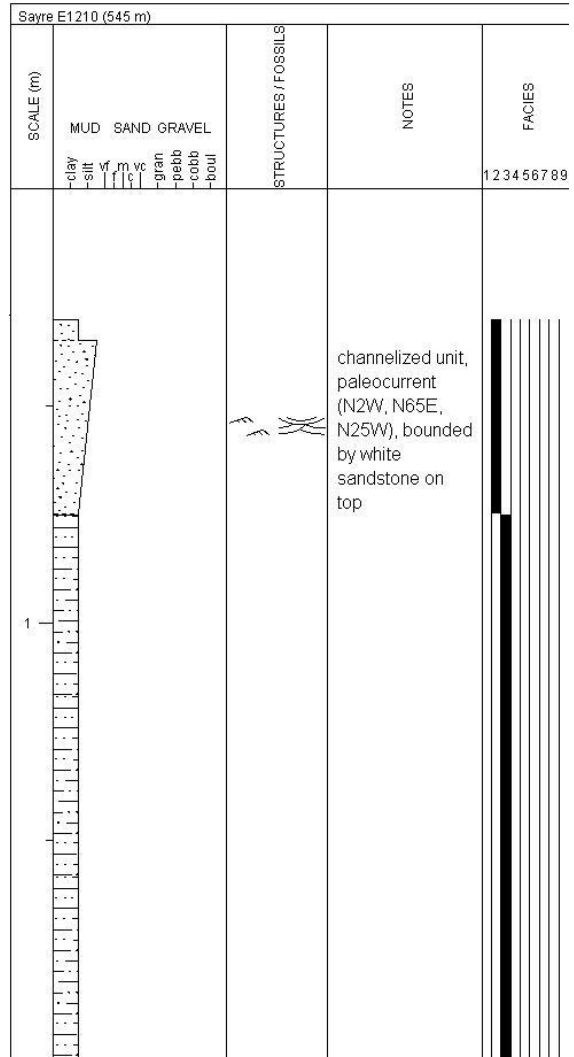
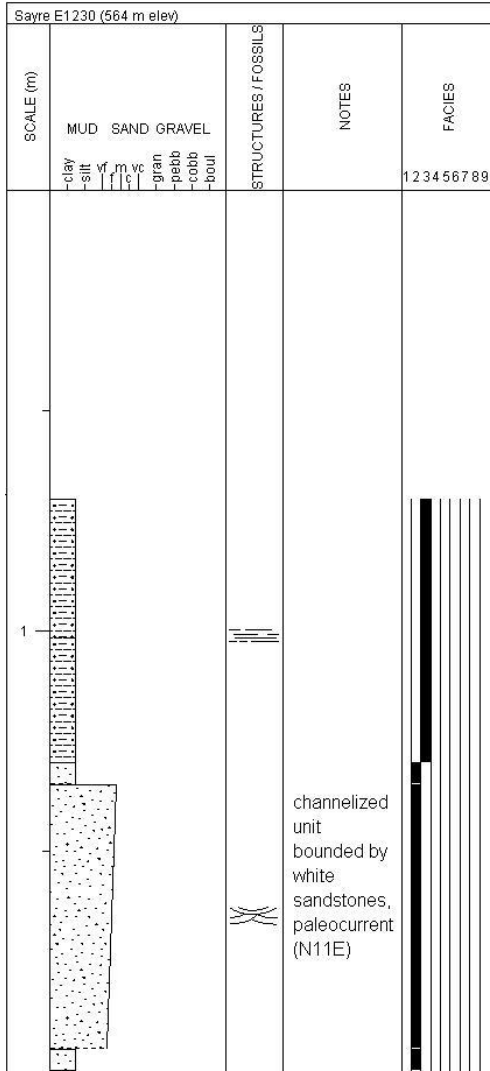


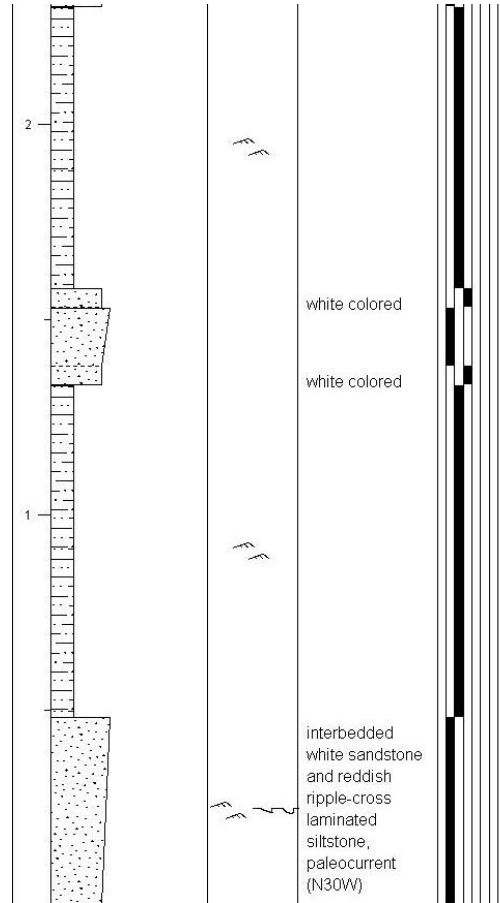
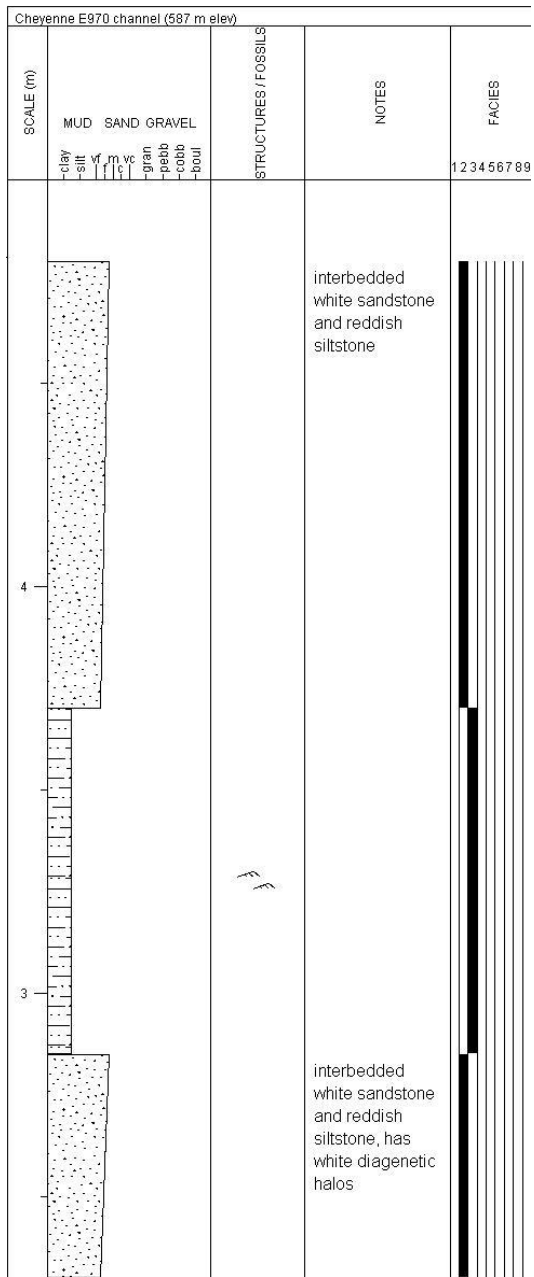




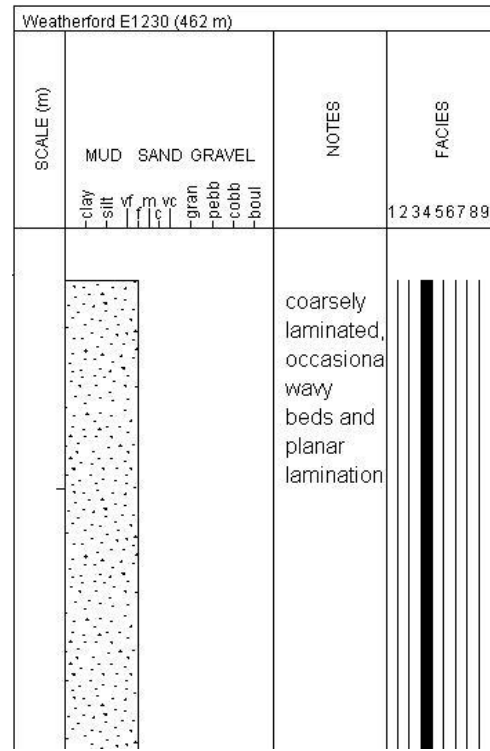
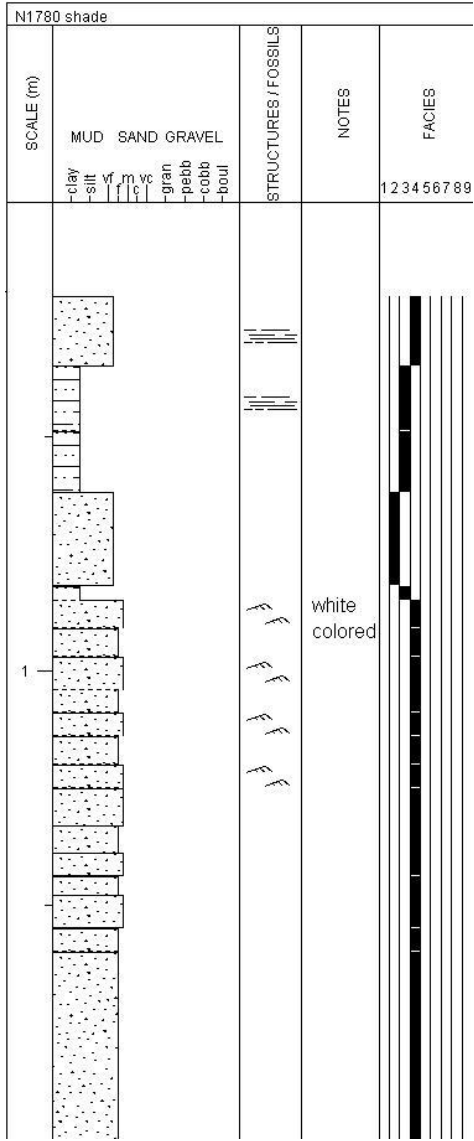




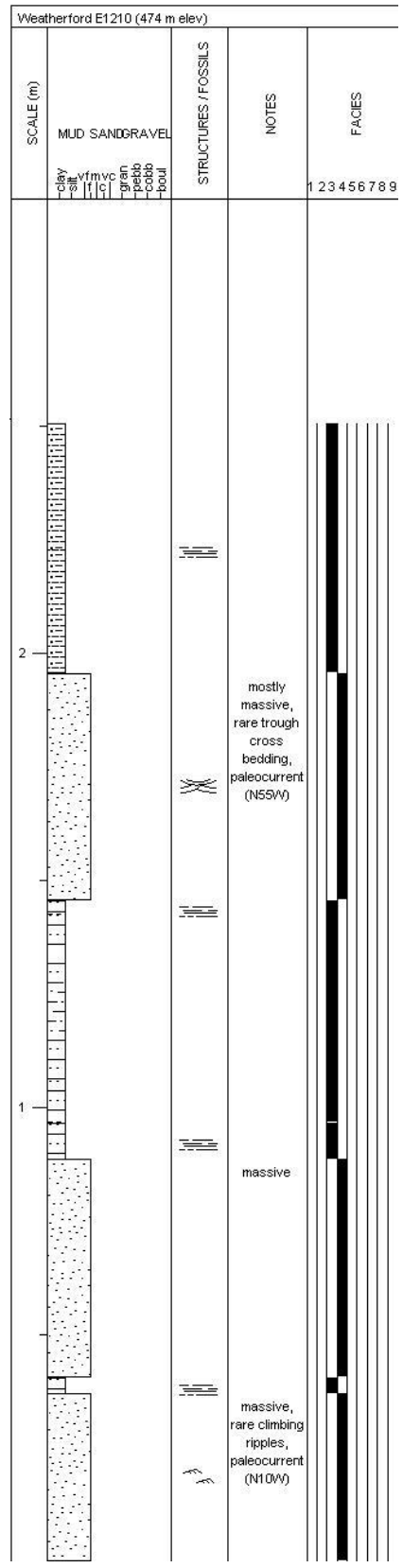
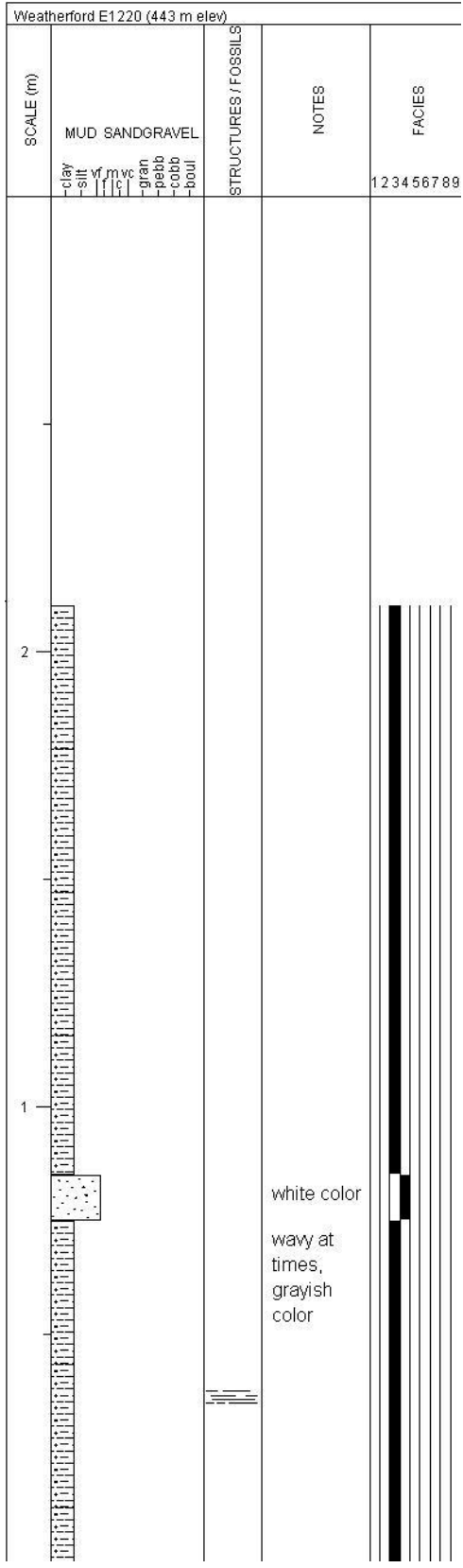






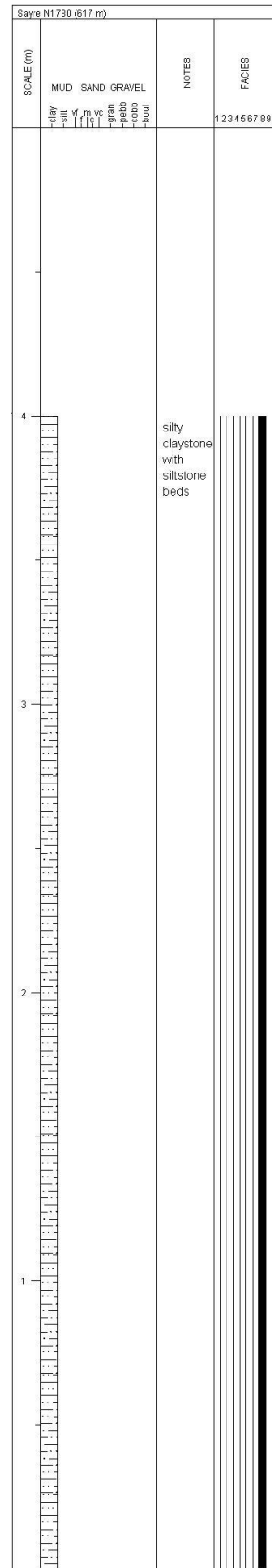
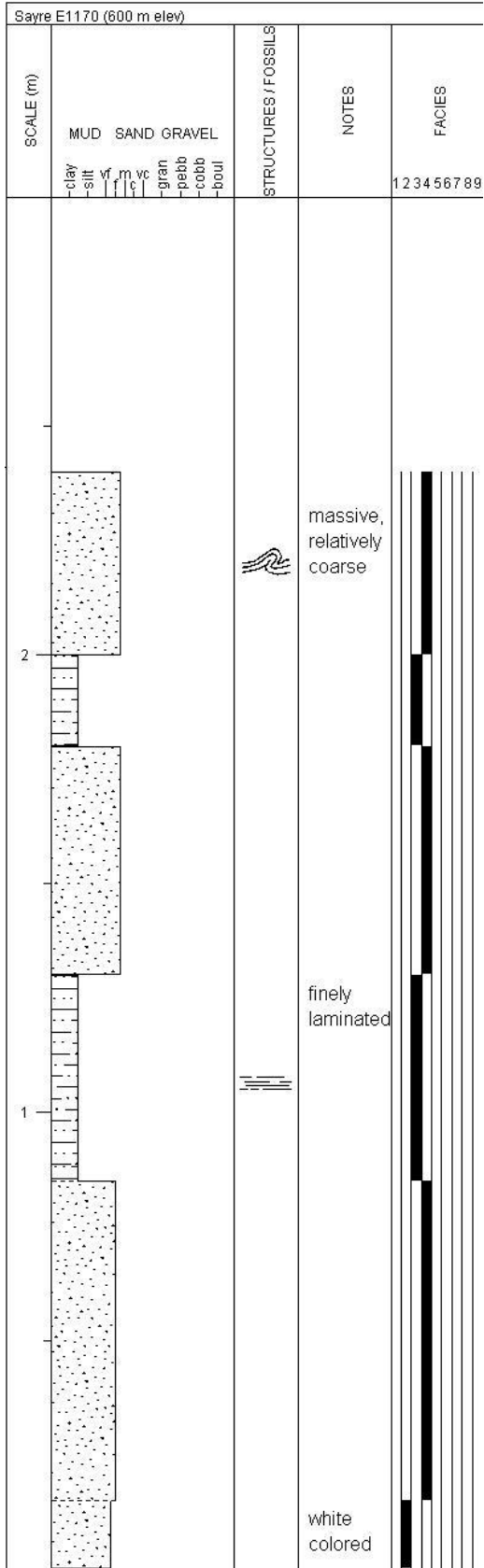


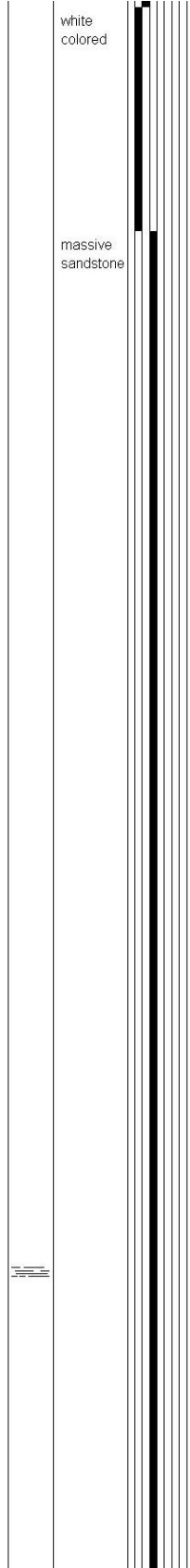
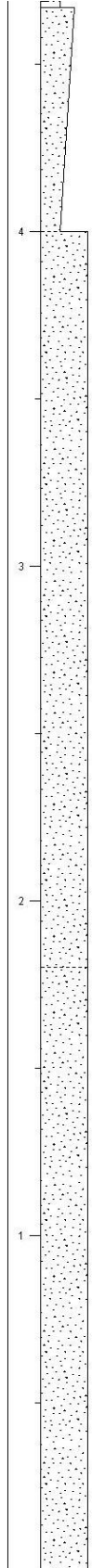
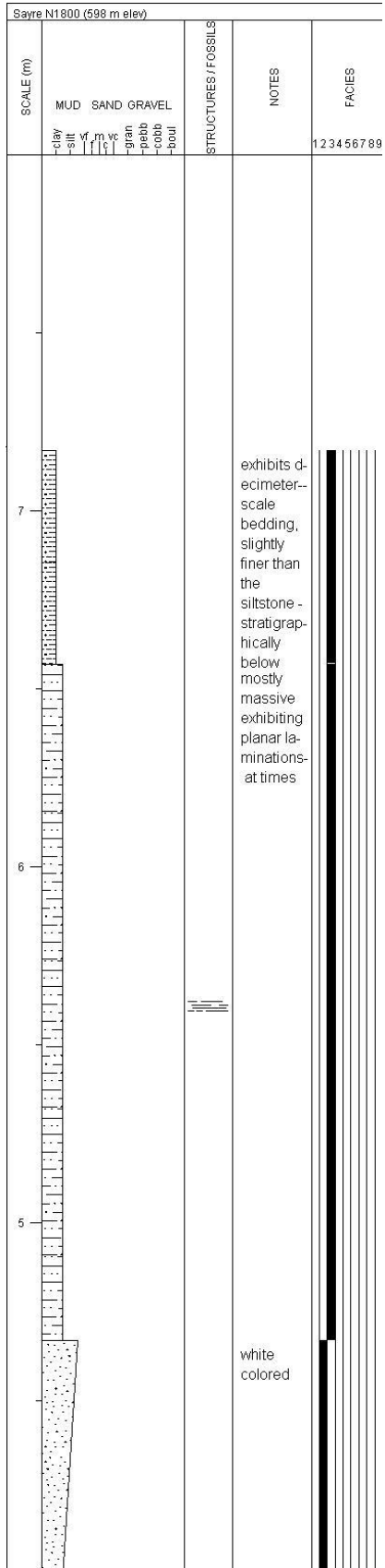


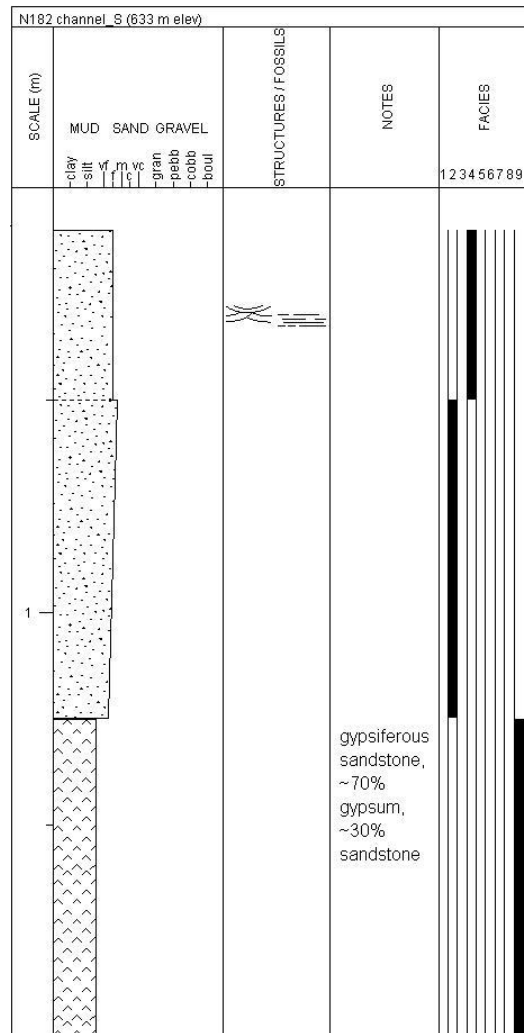
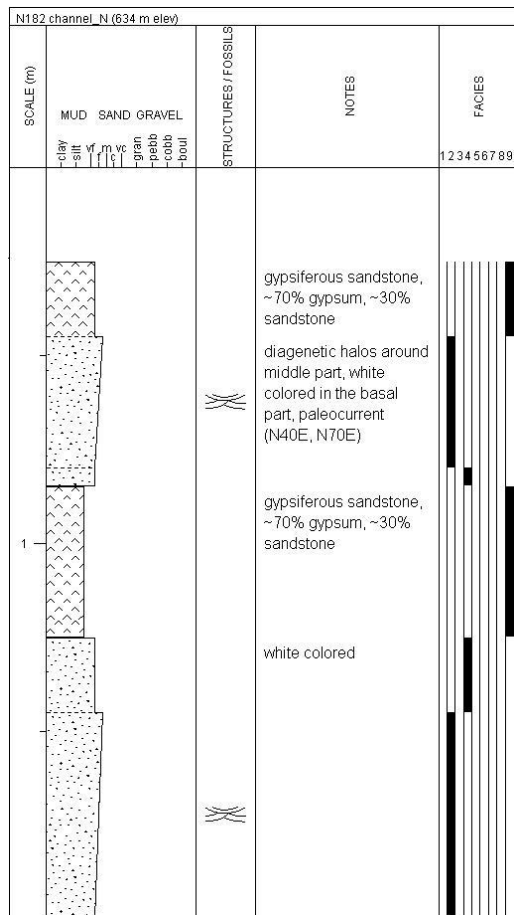


Weatherford E1090 (506 m elev)				
SCALE (m)	MUD SANDGRAVEL	STRUCTURES / FOSSILS	NOTES	FACIES
	-clay -silt -m -w -gran -pebb -cobb -boul		gypsum nodules (pebbles) within muddy matrix  massive, rare ripple cross laminations, white diagenetic halos, paleocurrent (N50E)	123456789

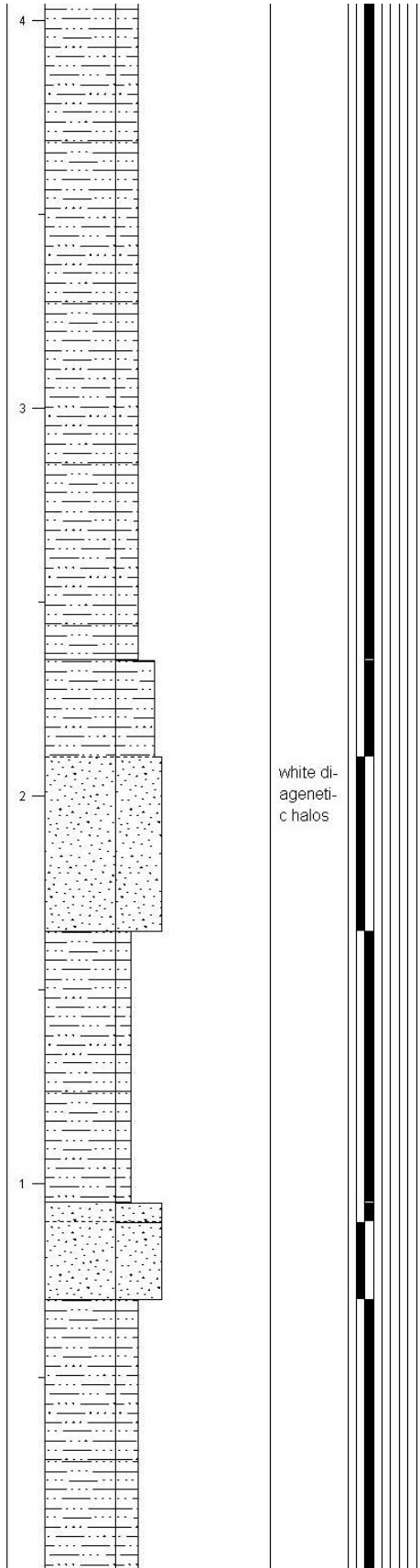
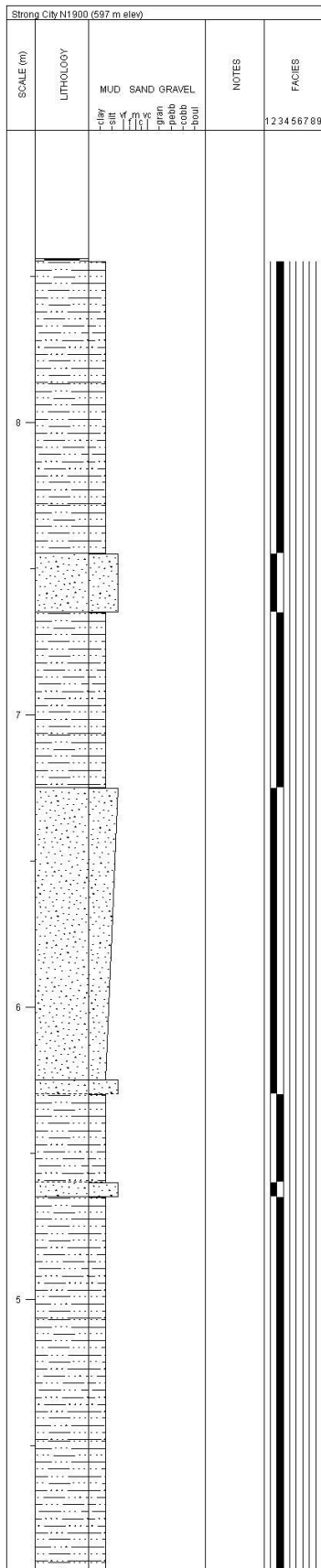
Savre E1200 (531 m elev)				
SCALE (m)	MUD SAND GRAVEL	STRUCTURES / FOSSILS	NOTES	FACIES
	-clay -silt -m -w -gran -pebb -cobb -boul		slightly more resistant than bottom layer, forms ledges, - paleocu- rrent (N35W)	123456789

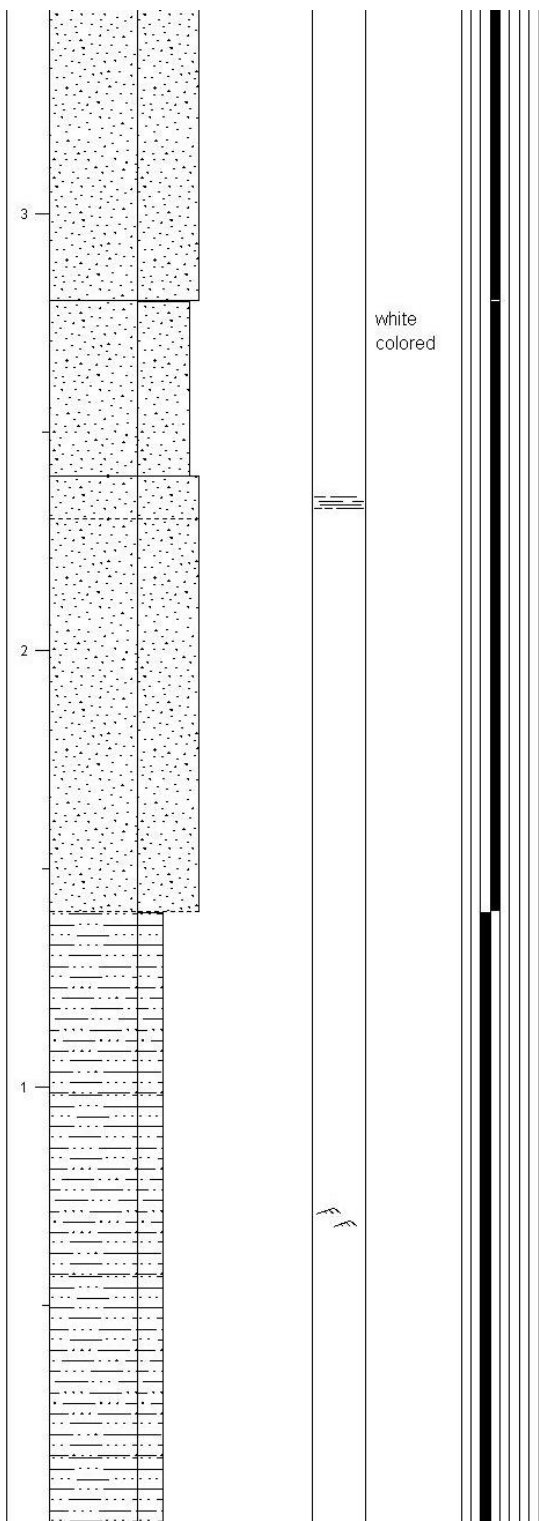
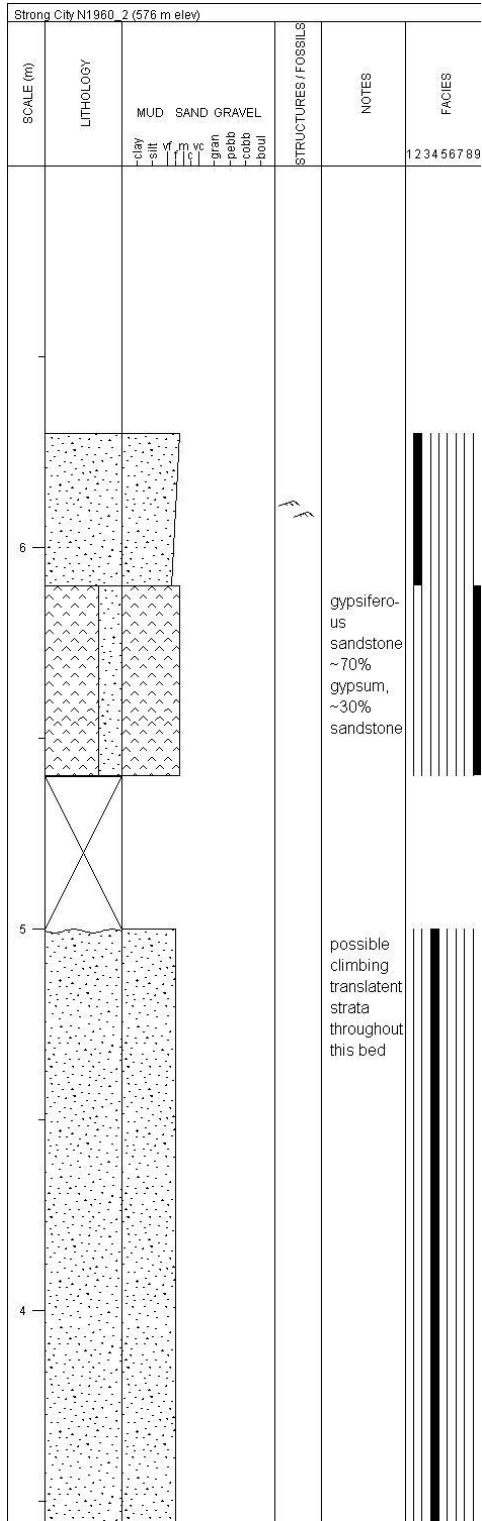




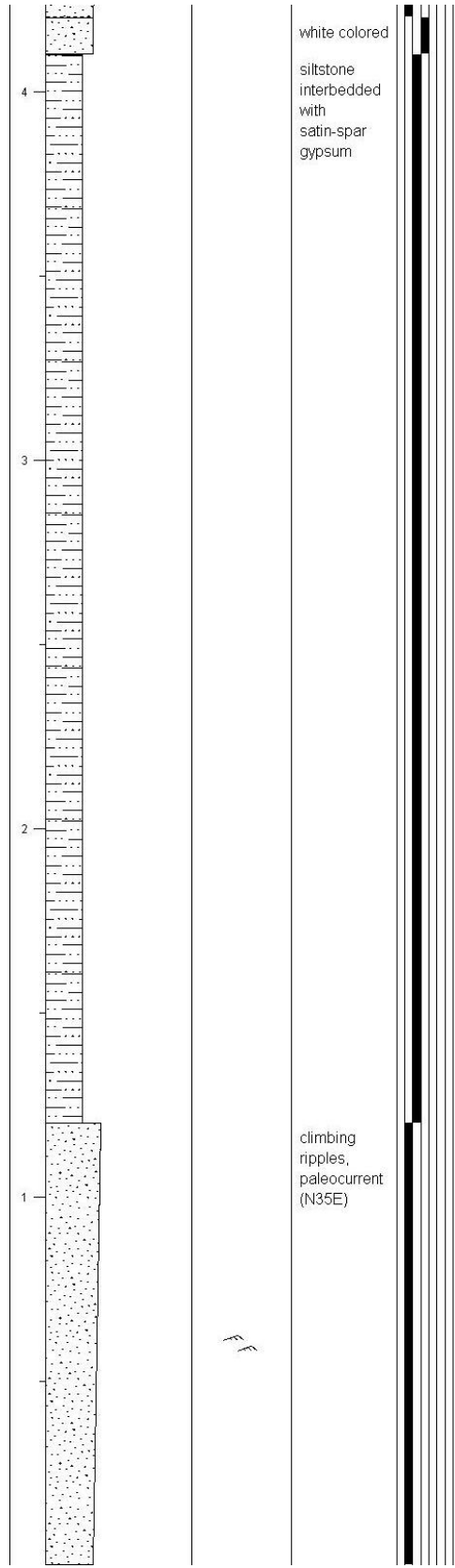
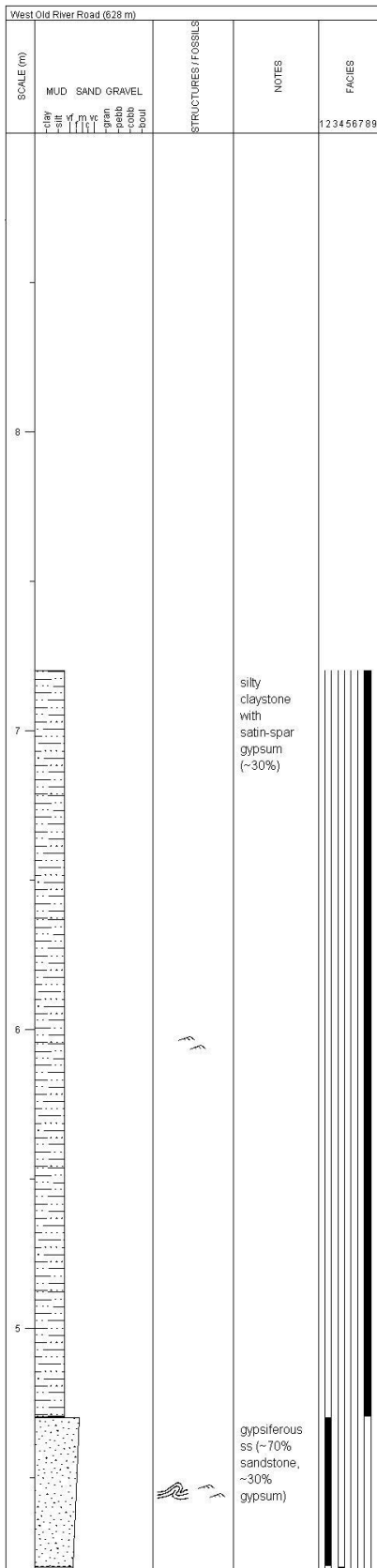


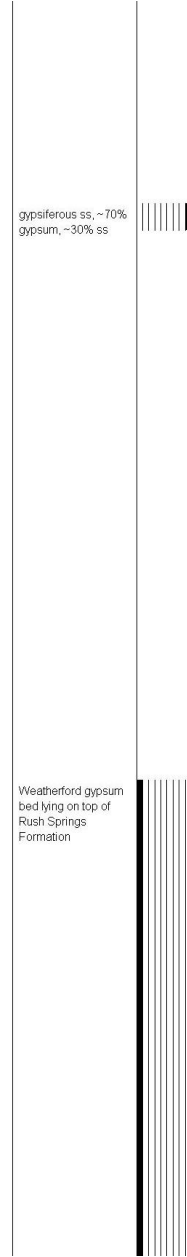
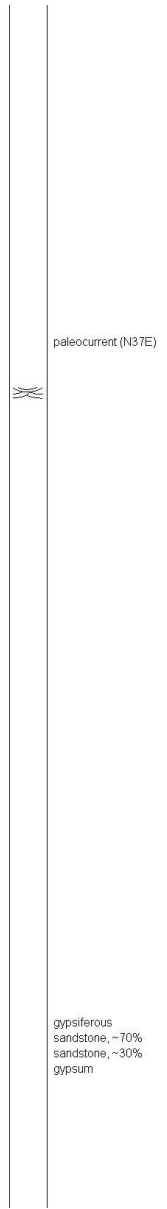
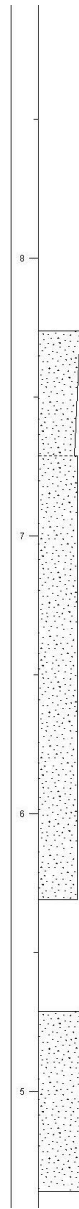
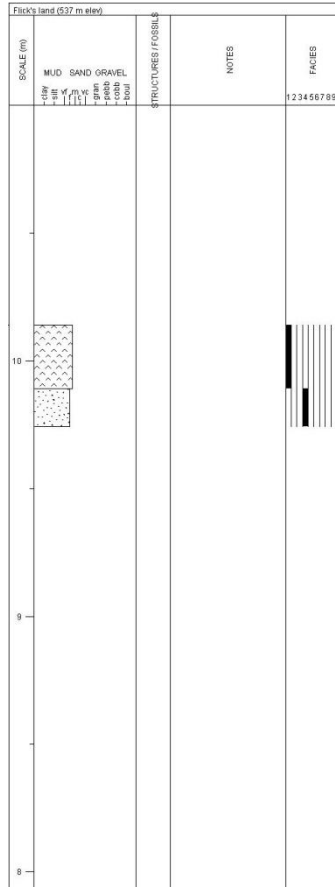


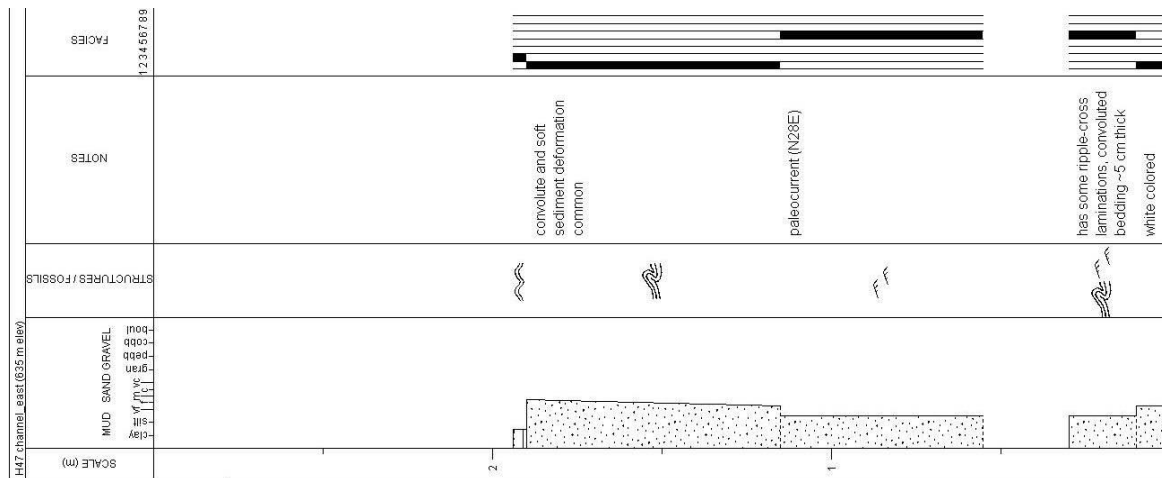












### Lithologies



Gypsum/Anhydrite



Sandstone



Siltstone



Mudstone



Dolomite

### Symbols



Trough cross bedding



Convolute lamination



Current ripple cross-lamination



Wave ripple cross-lamination



Horizontal planar lamination



Horizontal burrows

### Base Boundaries

— Sharp

- - - Gradational

~ Erosion

The facies column is divided into 9 types:

1 = evaporites (gypsum and dolomite)

6 = ripple-cross laminated sandstones

2 = channelized very fine sandstones

7 = interbedded sandstones and mudstones

3 = siltstones

8 = silty claystones

4 = thickly-bedded sandstones

9 = gypsiferous sandstones

5 = variegated mudstones